Conditional Moment Closure for Autoignition in Turbulent Flows

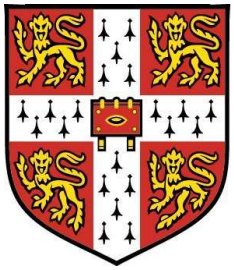

Giorgio De Paola – Fitzwilliam College

Department of Engineering

University of Cambridge

A thesis submitted for the degree of

Doctor of Philosophy

13th August 2007

Voglio dedicare questa tesi ai miei genitori Fulvio e Miriam, a mio fratello Luigi, mia sorella Lucia e ai miei nonni Cosimo e Marta, Luigi e Antonietta. Per essermi stati vicini in questi anni nonostante la distanza e soprattutto per essere la mia famiglia.

I would like to dedicate this thesis to my parents Fulvio and Miriam, to my brother Luigi, to my sister Lucia and to my grandparents Cosimo and Marta, Luigi and Antonietta. Thanks for being present throughout those years. Thanks for being my family.

Declaration

This dissertation is the result of my own work and includes nothing which is the outcome of work done in collaboration except where specifically indicated in the text. The dissertation contains approximately **42,000** words, **58** figures and **6** tables.

Hopkinson Laboratory, Cambridge *Giorgio De Paola*
13th August 2007

Acknowledgements

The work presented in this thesis could not be realized without the help of many people to whom I'm extremely grateful. I especially acknowledge my supervisor Dr. E. Mastorakos for the support, enthusiasm and guidance throughout this thesis and my advisor Dr. N. Swaminathan for the interesting discussions.

I'm indebted to all members of Dr. Mastorakos' research group for the stimulating environment in which this thesis and myself have grown. I would like to thank in particular C.N. Markides for the high quality measurements generously provided and the interesting discussions on mixing and autoignition but also for the invaluable friendship and company. I.S. Kim for the support and the contribution in the development of the numerical tools presented in this thesis. I'm extremely grateful to E.S. Richardson, my exact contemporary, for the interesting discussions, clever ideas and his patience throughout the development of the CMC code and especially his company during the last stages of editing the present work. T. Marchione for the long discussion on spray combustion but also for her friendship and all the other colleagues that made my stay here in the Hopkinson Laboratory unforgettable: T. Lovas, M. De la Cruz Garcia, R. Balachandran, H. Pedersen, C.W. Lee, S.F. Ahmed, A. Garmory, A. Triantafyllidis, P. Schroll, A. Pastore. A special thank you to P. Benie for his assistance and the technical support with the computers.

Impossible not to mention M. Tanfour for the rigour, the support, the technical discussions and non-, but in particular for his friendship across the distance. S. Karagiorgis who bear patiently a noisy italian for almost four years.

I would like to thank the engine research group at ETH Zurich, lead by Prof. K. Boulouchos, for the experimental data provided and the useful discussion on engine modelling. I am indebt to Y.M. Wright for his contribution in the development of the code but nonetheless for the enthusiasm in 'climbing' this research field.

For their technical input I would like to thank the N.I.C.E. consortium in particular the partner of the subproject B1. L. Vervish (I.N.S.A. Rouen), C. Angelberger (IFP), I. Magnusson, M. Balthasar (Volvo), F. Mauss (U. Cottbus), D. Suzzi (Daimler Chrysler) and the Ford Research centre (Aachen) W. Werner and G. Bikas. Financial support has been received from the European Project N.I.C.E. and Ford Research Center (Aachen). A final thank to T. Baritaud (Ferrari G.S.) that supported me in the decision to approach the research world of turbulent combustion.

I express my gratitude to all friends I have met here Cambridge during these years. In particular I will never forget my Spanish 'family', with the hope that the time spent together will always last. Elvira, Arantza, Javi, Josep, Josep-Maria and the Kiss of Klint, of course Fabio. All my friends from Italy 'la Casina Rosa', Andrea, Jonny, Dimma, Jhon, Penna, Simo, Matte, Tosco, Abi and also Elisa, Cate, Bea, Gio, Luchi, Danko, Alle, Antonio.

Publications

The results of this thesis have been partially published in the following journal articles:

1. Y.M. Wright, G. De Paola, K. Boulouchos and E. Mastorakos. Simulations of spray autoignition and flame establishment with two-dimensional CMC. *Combustion and Flame*, 143:402-419, 2005.
2. C.N. Markides, G. De Paola and E. Mastorakos. Measurements and simulations of mixing and autoignition of an n-heptane plume in a turbulent flow of heated air. *Experimental Thermal and Fluid Science*, 31(5):393-401, 2007.

and presented in the following conferences:

1. C.N. Markides, G. De Paola and E. Mastorakos. Measurements and simulations of mixing and autoignition of an n-heptane plume in a turbulent flow of heated air. *Proceeding of the* 4^{th} *Mediterranean Combustion Symposium*, 2005. Accepted for oral presentation.
2. G. De Paola and E. Mastorakos. Second-order Conditional Moment Closure simulations of autoignition of an n-heptane plume in a turbulent coflow of heated air. 2^{nd}*ECCOMAS thematic conference on computational combustion*, 2007. Accepted for oral presentation.
3. G. De Paola, Y.M. Wright, K. Boulouchos and E. Mastorakos. Diesel engine simulation with multi-dimensional conditional moment closure. 5^{th} *Mediterranean Combustion Symposium*, 2007. Submitted for oral presentation.

Other related works in preparation:

1. I.K. Kim, G. De Paola and E. Mastorakos, Simulation of diesel spray combustion and soot formation with two-dimensional CMC. (in preparation).
2. Y. M. Wright, R. Margari, G. De Paola, E. Mastorakos and K. Boulouchos. Experiments and simulations of n-heptane spray auto-ignition in a closed combustion chamber at Diesel engine conditions. (in preparation).
3. G. De Paola, Y.M. Wright, K. Boulouchos and E. Mastorakos, Diesel engine simulation with multi-dimensional conditional moment closure. (in preparation).
4. G. De Paola and E. Mastorakos. Second-order Conditional Moment Closure simulations of autoignition of an n-heptane plume in a turbulent coflow of heated air. (in preparation).

Abstract

This thesis presents the development and implementation of the CMC modelling approach for turbulent non-premixed autoignition with particular relevance to direct injection diesel engine simulations.

Initially the CMC model is presented. Special care has been taken to derive the conditional energy equation in the form of temperature at first and second-order. The numerical implementation for the cases analyzed is presented afterwards. Various numerical integration procedures have been considered based on the Method of Lines and the Operator Splitting method. Results have been analyzed in terms of accuracy and computational cost.

Transport equations for the two first conditional moments (i.e. conditional averages, conditional variances and covariances) have been implemented in a parabolic code to simulate autoignition of a n-heptane plume in a turbulent heated coflow. Results showed that autoignition occurs at the 'most reactive' mixture fraction and it is delayed by high value of conditional scalar dissipation rate. Also the mixture fraction statistics have an effect and in particular the width of the mixture fraction PDF, hence accounting for the different degrees of mixture homogeneities on autoignition. The effects of conditional fluctuations have been investigated and two methods have been employed: a Taylor expansion and a conditional joint PDF method. Closure using the full set of variances and covariances in the chemical mechanism has been attempted for the former whereas a simplified formulation based only on the conditional temperature PDF, presumed to be a β-function, has been used for the latter. The Taylor expansion method is numerically more efficient; however, the assumption of small but

still not negligible conditional fluctuations, necessary for the expansion, does not allow the method to proceed after autoignition. The conditional joint PDF method could predict autoignition and the hot kernel development resulting in a practical approach to include the conditional fluctuations in the CMC model. The effect of second-order closure has been found to be negligible if the conditional scalar dissipation rate decays rapidly; at these conditions, a first-order closure may suffice. The results are in good agreement with the experimental data.

The effect of turbulence of autoignition has been studied for a n-heptane spray in diesel engine-like conditions. Results show that, consistent with the experiments, turbulence shortens the autoignition delay mainly caused by a faster decay of the conditional scalar dissipation rate. Autoignition occurred at the edge of the spray towards its tip where the 'most reactive' mixture fraction coexisted with low values of the conditional scalar dissipation. The mechanisms of flame propagation have also been investigated.

The thesis concludes with the simulation of a diesel engine cycle using an elliptic three dimensional CMC. Results compare favourably with the experimental pressure traces. The level of insight that the CMC provides makes this model an effective diagnostic tool in the engine design process.

The present work provides a numerical and theoretical framework which can be extended in the future with more sophisticated models treating droplet evaporation, soot prediction and flame wall interaction in a RANS or LES formulation.

Contents

List of Figures

List of Tables

Chapter 1

Introduction

1.1 Motivation of this work

The demand of fossil fuel has closely accompanied the growth of the industrial development in our society. Irresponsible exploitations of this energy source are now posing environmental challenges related with pollutant emission and energy resources availability, raising the issue of a sustainable development.

Road transport has been identified as one of the main sources of environmental impact both in terms of pollutants (HC, NO_x and particulates) and greenhouse gases (GHG). Of particular concern are the CO_2 emissions that are strictly associated to the combustion efficiency and to the energy vector used. The transport sector is, unlike other sectors, almost completely dependent on a single fuel - oil. Considerable efforts are made by legislation to regulate car emission standards associated to adequate fuel specifications to meet the output of Kyoto protocol. However, even if a replacement of the fossil fuel might be foreseen in the long-term, a more efficient combustion process has to be pursued now.

Experimental and numerical research in turbulent combustion aims to provide better insight into the combustion phenomena, investigate new, more efficient, combustion modes and provide predictive tools to assist the design process. An efficient combustion mode is diesel combustion, which forms the focus of this work.

1.2 Diesel engine combustion

In the panorama of modern Internal Combustion (IC) engines, Direct Injection (DI) diesel engines represent the benchmark for the highest energy conversion efficiency. Combustion is controlled by autoignition, which is achieved due to the high temperatures at the end of the compression stroke (alternatively called Compression Ignition (CI) engines). The ability to stably burn under lean stratified conditions (i.e. low CO_2 emissions) has been the key of its success in the market in the last decade. Nevertheless, pollutants such as nitrogen oxides (NO_x) and particulates are the results of diesel engine combustion, the reason being the high temperatures attained during the combustion process combined with the excess of air and the highly stratified mixture in which combustion develops.

A picture of the 'conventional' diesel engine combustion is given in Heywood (1988). Injection occurs close to the Top Dead Center (TDC) at the end of the compression stroke. After a certain delay due to the evaporation, mixing and chemical processes, autoignition occurs. A premixed combustion phase follows, in which the fuel evaporated during the autoignition delay burns in a mainly chemistry-controlled combustion. This phase is responsible for the high heat release peak and consequent noise typical of diesel engines. A mixing-controlled combustion, or in other words a diffusion flame, comes after the premixed phase in which the heat release rate is determined by the mixing between fuel and oxidizer at high temperature.

Recent advancements in injector performance and in engine control allowed the development of new combustion modes. To reduce the pollutant emissions, Exhaust Gas Recirculation (EGR), multiple injection and Homogeneous Charge Compression Ignition (HCCI) became practical strategies. The common ground is an intent to reduce the combustion temperatures and have a more homogeneous reactive mixture. The presence of EGR in the background fluid rises the heat capacity of the mixture, hence, reducing the combustion temperatures and as consequence the NO_x. A multiple injector strategy (up to five injections par cycle) aim to create a reactive environment to reduce the premixed phase of combustion avoiding high peak of heat release rate which cause high temperatures and allow longer combustion enhancing soot post oxidation.

An alternative and most promising strategy to reduce diesel pollutant emission is represented by an HCCI type of combustion. A description is presented in Ryan and Callahan (1996). Opposite to the conventional diesel combustion, injection occurs during the compression stroke and ends before combustion takes place. The fuel attains a certain degree of homogeneity and autoignition appears simultaneously in multiple locations. The heat release rate presents two peaks, one due to the low temperature oxidation (i.e. cool flame) during the compression phase and the main one at the combustion of the full charge. It results in low NO_x and soot emissions due to the low temperatures attained during combustion and the high degree of homogeneity of the charge.

In the classic view of diesel engine combustion, the initial phase of combustion is mainly chemically-controlled due to the reactions at high temperatures while turbulent mixing has an effect during the diffusion flame to bring together the reactants. Traditionally diesel engine modelling followed this 'conventional' picture. Phenomenological models were developed, which linked sequentially autoignition (Halstead et al. (1977)) and diffusion flame (Magnussen (1981)) models for simplistic chemistries. Accurate predictions were achieved for engineering quantities such as pressure traces and heat release rate even though little could be said on pollutant prediction.

Moving toward new modes of combustion, which make uses of turbulence to control autoignition, an explicit treatment of the turbulence chemistry interaction is needed. In particular for HCCI combustion an accurate prediction of the autoignition delay is essential to predict the engine output in terms of engine performance and pollutant formation. Continuous research in turbulent combustion and in particular in autoignition might give better understanding of the phenomena involved and provide more refined tools for a better design or engine diagnostic.

1.3 Turbulent combustion modelling

1.3.1 Direct Numerical Simulation

Various computational tools are now in the hands of researcher to investigate turbulent combustion. The most accurate is Direct Numerical Simulation (DNS), which attempts to solve the Navier-Stokes equations and species conservation equations without any averaging or filtering procedure resolving the richness of spatio-temporal timescales, the high degree of non-linearities and the stochastic nature of turbulence.

Strong limitations preclude such an approach for most flows on interest in practical engineering applications. In part, the need of accurate boundary and initial conditions as well as the discretization method restrict the computational grid. A detailed description of the combustion chemical mechanism is needed. Since all the spatio-temporal scales for turbulence and chemistry need to be resolved, huge demands are placed on the computer memory and speed. In a non reactive case, the CPU time scales as the Reynolds number cubes (Pope (2000)). This places severe limitations on the simulated flowfield configuration and conditions.

Despite simplifying assumptions on the turbulent structure, which in some cases has been treated as two-dimensional, and on the chemical mechanism, often treated as a one-step reaction, to reduce the computational time, meaningful results can be achieved. DNS has become an indispensable tool in fundamental research to study and identify isolated phenomena, which cannot be investigated experimentally with the same degree of accuracy. Furthermore, it became increasingly important in statistical approaches to validate closure hypothesis and modelling assumptions.

DNS have been used extensively to study autoignition in turbulent flows, examples are given in Mastorakos et al. (1997a), Sreedhara and Lakshmisha (2002b), Im et al. (1998). To overcome the limitation of DNS, a number of modelling approaches have been proposed to make turbulent reacting flows more tractable for engineering applications.

1.3.2 Reynolds (Favre) Averaged Navier-Stokes equations modelling

The application of Reynolds Averaged Navier-Stokes (RANS) equations in turbulent reactive flows corresponds in solving transport equation for ensemble average quantities, in which the averages are defined as the statistical mean over time. For variable density flows, as is the case of combustion, the averaging procedure is replaced by a density weighted averaging. This procedure allows the solution of transport equations for continuity, momentum, species and energy in terms of mean values without resolving the fluctuations.

Additional terms appear in the equation due to the averaging procedure, depending on the covariance of the different velocity components (Reynolds stress, $\widetilde{\mathbf{v}''\mathbf{v}''}$ with double prime being the fluctuation above the density weighted mean) or in the covariance of velocity with respectively species and enthalpy (turbulent fluxes, $\widetilde{\mathbf{v}''Y''}$ and $\widetilde{\mathbf{v}''h''}$). Closures are needed for these extra terms. Standard practice is adopted in chapter 5 and 6 where additional transport equations for turbulent kinetic energy and its dissipation are solved ($k-\varepsilon$ model) and the Reynolds stress is closed using a turbulent viscosity as a function of k and ε. The turbulent flux is closed using a gradient diffusion hypothesis where a turbulent diffusion coefficient is defined in analogy to the laws of mass and energy diffusive transport of Fick and Fourier, respectively. As discussed in Pope (2000) these assumptions are not necessarily justified in strongly sheared flows. In this case, as reported in chapter 4, transport equations for the six component of the Reynolds stress tensor and for the dissipation are solved. Additional transport equation for the scalar flux can also be solved (Kim and Mastorakos (2006)).

The mean reaction rate in the species transport equation also requires modelling. In case of high fluctuations above the mean, a the moment method that uses the mean value of the scalars to calculate the mean reaction rate becomes inaccurate (Veynante and Vervisch (2002)). Various closure strategy have been proposed and will be better discussed in section 1.3.4.

RANS modelling does not need to resolve all spatial and temporal scales of the flow as opposite to DNS, allowing, in general, faster calculations and low

CPU requirements. Low-order discretization schemes yield, in turn, to more sophisticated meshes that well reproduce the most complicated geometries. The accuracy of the method clearly depends on the validity of the modelling assumptions. This high flexibility granted the spreading of RANS modelling in academic and industrial environment and will be adopted throughout the present thesis.

1.3.3 Large Eddy Simulations

Large Eddy Simulations (LES) attempt to solve directly for the larger scales of a turbulent flow while filtering the smaller ones. The filter dimension is within the inertial subrange of the turbulent spectrum (Lesieur and Metais (1996)), therefore modelling for the sub-filter processes is needed. In turbulent combustion these includes the filtered reaction rate and micromixing. Even if the LES shares this same shortcoming with RANS, as discussed by Pope (2000), in particular for flows involving strong unsteadiness of the large scales, e.g. vortex breakdown in gas turbine combustor, or unsteady separation and vortex shedding behind bluff bodies, LES can be expected to be more reliable and accurate than RANS.

LES generally employs higher resolution meshes and more accurate discretization schemes than RANS. Sophisticated initial conditions are in general required as well as long simulation times to achieve enough statistically independent samples for a proper comparison with experimental measurements. Given the unsteady nature of autoignition and its strong dependence on large scale motions (i.e. intermittency) and initial conditions (i.e. temperature fluctuations at the inlet) LES represent a very interesting tool to study autoignition as also demonstrated in Jones et al. (2007).

Model of complex geometries, with unstructured mesh, for real industrial applications has been recently achieved with LES as has been presented in Boudier et al. (2007) in case of a gas turbine combustor. Its application in IC engine modelling is also promising given the possibility to resolve the cycle-to-cycle variability not achievable with RANS (Richard et al. (2007)). The application of LES for industrial application is far yet to be mature. Difficulties still arise in the treatment of the near-wall regions, in which the high level of refinement required makes the simulations computationally very costly for IC engine calculations as

for confined flows in general. The variable boundaries, furthermore, represented by the valve and piston motions, increase the complexity of the problem. At present, engine modelling requires the sequential use of several computational meshes which get distorted and the solution interpolated on the new one over time. Despite the challenges involved, LES is expected in the near future to have a much broader use in industrial applications as a diagnostic tool although its employment in production calculation is still limited by the long computational time required.

1.3.4 Reaction rate closure

In turbulent reacting flows the chemical rate of reaction spans, in general, a broad range of timescales that, in some cases are of the same order than the flow physical timescales (Peters (2000)). When the timescales are comparable, it is expected that chemistry can not be treated as separate from turbulence. Turbulence is associated with scalar fluctuations. Closure of the mean/filtered reaction rate based on mean/filtered species mass fractions, i.e. neglecting turbulence effects, can therefore yield erroneous results given the strong non-linearities of the chemical source term Borghi (1988). Closure for the reaction and micro-mixing effect has became one of the most challenging problems in modelling turbulent reacting flows.

Different regimes of combustion have commonly been classified according to the state of mixedness and on the relative time-scales of chemistry and fluid mechanics (Bilger (1980), Borghi (1988)). It is worthwhile to recall that in diesel engine combustion different degrees of charge homogeneities are achieved (Conventional DI diesel engine, HCCI) and using EGR or early injection strategies the reaction are slow due to the low temperature and the chemical and fluid mechanical timescale at autoignition are expected to be strongly coupled. For practical applications, the need for a universal model able to span the different regimes of combustion is emphasized.

Flamelet models derived in Peters (1984), Peters (1986) and reviewed in Peters (2000), have been applied to both premixed and non-premixed combustion although in present work it will be referred only to the latter. Flamelet theory

is applicable to combustion regimes characterized by high Damköhler numbers defined as the ratio between turbulent and reaction timescales. In this conditions the thickness of the flame is small compared to the dimension of the eddies in the flow and the flame can be treated as a locally one-dimensional laminar flame sheet embedded in the turbulent flow. It is a conserved scalar approach, in which the state of mixing of the fluid particle is explicitly considered by the PDF of a scalar (i.e. marker) which is conserved during the reaction process. Transport inside the reaction zone is governed by molecular mixing, parameterized by the scalar dissipation rate. Despite the limited validity of the model due to the hypothesis made on the topology of the reaction zone, flamelets have been successfully applied in spray autoignition (Yu et al. (2001)) and in diesel engine combustion over a wide range of operating conditions (Pitsch et al. (1996)). It is worthwhile to mention the work done in the Eulerian Particle Flamelet approach (EPFM) in which multiple transient flamelets are employed solving an additional transport equation to obtain the probability of finding the corresponding flamelet in each CFD cell (Hergart and Peters (2001)). A two-mixture fraction formulation has also been derived to model split injections problem that could not be treated otherwise given the lack of interaction between the different flamelets (Hasse and Peters (2005)). Additional work in the context of the flamelet have been recently done by Lehtiniemi et al. (2006) to add the effect of transport in physical space, absent in a classical flamelet view, using a progress variable concept. It is worth to mention the work of Blanquart and Pitsch (2005) and Pitsch et al. (2003) who attempted to model scalar dissipation rate fluctuations through the use of a stochastic approach respectively for autoignition and flame with localized extinction/reignition.

The Conditional Moment Closure (CMC) independently derived by Bilger (1993) and Klimenko (1990) and later reviewed in (Klimenko and Bilger (1999)) is a conserved scalar based approach in analogy with the Flamelet method above presented. However, no assumption on the topology of the reaction zone was made in its derivation which generalizes its use to a broader range of turbulent reacting flow problems. A detailed description of the differences between the two models can be found in Klimenko (2001). It is important to underline that CMC allows an explicit treatment of the spatial transport using an elliptic formulation

which, in turn, allows the modelling of localized phenomena such as spatial variation of the scalar dissipation rate important in autoignition simulations (Wright et al. (2005)), edge-flame stabilization (Kim and Mastorakos (2005)) and propagation (Richardson and Mastorakos (2007)) and not less important in engine modelling, droplet evaporation and wall effects. The use of a higher-order closure allow to include the effect of conditional fluctuations, which are significant in flame with localized extinction/reignition and in autoignition problems. Developed for non-premixed combustion CMC can be used for premixed and partially premixed systems given a suitable definition of progress variable (Swaminathan et al. (1997), Bilger (2004)) or double conditioning (Kronenburg (2004)). CMC solves transport equations for conditional average mass fractions of scalars, the solution domain consists, therefore, of five independent variables respectively time, spatial coordinates and conserved scalar space. The increase in computational time with respect to the flamelet approach is evident. Its application to engine simulations is critical upon accurate and efficient solvers as discussed later in this thesis.

The transported Probability Density Function (PDF) model, developed by Pope (1985) and later reviewed by Pope (2000), shortly called PDF method, allows a general description for most types of turbulent reacting flows. Solving transport equation for the joint PDF of composition and velocity the chemical source term appears in a closed form which is the main advantage of this method. However, the micro-mixing term remains unclosed. Even though the PDF method have attained a certain degree of maturity, research is still active in this direction. To solve numerically the joint PDF transport equations, numerical integrations based on stochastic methods have been employed. Reference for a lagrangian Monte Carlo approach is reported in Pope (1985) whereas the Eulerian Stochastic Field method is described in Valiño (1998) and Mustata et al. (2006). The use of a stochastic methodologies imply a high number of realizations to achieve a statistical convergent solution which makes this method one the most computationally expensive. The use of a deterministic solution for the flow field, combined with a stochastic solution for the concentration joint PDF or for the joint velocity and concentration PDF (Pope (1985)), allows to reduce the number of statistical realizations needed, furthermore recent advancement in chemistry

tabulation (i.e. In Situ Adaptive Tabulation (ISAT)) have finally allowed the use of this method for a variety of turbulent reacting flows. Examples of transported PDF method employed to model autoignition can be found in Lakshmisha et al. (1992) and more recently in Blouch et al. (2003), Gkagkas and Lindstedt (2007), Jones et al. (2007).

1.4 Objective of this study

The present work aims to study turbulent autoignition in inhomogeneous flows and to provide an accurate and numerical efficient tool capable to predict turbulent non-premixed combustion, with special emphasis on diesel engine simulations.

Asymptotic analysis (Liñan and Crespo (1976)) and DNS studies (Mastorakos et al. (1997a), Sreedhara and Lakshmisha (2002b), Im et al. (1998), Echekki and Chen (2003) as examples among the works proposed) have attempted to describe the topology of the autoignition spot. It has been recognized that turbulent inhomogeneous autoignition occurs at a well defined mixture fraction called the 'most reactive' for low valued of conditional scalar dissipation rate. The fluctuations of the conditional scalar dissipation rate also have an effect on the evolution of autoignition following the work done by Mastorakos and Bilger (1998) and Blanquart and Pitsch (2005).

The Conditional Moment Closure method resolves explicitly mixture fraction space giving an accurate modelling of the micro-mixing. Using a higher conditional moment formulation allows to include the effects of the conditional scalar dissipation rate statistics. CMC represents, therefore, a very promising approach to study autoignition and will be used throughout the present thesis. Detailed literature review on turbulent in-homogeneous autoignition in jet and spray as well as on the various modelling approaches is reported in the appropriate chapters.

The CMC transport equation are derived in chapter 2 following Klimenko and Bilger (1999) at first and second-order closure. Special care has been taken in the derivation of the conditional temperature transport equations, including the effects of variable specific heat capacities, and new additional terms have been

derived for both first and second-order. Chapter 3 describes the numerical methods employed to efficiently implement the CMC combustion code coupled with a CFD solver for transient calculation. Chapter 4, by means of a well thought experiment intends to investigate the capability of the CMC to model turbulent in-homogeneous autoignition in gaseous fuels. The effects of the statistics of mixture fraction and the use of a second order closure are carefully investigated. Chapter 5 presents the application of CMC for a transient spray-driven combustion in a diesel-engine like environment, in which the physics highlighted in chapter 4 can be reviewed in terms of a spray simulation. Chapter 6 closes this work with an example of diesel engine combustion, which demonstrates the practical usefulness of the methods and solvers developed in this work.

All the simulation performed used an unsteady-RANS approach. The transport equations derived for the conditionally filtered species mass fractions in the framework of CMC with LES (Navarro-Martinez et al. (2005)) are analogous to the one derived in a RANS approach. The code developed here can, therefore, be considered more general and applicable to a broader range of turbulence treatment, given an accurate validation of the sub-models used. The use of the present solver in a LES framework is not yet mature and is matter of future research work, however we feel that most of the background numerical work has been completed.

Chapter 2

Conditional Moment Closure

2.1 Chapter objective

The scope of this chapter is to present the Conditional Moment Closure (CMC) equations and closures as will be later implemented in chapter 3. Using the decomposition methodology as in Bilger (1993), new transport equations have been derived for the conditional temperature, its variance and species covariances in case of variable specific heat capacities. The novelty being that starting from the instantaneous temperature equation rather than enthalpy, additional terms appear that are not negligible and might be important in autoignition calculations. Second conditional moments modelling is still a young field of research in particular for autoignition applications. It is in the aim of this chapter to underline the strengths and deficiencies of the available sub-models particulary for the conditional reaction rate closure.

The application of the CMC closure to practical problems as for diesel engine combustion, requires to address additional considerations to the wall-boundary treatment, to the CMC formulation in the presence of a sliding grid and in case of a dispersed evaporating phase. Each of these are interesting fields of research that cannot be extensively examined in the present thesis because of lack of time. Nevertheless, some efforts have been made to provide a viable treatment and ideas for future developments. A model for the heat transfer to the wall and a formulation to account for the effects of a moving grid have been proposed.

2.2 PDFs and conditional statistics

Turbulent flows are generally defined as random processes. Velocity components and scalars concentrations are fluctuating quantities often described in terms of their probabilities. Reference to the stochastic nature of turbulence and its statistical treatment can be found in Pope (1985, 2000), Hinze (1987) and Davidson (2004). Here only few basic concepts will be underlined to be able to better understand the physical meaning of turbulent reactive flow modelling and of CMC.

In turbulent flows, a random variable $f \equiv f(\mathbf{x}, t)$ (we assume functional dependence on position and time) can assume any value within its sample space Z. By definition the sample space is the space of all possible realizations of the stochastic variable, for generality is assumed $Z \in [a, b]$. The two bounds a and b are respectively Z_{min}, Z_{max} which take the values of $-\infty, \infty$ in case of an unbounded scalar. The probability p of f assuming a value within an infinitesimal range dZ can be given in terms of its probability density function (PDF) $P(Z)$ as

$$p\ (Z \leq f(\mathbf{x}, t) \leq Z + dZ) = P(Z; \mathbf{x}, t)\ dZ \tag{2.1}$$

where the semicolon indicates that P is a probability density in Z-space and function of $\mathbf{x}$, t as it is f. In the following, to simplify the notation, the dependence of P on $\mathbf{x}$ and t is dropped. It can also be written that the probability of finding f in the whole of its sample space is by definition certain so that, as normalization condition, we can write

$$\int_b^a P(Z)dZ = 1 \tag{2.2}$$

Knowing the $P(Z)$ the n^{th} moment of f is defined as

$$\langle f^n \rangle = \int_b^a Z^n P(Z)dZ \tag{2.3}$$

where the first moment $\langle f \rangle$ is the mean. Analogously the n^{th} central moment is written as

$$\langle f'^n \rangle = \langle (f - \langle f \rangle)^n \rangle = \int_b^a (Z - \langle f \rangle)^n P(Z)dZ \tag{2.4}$$

where the second central moment $\langle f'^2 \rangle$ is the variance.

It is useful to underline that the moments of a stochastic scalar can be explicitly calculated using its PDF. On the other hand this last is often computationally too expensive to be calculated even using a stochastic particle method. Presumed functions, parameterized on the mean and the variance of the stochastic scalar, are often used (i.e. gaussian-type or β-function PDF) for a single-scalar PDF, see section 2.4.5.

Equation 2.3 can be applied to any function $F(f)$ so that its mean value can be calculated as

$$\langle F(f) \rangle = \int_b^a F(Z) P(Z) dZ \tag{2.5}$$

In case of a function dependent on n stochastic variables $\mathbf{f}$, the previous definitions can be extended using the concept of joint-PDF $P(\mathbf{Z})$ integrated over a n-dimensional sample space $\mathbf{Z}$ so that equation (2.3) can be rewritten as

$$\langle F(\mathbf{f}) \rangle = \int_b^a ... \int_{b'}^{a'} F(\mathbf{Z}) P(\mathbf{Z}) d\mathbf{Z} \tag{2.6}$$

As it can be seen from equation (2.6), it is not generally true that the mean of a function is its value evaluated at the mean of its independent variables $\langle F(\mathbf{f}) \rangle \neq F(\langle \mathbf{f} \rangle)$. It becomes equivalent only in the particular case that the $P(\mathbf{Z})$ approaches the δ-function in $\mathbf{Z}$-space or if F is linear function of $\mathbf{f}$. This is an important principle that will be used in section 2.4.4 in the evaluation of the chemical source term.

If we consider two stochastic variables $\mathbf{f} \equiv (f_1, f_2)$, using the Bayes theorem, the joint-PDF $P(Z_1, Z_2)$ can be decomposed as

$$P(Z_1, Z_2) = P(Z_1 | f_2 = Z_2) P(Z_2) \tag{2.7}$$

where the value of Z_1 is conditional on f_2 respecting the condition on the right side of the vertical bar. $P(Z_1 | f_2 = Z_2)$ is called shortly conditional PDF of Z_1 with respect to Z_2. Using equation 2.7 we can define the conditional mean of the scalar f_1 on the condition that $f_2 = Z_2$ as

$$\langle Z_1 | f_2 = Z_2 \rangle = \int_b^a Z_1 P(Z_1 | f_1 = Z_2) dZ_1 = \frac{\int_b^a Z_1 P(Z_1, Z_2) dZ_1}{P(Z_2)} \tag{2.8}$$

and calculate the mean value $\langle Z_1 \rangle$ in terms of the conditional mean using equation 2.8

$$\langle Z_1 \rangle = \int_b^a \langle f_1 | f_2 = Z_2 \rangle P(Z_2) dZ_2 \tag{2.9}$$

2.3 Conservation equations

Turbulent reactive flows modelling is based on the solution of the Navier-Stokes equations in conjunction with transport equation for energy and chemical species. For a single-phase Newtonian fluid with non constant density the conservation equations can be written as follows:

Continuity

$$\frac{\partial \rho}{\partial t} + \nabla \cdot (\rho \mathbf{v}) = 0 \tag{2.10}$$

Momentum

$$\frac{\partial \rho \mathbf{v}}{\partial t} + \nabla \cdot (\rho \mathbf{v}\mathbf{v}) = -\nabla p + \nabla \cdot \underline{\underline{\tau}} + \rho \mathbf{g} \tag{2.11}$$

where the first and last term on the right-hand side are body forces term due to the pressure gradient and buoyancy effects. The second term on the right-hand side is the molecular transport due to the viscosity. Here $\underline{\underline{\tau}}$ is the viscous stress tensor that for newtonian fluid can be rewritten as

$$\underline{\underline{\tau}} = \mu \left(2\mathbf{S} - \frac{2}{3}\delta \nabla \cdot \mathbf{v} \right) \text{ and } \quad \mathbf{S} = \frac{1}{2} \left(\nabla \mathbf{v} + \nabla \mathbf{v}^T \right) \tag{2.12}$$

with $\nabla \mathbf{v}^T$ is the transpose of the velocity gradient and μ the dynamic viscosity.

Species

$$\rho \frac{\partial Y_i}{\partial t} + \rho \mathbf{v} \cdot \nabla Y_i - \nabla \cdot (\rho D_i \nabla Y_i) = \rho W_i \tag{2.13}$$

where Y_i is the species i mass fraction, W_i its reaction rate and D_i its mass diffusivity. The diffusivity is related to the viscosity through the Schmidt number $Sc_i = \mu / \rho D_i$. In the equation 2.13, Fick's law of diffusion is assumed for the diffusive fluxes and the Soret effect is neglected.

Energy

In a reactive mixture, the enthalpy h is the mass-weighted sum of the species specific enthalpies h_i of species i

$$h = \sum_{i=1}^{n} Y_i h_i \tag{2.14}$$

where h_i can be decomposed in enthalpy of formation $h_{i,ref}$ and sensible enthalpy h_s so that $h_i(T) = h_{i,ref} + h_{i,s}(T)$. By definition of sensible enthalpy we can rewrite

$$h_i = h_{i,ref} + \int_{T_{ref}}^{T} c_{p,i}(T)dT \tag{2.15}$$

Here $c_{p,i}$ is the specific heat capacity of species i at constant pressure and T is temperature in Kelvin. The enthalpy balance equation can be derived from the first law of thermodynamics (Williams (1985)) as

$$\begin{aligned} \rho\frac{\partial h}{\partial t} + \rho\mathbf{v}\cdot\nabla h &= \frac{\partial p}{\partial t} + \nabla\cdot\left(\frac{\lambda}{c_p}\nabla h\right) + \rho W_R + \\ &- \sum_{i=1}^{n} h_i \nabla\cdot\left[\left(\frac{\lambda}{c_p} - \rho D_i\right)\nabla Y_i\right] \end{aligned} \tag{2.16}$$

Here λ is the thermal conductivity, W_R the source term due to radiation and c_p the specific heat capacity at constant pressure of the mixture calculated as $c_p = \sum_{i=1}^{n} Y_i c_{p,i}$. In equation 2.16 the assumption of low speed flow and low Mach number allowed the simplification of terms involving the viscous stress tensor and the pressure gradient.

Another form of the energy equation can be written in terms of temperature as

$$\begin{aligned} \rho c_p\frac{\partial T}{\partial t} + \rho c_p\mathbf{v}\cdot\nabla T &= \frac{\partial p}{\partial t} + \nabla\cdot(\lambda\nabla T) - \rho W_R \\ &- \sum_{i=1}^{n} c_{p,i}\,\rho D_i \nabla Y_i\cdot\nabla T - \rho\sum_{i=1}^{n} h_i W_i \end{aligned} \tag{2.17}$$

In the derivation of equation 2.17 it has been implicitly assumed constant species heat capacities ($c_{p,i}$) within the time or space interval of derivation so that c_p could be carried outside the derivative. For simplicity it can also be assumed that all mass diffusivities D_i are proportional to the thermal diffusivity.

$$D = \frac{\lambda}{\rho c_p} \tag{2.18}$$

such that the Lewis numbers are constant

$$Le_i = \frac{\lambda}{\rho c_p D_i} = \frac{D}{D_i} \tag{2.19}$$

Under the assumption of unity Lewis number, the last term on the right-hand side of equation 2.16 disappears. And the enthalpy equation can be written in the same form then the reactive species equations. We notice that even with this last simplification the temperature equation maintains an additional term dependent on the scalar product between species and temperature gradient. Further analysis on the energy equation in the context of the CMC can be found in section 2.4.3 and 2.5.2.

Mixture Fraction

$$\rho \frac{\partial \xi}{\partial t} + \rho \mathbf{v} \cdot \nabla \xi - \nabla \cdot (\rho D_\xi \nabla \xi) = 0 \tag{2.20}$$

In turbulent non-premixed combustion in presence of a two stream-mixing problem, mixture fraction fully describes the state of mixing of the fluid (if equal diffusivity of the species is assumed). It is defined as a conserved scalar that can be defined as the normalized mass fraction of an inert tracer introduced with the fuel. For a single-phase fluid its transport equation is analogous to equation 2.13 without the source term. In a RANS approach, mixture fraction statistics can be inferred solving transport equation for the Favre average mean and its variance.

2.4 First-order closure

The CMC originates conceptually in the hypothesis that most of the fluctuation in the scalar quantities of interest can often be associated with the fluctuation of (usually) only one key quantity (Klimenko and Bilger (1999)). In turbulent non-premixed combustion the reactive scalars can be related (conditioned) to mixture fraction so that the fluctuation above its conditional average value is smaller than above its unconditional one, as shown in Masri et al. (1992). Using a conserved scalar approach, CMC attempts to rigorously close the problem of the turbulence-chemistry interaction crucial in turbulent reacting flow modelling. Under the assumption of negligible conditional fluctuations, the conditional reaction rate

can be evaluated based on the conditional mean species concentration. This requires the solution of the first conditional moments (conditional means) of the conditional species mass fractions, which will be shortly called 'first-order closure'. This closure may not be accurate in case of localized extinction/reignition or at autoignition, in which the effects of conditional fluctuations might have a significant effect. In these cases the solution of the second conditional moments (conditional variances and covariances) is important, shortly called 'second-order on higher-order closure'. A more detailed analysis of the conditional reaction rate closure can be found in section 2.4.4.

CMC was independently derived by Klimenko (1990) and Bilger (1993) following two different methodologies, respectively the joint PDF and the decomposition method. Throughout this thesis Bilger's decomposition method is used. In the following the CMC equations derivation are reviewed for completeness and to better appreciate the validity of the model.

2.4.1 Conditional mean species equations

The conditional mean or first conditional moment of scalar Y can be defined as $Q(\eta, \mathbf{x}, t) \equiv \langle Y(\mathbf{x}, t)|\eta\rangle$ where η is the sample space for the conserved scalar ξ (mixture fraction) and the operator $\langle\cdot|\xi(\mathbf{x}, t) = \eta\rangle$, shortly $\langle\cdot|\eta\rangle$, denotes ensemble averaging subject to the fulfilment of the condition on the right of the vertical bar.

The mean value $\langle Y(\mathbf{x}, t)\rangle$ of a reactive scalar can then be calculated from its conditional mean using the conserved scalar PDF $P(\eta, \mathbf{x}, t)$ as

$$\langle Y(\mathbf{x}, t)\rangle = \int_0^1 \langle Y(\mathbf{x}, t)|\eta\rangle P(\eta; \mathbf{x}, t) d\eta \tag{2.21}$$

The instantaneous value of Y can be decomposed as

$$Y(\mathbf{x}, t) = Q(\xi(\mathbf{x}, t), \mathbf{x}, t) + Y''(\mathbf{x}, t) \tag{2.22}$$

where Y'' is the conditional fluctuation above the conditional mean. Applying the time derivative and the gradient operator to equation 2.22 we obtain

$$\frac{\partial Y}{\partial t} = \frac{\partial Q}{\partial t} + \frac{\partial Q}{\partial \eta}\frac{\partial \xi}{\partial t} + \frac{\partial Y''}{\partial t} \tag{2.23}$$

$$\nabla Y = \nabla Q + \frac{\partial Q}{\partial \eta}\nabla\xi + \nabla Y'' \tag{2.24}$$

From equation 2.24 the molecular diffusion term in the transport equation for Y (equation 2.13) can be rewritten as

$$\begin{aligned}\nabla\cdot(\rho D\nabla Y) &= \nabla\cdot(\rho D\nabla Q) + \frac{\partial Q}{\partial\eta}\nabla\cdot(\rho D\nabla\xi)\\ &\quad +\rho D(\nabla\xi)^2\frac{\partial^2 Q}{\partial\eta^2} + \rho D\nabla\xi\cdot\nabla\frac{\partial Q}{\partial\eta}\\ &\quad +\nabla\cdot(\rho D\nabla Y'')\end{aligned} \tag{2.25}$$

Introducing equation 2.23, 2.24 and 2.25 into equation 2.13 and rearranging

$$\begin{aligned}\rho W &= \rho\frac{\partial Q}{\partial t} + \rho\mathbf{v}\cdot\nabla Q - \rho D(\nabla\xi)^2\frac{\partial^2 Q}{\partial\eta^2}\\ &\quad -\nabla\cdot(\rho D\nabla Q) - \rho D\nabla\xi\cdot\nabla\frac{\partial Q}{\partial\eta}\\ &\quad +\rho\frac{\partial Y''}{\partial t} + \rho\mathbf{v}\cdot\nabla Y'' - \nabla\cdot(\rho D\nabla Y'')\\ &\quad +\left(\rho\frac{\partial\xi}{\partial t} + \rho\mathbf{v}\cdot\nabla\xi - \nabla\cdot(\rho D_\xi\nabla\xi)\right)\frac{\partial Q}{\partial\eta}\\ &\quad +\nabla\cdot(\rho(D_\xi - D)\nabla\xi)\frac{\partial Q}{\partial\eta}\end{aligned} \tag{2.26}$$

From equation 2.20 the last term in equation (2.26) vanishes. Taking the conditional expectation of equation 2.26, conditional on $\xi(\mathbf{x},t) = \eta$, defining as $N \equiv D_\xi(\nabla\xi)^2$ one-half of the instantaneous mixture fraction dissipation rate, yields

$$\rho_\eta\frac{\partial Q}{\partial t} + \rho_\eta\langle\mathbf{v}|\eta\rangle\nabla Q - \rho_\eta\frac{D}{D_\xi}\langle N|\eta\rangle\frac{\partial^2 Q}{\partial\eta^2} = \rho_\eta\langle W|\eta\rangle + e_Q + e_Y \tag{2.27}$$

with

$$\begin{aligned}e_Q \equiv &\left\langle \nabla\cdot(\rho D\nabla Q) + \rho D\nabla\xi\cdot\nabla\frac{\partial Q}{\partial\eta}\,\middle|\,\xi(\mathbf{x},t)=\eta\right\rangle\\ &+\left(\frac{D}{D_\xi}-1\right)\langle\nabla\cdot(\rho D_\xi\nabla\xi)|\eta\rangle\frac{\partial Q}{\partial\eta}\end{aligned} \tag{2.28}$$

$$e_Y \equiv -\left\langle \rho\frac{\partial Y''}{\partial t} + \rho\mathbf{v}\cdot\nabla Y'' - \nabla\cdot(\rho D\nabla Y'')\,\middle|\,\xi(\mathbf{x},t)=\eta\right\rangle \tag{2.29}$$

where $\rho_\eta \equiv \langle \rho | \eta \rangle$ is the conditional density. In the above the ratio of diffusivities that appears in the last term of equation 2.28 was assumed constant even though the single diffusivity might vary (Klimenko and Bilger (1999)). In fact this last term can be rewritten as

$$e_{Q,3} \equiv \rho_\eta \left(\frac{D}{D_\xi} - 1 \right) \langle M | \eta \rangle \frac{\partial Q}{\partial \eta} \tag{2.30}$$

Where M_η is the conditional diffusion defined as

$$\langle M | \eta \rangle \equiv \frac{1}{\rho_\eta} \langle \nabla \cdot (\rho D_\xi \nabla \xi) | \eta \rangle \tag{2.31}$$

It is the only term with the explicit difference of diffusivities between the reactive species and mixture fraction and is considered responsible for differential diffusion effects (Klimenko and Bilger (1999)).

Note that equation 2.27 represents the unclosed transport equation for Q. No assumptions on the small scale structure of the reaction zone or on the relative timescale between chemistry and turbulence have been made. Its mathematical derivation holds for any non-premixed system. The conditional density fluctuations ρ'' has been neglected. In case of system near extinction equation 2.27 we can relax this hypothesis introducing the concept of conditional Favre averaging (Klimenko and Bilger (1999)) with the new definition of the conditional averaging operator being defined as $\langle \cdot | \eta \rangle \equiv \langle \cdot \rho | \xi = \eta \rangle / \rho_\eta$ and hence, the conditional mean $Q \equiv \langle Y \rho | \xi = \eta \rangle / \rho_\eta$.

2.4.2 Primary closure hypothesis

The closure of equation 2.27 requires modelling assumptions for the two last terms named e_Q and e_Y.

Following the scaling arguments presented in Klimenko and Bilger (1999), for high Reynolds number flows, the effects of macro-transport by molecular diffusion becomes negligible with respect to the turbulent transport and the first two terms in equation 2.28 can be neglected. This does not mean that the molecular diffusion effects are neglected, since the term depending on the scalar dissipation rate is still determined by the small scale diffusion processes. The third term named $e_{Q,3}$ even at high Reynolds number remains finite as the conditional diffusion ($\langle M | \eta \rangle$)

is related to the conditional dissipation by equation 2.32 (Klimenko and Bilger (1999))

$$\langle M|\eta\rangle = \frac{1}{\rho_\eta P(\eta)} \frac{\partial \langle N|\eta\rangle P(\eta)\rho_\eta}{\partial \eta} \tag{2.32}$$

To estimate the e_Y term we recall that, from the decomposition equation 2.22, $\langle Y''|\eta\rangle = 0$ and therefore, $\langle Y''\rangle = 0$. This does not imply that $\langle \nabla Y''|\eta\rangle = 0$ or $\langle \partial Y''/\partial t|\eta\rangle = 0$. Nevertheless, we can still say that $\langle \nabla Y''\rangle = \nabla\langle Y''\rangle = 0$ and $\langle \partial Y''/\partial t|\eta\rangle = \partial\langle Y''\rangle/\partial t = 0$ or written is a different form

$$\int_0^1 \langle \nabla Y''|\eta\rangle P(\eta) d\eta = 0 \tag{2.33}$$

$$\int_0^1 \langle \partial Y''/\partial t|\eta\rangle P(\eta) d\eta = 0 \tag{2.34}$$

If we convolute the e_Y term with $P(\eta)$ to find its unconditional contribution, we obtain

$$\begin{aligned} -\int_0^1 e_Y P(\eta) d\eta &= \left\langle \frac{\partial \rho Y''}{\partial t} + \nabla\cdot(\rho \mathbf{v} Y'') - \nabla\cdot(\rho D \nabla Y'') \right\rangle \\ &= \frac{\partial \langle \rho Y''\rangle}{\partial t} + \nabla\cdot(\langle \rho \mathbf{v} Y''\rangle) - \nabla\cdot(\langle \rho D \nabla Y''\rangle) \\ &= \nabla\cdot(\langle \rho \mathbf{v}'' Y''\rangle) = \nabla\cdot\left(\int_0^1 \rho_\eta \langle \mathbf{v}'' Y''|\eta\rangle P(\eta) d\eta\right) \\ &= \int_0^1 \nabla\cdot(\rho_\eta \langle \mathbf{v}'' Y''|\eta\rangle P(\eta) d\eta) \end{aligned} \tag{2.35}$$

In the derivation of equation 2.35, the continuity equation 2.10 multiplied by Y'' has been conditional averaged and added to equation 2.29. The conditional fluctuations of density and molecular diffusivity have been neglected. The diffusion term has been transformed as $\langle \rho D \nabla Y''\rangle = \nabla\langle \rho D Y''\rangle - \langle Y''(\nabla \rho D)\rangle = 0$. The velocity has been decomposed into conditional mean and fluctuation as $\mathbf{v} = \langle \mathbf{v}|\eta\rangle + \mathbf{v}''$ and substituted. By the equivalence of the integrals it has been assumed that also the integrand functions are equal. This is not generally true, but it is assumed that the error committed would vanish in the evaluation of the mean value. From equation 2.35 we can write

$$e_Y P(\eta) = -\nabla\cdot(\rho_\eta \langle \mathbf{v}'' Y''|\eta\rangle P(\eta)) \tag{2.36}$$

The resulting transport equation for Q can finally be rewritten for the case of of equal species diffusivity $D = D_i = D_\xi$ as

$$\frac{\partial Q}{\partial t} + \langle \mathbf{v}|\eta\rangle \cdot \nabla Q + \frac{\nabla \cdot (\rho_\eta P(\eta)\langle \mathbf{v}'' Y''|\eta\rangle)}{\rho_\eta P(\eta)} - \langle N|\eta\rangle \frac{\partial^2 Q}{\partial \eta^2} = \langle W|\eta\rangle \tag{2.37}$$

The first term on the left-hand side is the unsteady or accumulative term, the second and third term represent respectively the transport by convection, through the conditional velocity, and by conditional fluctuations. The last term on the left-hand side represents the diffusion in conserved scalar space and is proportional to the conditional scalar dissipation rate. The term on the right-hand side is the conditional chemical source term.

For completeness we report the conditional average Q transport equation as obtained using the joint PDF method (Klimenko and Bilger (1999) for the equal species diffusivities.

$$\begin{aligned} \frac{\partial \rho_\eta Q P(\eta)}{\partial t} &+ \nabla \cdot (\rho_\eta P(\eta)\langle \mathbf{v} Y|\eta\rangle) \\ &= \rho_\eta \langle W|\eta\rangle P(\eta) - \frac{\partial^2 \rho_\eta \langle N|\eta\rangle P(\eta)}{\partial \eta^2} Q + \rho_\eta \langle N|\eta\rangle P(\eta) \frac{\partial^2 Q}{\partial \eta^2} \end{aligned} \tag{2.38}$$

that joined with the transport equation for the PDF of mixture fraction

$$\frac{\partial \rho_\eta P(\eta)}{\partial t} + \nabla \cdot (\rho_\eta P(\eta)\langle \mathbf{v}|\eta\rangle) = -\frac{\partial^2 \rho_\eta \langle N|\eta\rangle P(\eta)}{\partial \eta^2} \tag{2.39}$$

can be written as equation 2.37. The boundary conditions for equation 2.37 are discussed in section 2.4.6.

An analysis of the primary closure hypothesis has been considered in Kim (2002). It was argued that the equivalence of the integrand functions given the equality of the integrals is a too strict hypothesis. An additional term can be added whose contribution in the unconditional mean is zero so that

$$e_Y P(\eta) = -\nabla \cdot (\rho_\eta \langle \mathbf{v}'' Y''|\eta\rangle P(\eta)) + F_{Y''} \tag{2.40}$$

given that

$$\int \rho_\eta F_{Y''} P(\eta) d\eta = 0 \tag{2.41}$$

The term $F_{Y''}$ can be derived using the joint PDF method having the form

$$F_{Y''} = \frac{1}{\rho_\eta P(\eta)} \frac{\partial J_{Y''}}{\partial \eta} \tag{2.42}$$

with

$$J_{Y''} \equiv -\frac{\partial \rho_\eta \langle N'' Y'' | \eta \rangle P(\eta)}{\partial \eta} + 2\rho_\eta \langle D \nabla Y'' \cdot \nabla \xi | \eta \rangle P(\eta) \tag{2.43}$$

Closure using equation 2.36 neglects the effects of the conditional fluctuations in mixture fraction space. The assumption of a negligible $J_{Y''}$ term, is analogous to implicitly assume for the first term of equation 2.43 no correlation between mixture fraction dissipation and the scalar, while for the second term a perfect alignment between the scalar and the mixture fraction gradients which is not generally true in non-premixed turbulent flames. DNS by Mell (1995) investigated the magnitude of the two terms in equation 2.43. It was found that even though the magnitude can be significant with respect to the retained terms in particular for high Damköhler number, the sum of the two is such that the whole $J_{Y''}$ term almost cancels. Bushe and Bilger (1999) analyzed equation 2.38 in the context of DNS simulations of flame with significant extinction re-ignition and concluded that the term $J_{Y''}$ is indeed small (although no explicit analysis of its first derivative was presented). Following (Klimenko and Bilger (1999)) in the present formulation $F_{Y''} \equiv 0$ although further investigations are worth. It is important to notice here, as was explained in Kim (2002), that this additional term can not be neglected in the derivation of the second-order closure transport equations in section 2.5.

2.4.3 Conditional energy equation

As it can be seen from section 2.3, the unconditional enthalpy conservation, equation 2.16, can be rewritten in terms of equal diffusivity of the scalars and using equation 2.18 as

$$\rho \frac{\partial h}{\partial t} + \rho \mathbf{v} \cdot \nabla h = \frac{\partial p}{\partial t} + \nabla \cdot (\rho D \nabla h) - \rho W_R \tag{2.44}$$

where $\partial p / \partial t$ is the pressure work and ρW_R is the heat loss due to radiation. Since total enthalpy is conserved in the reaction process no chemical source term

is present. The structure of equation 2.44 is similar to equation (2.13) used to derive the transport equation for the conditional scalar Q. In analogy with the derivation in section 2.4, the conditional energy transport equation can be written in terms of total enthalpy with $Q_h \equiv \langle h|\eta\rangle$ as

$$\begin{aligned}\frac{\partial Q_h}{\partial t} &+ \langle \mathbf{v}|\eta\rangle \cdot \nabla Q_h + \frac{\nabla \cdot (\rho_\eta P(\eta)\langle \mathbf{v}'' h''|\eta\rangle)}{\rho_\eta P(\eta)} \\ &= \langle N|\eta\rangle \frac{\partial^2 Q_h}{\partial \eta^2} + \frac{1}{\rho_\eta}\left\langle \frac{\partial p}{\partial t}\middle| \eta \right\rangle - \langle W_R|\eta\rangle \end{aligned} \tag{2.45}$$

It is worth to remind that if the effect of differential diffusion has to be considered, an additional term with respect to equation (2.26) appears due to the last term in equation (2.16) (Kronenburg and Bilger (2001)). The conditional temperature $Q_T \equiv \langle T|\eta\rangle$ that enters in the reaction rate expression (2.57) can be calculated iteratively knowing the composition given the function $h_i = h_i(T)$ is explicitly known.

An alternative procedure can be the explicit solution for the conditional energy equation in terms of temperature. We notice that equation 2.17 has an explicit dependence on the specific heat capacities c_P and an extra term function of $\nabla Y_i \nabla T$ that deserve better considerations. The derivation of the conditional temperature equation follows the same procedure as in section 2.4.

The decomposition method applied to temperature reads

$$T(\mathbf{x}, t) = Q_T(\xi(\mathbf{x}, t), \mathbf{x}, t) + T''(\mathbf{x}, t) \tag{2.46}$$

substituting equations 2.23 - 2.25 written in terms of conditional enthalpy into equation 2.17 and rearranging, we obtain

$$\begin{aligned}\rho c_p \frac{\partial Q_T}{\partial t} &+ \rho c_p \mathbf{v} \cdot \nabla Q_T - \lambda (\nabla \xi)^2 \frac{\partial^2 Q_T}{\partial \eta^2} \\ &- \nabla \cdot (\lambda \nabla Q_T) - \lambda \nabla \xi \cdot \nabla \frac{\partial Q_T}{\partial \eta} \\ &+ \rho c_p \frac{\partial T''}{\partial t} + \rho c_p \mathbf{v} \cdot \nabla T'' - \nabla \cdot (\lambda \nabla T'') \\ &+ \frac{\partial Q_T}{\partial \eta}\left(\rho c_p \frac{\partial \xi}{\partial t} + \rho c_p \mathbf{v} \cdot \nabla \xi - \nabla \cdot (\lambda \nabla \xi)\right) \\ &= \frac{\partial p}{\partial t} - \rho \sum_{i=1}^{n} h_i W_i - \rho W_R \end{aligned}$$

$$
\begin{aligned}
&- \sum_{i=1}^{n} c_{p,i}\, \rho D_i \left(\nabla Q_i + \frac{\partial Q_i}{\partial \eta} \nabla \xi + \nabla Y_i'' \right) \\
&\cdot \left(\nabla Q_T + \frac{\partial Q_T}{\partial \eta} \nabla \xi + \nabla T'' \right)
\end{aligned} \tag{2.47}
$$

using equation 2.18, assuming equal diffusivities among the scalars and $Le = 1$

$$
\nabla \cdot (\lambda \nabla \xi) = \nabla \cdot (\rho c_p D \nabla \xi) = c_p\, \nabla \cdot (\rho D \nabla \xi) + \rho D \nabla \xi \cdot \nabla c_p \tag{2.48}
$$

Making explicit the dependence $c_p = c_p(\xi(\mathbf{x}, t), \mathbf{x}, t)$. Applying the decomposition $c_p = c_{p_\eta}(\xi(\mathbf{x}, t), \mathbf{x}, t) + c_p''(\mathbf{x}, t)$ with $c_{p_\eta} \equiv \langle c_p | \eta \rangle \equiv \sum_{i=1}^{n} Q_i c_{p,i_\eta}(Q_T)$ and the differentiating rules from equations 2.23, 2.24, we can substitute equations 2.20, 2.48 into equation 2.47

$$
\begin{aligned}
\rho c_p \frac{\partial Q_T}{\partial t} &+ \rho c_p \mathbf{v} \cdot \nabla Q_T - \rho c_p D (\nabla \xi)^2 \frac{\partial^2 Q_T}{\partial \eta^2} \\
&- \nabla \cdot (\rho c_p D \nabla Q_T) - \rho c_p D \nabla \xi \cdot \nabla \frac{\partial Q_T}{\partial \eta} \\
&+ \rho c_p \frac{\partial T''}{\partial t} + \rho c_p \mathbf{v} \cdot \nabla T'' - \nabla \cdot (\rho c_p D \nabla T'') \\
&+ \frac{\partial Q_T}{\partial \eta} \rho D \nabla \xi \cdot \left(\nabla c_{p_\eta} + \frac{\partial c_{p_\eta}}{\partial \eta} \nabla \xi + \nabla c_p'' \right) \\
&= \frac{\partial p}{\partial t} - \rho \sum_{i=1}^{n} h_i W_i - \rho W_R \\
&- \rho D \sum_{i=1}^{n} c_{p,i} \left(\nabla Q_i + \frac{\partial Q_i}{\partial \eta} \nabla \xi + \nabla Y_i'' \right) \\
&\cdot \left(\nabla Q_T + \frac{\partial Q_T}{\partial \eta} \nabla \xi + \nabla T'' \right)
\end{aligned} \tag{2.49}
$$

taking the conditional expectation of equation (2.49) conditional on $\xi(\mathbf{x}, t) = \eta$

$$
\begin{aligned}
\rho_\eta c_{p_\eta} \frac{\partial Q_T}{\partial t} &+ \rho_\eta c_{p_\eta} \langle \mathbf{v} | \eta \rangle \cdot \nabla Q_T - \rho_\eta c_{p_\eta} \langle N | \eta \rangle \frac{\partial^2 Q_T}{\partial \eta^2} \\
&- \rho_\eta \langle N | \eta \rangle \frac{\partial c_{p_\eta}}{\partial \eta} \frac{\partial Q_T}{\partial \eta} - \rho_\eta \langle N | \eta \rangle \sum_{i=1}^{n} c_{p,i_\eta} \frac{\partial Q_i}{\partial \eta} \frac{\partial Q_T}{\partial \eta} \\
&= \left\langle \frac{\partial p}{\partial t} \middle| \eta \right\rangle - \rho_\eta \left\langle \sum_{i=1}^{n} h_i W_i - W_R \middle| \eta \right\rangle + e_{Q_T} + e_T + e_{c_p}
\end{aligned} \tag{2.50}
$$

with

$$e_{Q_T} \equiv \left\langle \nabla \cdot (\rho c_p D \nabla Q_T) + \rho c_p D \nabla \xi \cdot \nabla \frac{\partial Q_T}{\partial \eta} \middle| \xi(\mathbf{x}, t) = \eta \right\rangle \tag{2.51}$$

$$e_T \equiv -\left\langle \rho c_p \frac{\partial T''}{\partial t} + \rho c_p \mathbf{v} \cdot \nabla T'' - \nabla \cdot (\rho c_p D \nabla T'') \middle| \xi(\mathbf{x}, t) = \eta \right\rangle \tag{2.52}$$

$$\begin{aligned} e_{c_p} \equiv & \left\langle \rho N'' \sum_{i=1}^{n} c''_{p,i} \frac{\partial Q_i}{\partial \eta} \frac{\partial Q_T}{\partial \eta} + \frac{\partial Q_T}{\partial \eta} \rho D \nabla \xi \cdot (\nabla c_{p_\eta} + \nabla c''_p) \right. \\ & + \rho D \sum_{i=1}^{n} c_{p,i} \ (\nabla Q_i + \nabla Y_i'') \cdot \nabla \xi \frac{\partial Q_T}{\partial \eta} \\ & + \rho D \sum_{i=1}^{n} c_{p,i} \frac{\partial Q_i}{\partial \eta} \nabla \xi \cdot (\nabla Q_T + \nabla T'') \\ & + \left. \rho D \sum_{i=1}^{n} c_{p,i} \ (\nabla Q_i + \nabla Y_i'') \cdot (\nabla Q_T + \nabla T'') \middle| \xi(\mathbf{x}, t) = \eta \right\rangle \end{aligned} \tag{2.53}$$

Equation 2.50 represents the unclosed form of the conditional temperature equation. If we compare equation (2.50) with equation 2.27 we can notice two additional terms acting in mixture fraction space and proportional to the conditional scalar dissipation rate. The last three terms on the right-hand side of equation (2.50) can be treated as in section 2.4.2. The term e_{Q_T} can be neglected under the assumption of high Reynolds number. Following the primary closure hypothesis and assuming negligible c''_p, the e_T term can be closed as

$$e_T P(\eta) = -c_{p_\eta} \nabla \cdot (\rho_\eta \langle \mathbf{v}'' T'' | \eta \rangle P(\eta)) \tag{2.54}$$

Starting from the instantaneous transport equation for temperature instead of enthalpy, the 'canonical' transport equation for the conditional temperature (Kim and Mastorakos (2005)) has been recovered. Nevertheless, a new additional term e_{c_p} appears that, to the author knowledge, has never been presented in the literature before and to which special considerations need to be addressed. Applying the rescaling arguments proposed in (Klimenko and Bilger (1999)) for high Reynolds number flows this term can not be neglected. The first term in fact does not depend on the molecular diffusivity D and remains finite. The following ones

have an explicit dependence on D. However, for high Reynolds number flows, when D appears as factor of the scalar product of two gradients of instantaneous quantities (non means), the whole term remains finite. The magnitude of e_{c_p} needs to be estimated from DNS databases before drawing any conclusion. The CMC implementation in the present thesis neglects the e_{c_p} term, however, better analysis is worth to estimate the error of this assumptions. The conditional transport equation of temperature can be then written as

$$\begin{aligned}\frac{\partial Q_T}{\partial t} &+ \langle \mathbf{v}|\eta\rangle \cdot \nabla Q_T = -\frac{\nabla\cdot(\rho_\eta P(\eta)\langle \mathbf{v}''T''|\eta\rangle)}{\rho_\eta P(\eta)} \\ &+ \langle N|\eta\rangle \left[\frac{1}{c_{p_\eta}}\left(\frac{\partial c_{p_\eta}}{\partial \eta} + \sum_{i=1}^{n} c_{p,i_\eta}\frac{\partial Q_i}{\partial \eta}\right)\frac{\partial Q_T}{\partial \eta} + \frac{\partial^2 Q_T}{\partial \eta^2}\right] \\ &+ \frac{1}{c_{p_\eta}\rho_\eta}\left\langle \frac{\partial p}{\partial t}\middle| \eta\right\rangle - \frac{1}{c_{p_\eta}}\left\langle \sum_{i=1}^{n} h_i W_i \middle| \eta\right\rangle - \frac{\langle W_R|\eta\rangle}{c_{p_\eta}}\end{aligned} \tag{2.55}$$

2.4.4 Conditional chemical source term

An accurate estimation of the chemical reaction rate is essential in turbulent combustion modelling. The description of the chemistry, depending on its complexity, is given by a set of one or more Arrehenius type of reactions that given an initial composition of reactants, returns the rate of change of all the reactive species as

$$W_i = W_i(\mathbf{Y}, T) \tag{2.56}$$

Being a non-linear function of species and temperature, the evaluation of the average reaction rate based on the average of its arguments can yield to an error dependent on the magnitude of the fluctuations. In turbulent combustion, species fluctuations are in general large in the reaction zone so that $\langle W_i\rangle \neq W_i(\langle \mathbf{Y}\rangle, \langle T\rangle)$.

Solving for conditional scalars, CMC associates the fluctuations of the scalars to the fluctuations of mixture fraction. Experimental evidence (Masri et al. (1992)) shows that the conditional fluctuations are of smaller order than the unconditional ones, i.e. $Y'' \ll Y'$. In some cases $Y'' \to 0$ and can be neglected, hence the conditional reaction rate term can be calculated based on the conditional mean of the scalars as

$$\langle W_i(\mathbf{Y}, T)|\eta\rangle \approx W_i(\mathbf{Q}, Q_T) \tag{2.57}$$

In presence of localized extinction and reignition, the conditional fluctuations can not be neglected in the estimation of the reaction rate, hence, a more general formulation need to be applied. The exact expression of the conditional chemical source term can be written as:

$$\langle W_i(\mathbf{Y})|\eta\rangle \equiv \int_{\infty} W_i(\mathbf{Y}^*)P(\mathbf{Y}^*|\eta)d\mathbf{Y}^* \tag{2.58}$$

where $Y_1, ..., Y_{n-1}$ are the species mass fraction, $Y_n \equiv h$ $(or\ T)$ and $\mathbf{Y}^*$ is the n-dimensional sample space of $\mathbf{Y}$. $P(\mathbf{Y}^*|\eta)$ is the conditional joint PDF of the reactive species. Closure of equation (2.58) requires a model for $P(\mathbf{Y}^*|\eta)$. Klimenko and Bilger (1999) suggested a presumed conditional joint gaussian shape calculated based on the first two conditional moments (i.e. conditional mean and conditional variances and covariances). Defining G_{ij} and g_{ij} as respectively the conditional covariance matrix and its inverse we can write

$$P(\mathbf{Y}^*|\eta) = \frac{1}{((2\pi)^n\ det(G_{ij}))^{1/2}}\ exp\left[-\frac{1}{2}\ g_{ij}(Y_i^* - Q_i)(Y_j^* - Q_j)\right] \tag{2.59}$$

Alternatively Kim et al. (2002) proposed the maximum entropy PDF as

$$P(\mathbf{Y}^*|\eta) = exp\left(\alpha_0 + \alpha_i Y_i^* + \beta_{jk} Y_j^* Y_k^*\right) \tag{2.60}$$

with the coefficients α_0, α_i and β_{jk} given from the relationships:

$$\int_{\Omega_\eta} P(\mathbf{Y}^*|\eta)d\mathbf{Y}^* = 1 \tag{2.61}$$

$$\int_{\Omega_\eta} Y_i^* P(\mathbf{Y}^*|\eta)d\mathbf{Y}^* = Q_i \tag{2.62}$$

$$\int_{\Omega_\eta} (Y_i^* - Q_i)(Y_j^* - Q_j)P(\mathbf{Y}^*|\eta)d\mathbf{Y}^* = G_{ij} \tag{2.63}$$

It has to be noticed that the coefficients are not explicitly defined and an algebraic system of $1 + n + n \times (n+1)/2$ equations has to be solved.

A different expression for the conditional reaction rate can be achieved applying a Taylor expansion method to equation (2.56). Assuming a small but not negligible perturbation Y'' from the conditional mean and neglecting the third-order terms, we can write (Kim et al. (2002))

$$\begin{aligned} W(\mathbf{Y}) &= W(\mathbf{Q}) \\ &+ \left.\frac{\partial W}{\partial Y_i}\right|_{\mathbf{Y}=\mathbf{Q}} Y_i'' + \frac{1}{2}\left.\frac{\partial^2 W}{\partial Y_i \partial Y_j}\right|_{\mathbf{Y}=\mathbf{Q}} Y_i'' Y_j'' + \mathcal{O}(Y_i'' Y_j'' Y_k'') \end{aligned} \tag{2.64}$$

taking the conditional expectation for $\xi(\mathbf{x},t)=\eta$

$$\langle W(\mathbf{Y})|\eta\rangle \approx \langle W(\mathbf{Q})|\eta\rangle + \frac{1}{2}\left.\frac{\partial^2 W}{\partial Y_i \partial Y_j}\right|_{\mathbf{Y}=\mathbf{Q}} \langle Y_i'' Y_j''|\eta\rangle \tag{2.65}$$

Alternatively, applying (2.65) to each of the reactions in the chemical mechanism, assuming second order one-step reactions of the form $A+B\rightarrow P$, so that $W=\rho k Y_A Y_B$ with $k=A_0 T^{\beta} exp[-T_a/T]$, we can rewrite the conditional reaction rate, for every reaction as (Klimenko and Bilger (1999))

$$\begin{aligned}\langle W|\eta\rangle \;\approx\; & \langle\rho|\eta\rangle k(Q_T) Q_A Q_B \\ & \left(1+\frac{\langle Y_A'' Y_B''|\eta\rangle}{Q_A Q_B}+\left(\beta+\frac{T_a}{Q_T}\right)\left(\frac{\langle Y_A'' T''|\eta\rangle}{Q_A Q_T}+\frac{\langle Y_A'' T''|\eta\rangle}{Q_B Q_T}\right)\right. \\ & \left.+\frac{1}{2}\left(\beta(\beta-1)+\frac{2(\beta-1)T_a}{Q_T}+\frac{T_a^2}{Q_T^2}\right)\frac{\langle T''^2|\eta\rangle}{Q_T^2}\right)\end{aligned} \tag{2.66}$$

Equations 2.65 and 2.66 are analogous. The first applies to the global reaction rate of the species Y, whereas the second to every elementary reaction in the chemical mechanism. As validation, both methods described recover the first order solution for $\langle Y''|\eta\rangle \rightarrow 0$.

An interesting analysis of different conditional reaction rate closures was presented in Cha and Pitsch (2002) for the DNS database of Sripakagorn et al. (2000). Four different closures of the chemical source term were implemented: (i) first-order, (ii) second-order Taylor expansion (iii) third-order Taylor expansion and a (iv) presumed PDF closure using a β-function for only the conditional (normalized) temperature. The DNS simulated a non-premixed flame that subjected initially to strong scalar dissipation rate exhibits local extinction events, the higher the scalar dissipation rate, the higher the 'level of extinction, the lower the conditional temperature attained. Proceeding in time, due to the scalar dissipation decay, a gradual reignition is achieved. It was shown that only closures higher than first-order were able to predict extinction/re-ignition. For 'moderate extinction' (the conditional PDF of temperature was uni-modal) the Taylor expansion method could predict well the onset of re-ignition. Nevertheless, in the presence of high skewness of the PDF a third order closure was necessary. For 'higher extinction level' (bimodal conditional PDF of temperature with low value of the skewness) both the second and third-order closure were giving very

similar results overpredicting the re-ignition. Despite the fact that the presumed β-PDF is based on only the first two moments, surprisingly good agreement was presented for case (iv) with little sensitivity on the variance estimation. This was explained as a cancelation of error between the modelling with a presumed β-PDF shape and the strong non-linearity of the chemical source term. The hypothesis that for hydrocarbon combustion the performance of the β-PDF function would improve and the model would be a valuable alternative to predict flame with localized extinction/re-ignition was put forward. A similar conclusion was drawn by Kronenburg and Kostka (2005) for Sandia Flame D, E and F using sensible enthalpy instead of temperature.

Valuable discussions on the shape of the conditional joint PDF were presented in Swaminathan and Bilger (1999). Using a two step chemical mechanism to allow extinction and reignition, it was found that the joint PDF may assume a log-normal or a gaussian shape depending on the existence or not of localized extinction.

The aim of the present work is to study the effect of scalar conditional fluctuations on autoignition. The autoignition phenomenon is strongly related to the value of the conditional scalar dissipation rate and its level of conditional fluctuations. Second order closure explicitly considers this effect on the evaluation of the chemical source term (see section 2.5 later in this chapter). It is expected that before the thermal runaway, that characterises the ignition event, the conditional fluctuations are small, but still not negligible. Thus, it has been chosen to close the chemical source term using a Taylor expansion formulation following equation (2.65). The methodology used relies on the numerically evaluation of the Hessian function of the reaction rate to calculate the second order correction. Additional tests will be considered following Cha and Pitsch (2002) restricting the conditional joint PDF of reactive scalars only to the temperature and presuming its conditional PDF by a β-function.

2.4.5 Sub-models

Mixture fraction PDF

The knowledge of the conserved scalar PDF provides information about the local state of mixing of the fluid. In turbulent combustion modelling when it is not directly calculated using a stochastic particle method (Monte Carlo), it is presumed based on its mean and variance. Additional transport equations for the first two moments need to be solved. In this thesis two presumed function have been used:

Clipped Gaussian

$$\begin{aligned}
\tilde{P}(\eta) &= \gamma_1\delta(\eta) + (1-\gamma_1-\gamma_2)\frac{G(\eta)}{I_g} + \gamma_2\delta(1-\eta) \\
G(\eta) &\equiv \frac{1}{\sqrt{2\pi\widetilde{\xi''^2}}}\, exp\left(-\frac{(\eta-\tilde{\xi})^2}{2\widetilde{\xi''^2}}\right) \\
I_g &= \int_0^1 G(\eta)d\eta \\
\gamma_1 &= \int_{-\infty}^0 G(\eta)d\eta \;\; ; \quad \gamma_2 = \int_1^\infty G(\eta)d\eta
\end{aligned} \tag{2.67}$$

where $\delta(x)$ represents the Dirac delta function and γ_1 and γ_2 are the strengths of the delta function at $\eta = 0$ and $\eta = 1$ respectively.

β-function

$$\begin{aligned}
\tilde{P}(\eta) &= \frac{\eta^{r-1}(1-\eta)^{s-1}}{I_b} \\
I_b &\equiv \int_0^1 \eta^{r-1}(1-\eta)^{s-1}d\eta \\
r &= \tilde{\xi}\left(\tilde{\xi}\frac{1-\tilde{\xi}}{\widetilde{\xi''^2}} - 1\right); \quad s = r\frac{1-\tilde{\xi}}{\tilde{\xi}}
\end{aligned} \tag{2.68}$$

Both $\widetilde{\xi}$ and $\widetilde{\xi''^2}$ are positive quantities and with the variance limited between $0 < \widetilde{\xi''^2} < \tilde{\xi}(1-\tilde{\xi})$.

The prediction of the PDF is still an active field of research. It is worth to mention the work of Mortensen (2005) who derived transport equation for the i^{th} central moment of mixture fraction and Mortensen and Bengt (2006) who described the PDF shape using a mapping function.

Conditional mixture fraction dissipation rate

The conditional mixture fraction dissipation rate, appearing in equations 2.38-2.39 represents the effect of diffusion at the small scales. Two different well established models have been used throughout this work, given below:

Amplitude Mapping Closure (AMC) model

$$\begin{aligned} \langle N|\eta\rangle &= \frac{G(\eta)}{\int_0^1 G(\eta)\tilde{P}(\eta)d\eta}\frac{\tilde{\chi}}{2} \\ G(\eta) &= \exp(-2(\mathrm{erf}^{-1}(2\eta-1))^2) \end{aligned} \tag{2.69}$$

where erf^{-1} is the inverse error function. Proposed by O'Brien and Jiang (1991), the AMC model represents the conditional scalar dissipation rate profile in a counterflow configuration, its formulation provide accurate prediction in inhomogeneous conditions (Kim (2005)). In the present work it is considered as the standard choice in transient calculation given its computationally inexpensive formulation.

Girimaji model

$$\begin{aligned} \langle N|\eta\rangle &= -2\frac{\tilde{\xi}(1-\tilde{\xi})}{\left(\widetilde{\xi''^2}\right)^2}\frac{I(\xi)}{\tilde{P}(\eta)}\frac{\tilde{\chi}}{2} \\ I(\eta) &= \int_0^\eta \left(\tilde{\xi}\left(\ln\eta'-G_1\right)+(1-\tilde{\xi})\left[\ln(1-\eta')-G_2\right]\right)\tilde{P}(\eta')(\eta-\eta')d\eta' \\ G_1 &= \int_0^1 \ln(\eta)\tilde{P}(\eta)d\eta;\;\; G_2=\int_0^1 \ln(1-\eta)\tilde{P}(\eta)d\eta \end{aligned} \tag{2.70}$$

Proposed by Girimaji (1992), its a more generic formulation than the AMC, it assumes a β-function profile for the mixture fraction PDF. In this thesis, it is used in chapter 4. More recent approaches to model the conditional scalar dissipation rate have been proposed in Devaud et al. (2004) and in Mortensen (2005).

Conditional velocity

The conditional velocity has been modeled using a linear approximation (Klimenko and Bilger (1999)).

$$\langle \mathbf{v}|\eta\rangle = \tilde{\mathbf{v}}+\frac{\widetilde{\mathbf{v}'\xi'}}{\widetilde{\xi''^2}}(\eta-\tilde{\xi})$$

$$\widetilde{\mathbf{v}'\xi'} = -D_t \nabla \tilde{\xi} \tag{2.71}$$

The model is expected to perform well close to the mean mixture fraction. Validation of the present model can be found in Li and Bilger (1993b). Additional analysis has been carried by in Mortensen (2005) who concluded that the linear model is not consistent with a β-function to model the mixture fraction PDF and a PDF model following Pope (1985) should be used. However, because of its simplicity and its stability of implementation, the linear model remains still widely used.

Conditional turbulent flux

Closure for the conditional turbulent flux has been modeled by analogy with the unconditional scalar flux (Klimenko and Bilger (1999)).

$$\langle \mathbf{v}'' Y_i'' | \eta \rangle = -D_t \nabla Q_i \tag{2.72}$$

Equation 2.72 has demonstrated to be an important term in the stabilization of a lifted flame (Kim and Mastorakos (2005)). Its validation has been recently presented by Richardson et al. (2007) for a DNS database of propagating flame edge flame. Significant counter gradient diffusion was found as it may be expected from the literature in turbulent premixed flame (Veynante and Vervisch (2002)). Transport equation for the conditional turbulent flux were derived, however its integration seem impractical. An additional term has been proposed in Richardson and Mastorakos (2007) to account for the effect of dilatation whose application may be considered in future work.

2.4.6 Boundary conditions

CMC clearly links the conditional scalar transport equations to the mixture fraction PDF. An intuitive physical property of the conditional averages can be seen from the mathematical formulation of equations 2.38 and 2.39, in the limit of $P(\eta) \to 0$ they are undetermined. In other words, a conditional average loses its meaning in region of the conserved scalar sample space that are not realized. Hence, equation 2.37 is defined within the limit of realizability $\eta \in [\eta_{min}, \eta_{max}]$ and requires boundary conditions in physical as well as in mixture fraction space.

Boundary conditions in conserved scalar space have been derived for the mixture fraction PDF transport equation being (Klimenko and Bilger (1999))

$$P(\eta)\langle N|\eta\rangle \to 0 \qquad \eta \to \eta_{min}, \eta_{max} \tag{2.73}$$

with the additional property for non-intermittent PDF

$$\frac{\partial(P(\eta)\langle N|\eta\rangle)}{\partial\eta} \to 0 \qquad \eta \to \eta_{min}, \eta_{max} \tag{2.74}$$

The boundary conditions for equation 2.37 has been proved for smooth PDF with fixed bounds (Klimenko and Bilger (1999)) to be restricted by equation 2.37 itself so that in can be written

$$\left[\frac{\partial Q}{\partial t} + \langle \mathbf{v}|\eta\rangle \cdot \nabla Q + \frac{\nabla \cdot (\rho_\eta P(\eta)\langle \mathbf{v}'' Y''|\eta\rangle)}{\rho_\eta P(\eta)} - \langle W|\eta\rangle\right]_{min,max} = 0 \tag{2.75}$$

This shows that if the boundary fluid is allowed to react, there must be a temporal and spacial variation in the boundary value for Q. This would occur in partially premixed flame in which the fuel stream entering the domain is already a reactive mixture and even at its boundary value should be allowed to react.

In transient simulations the $P(\eta)$ and its boundaries evolve over time. An initialization of η-space is required for those regions previously non realizable. In this work, the approach of a linear interpolation between the value at η_{min}, η_{max} and respectively the value at $\eta = 0$ and $\eta = 1$ is proposed in the aim of mimic a process of inert mixing between the known boundary values. This choice is particularly interesting in situation in which two different combustion events occur sequentially and interact as in a diesel combustion with multiple injections. Asymptotically, if the time between the two injections is large, the second injection occurs in a homogeneous environment prepared by the reaction of the first. The initial conditions should respect an inert mixing between a left boundary value shifted with respect to $\eta = 0$ determined by the first combustion and the right boundary condition determined by the new inlet fuel.

The limit of realizability of $P(\eta)$ reduces the actual domain of solution to a sub-domain of the physical space itself. Dirichlet boundary conditions (defined value) are imposed in the inlet whilst Von Neumann boundary conditions (zero gradient) are applied in the outflow in physical space and at the boundary of

finite probability in mixture fraction space. It is important to underline that for an accurate boundary treatment the domain of finite probability of η should be well resolved in physical space. This implies a careful definition of the mesh in physical space and of the integration timestep. However, this is not necessarily guaranteed using a presumed form for $P(\eta)$.

The formulation of the CMC at the physical boundary is still an open subject of research. In case of engine combustion, heat flux trough the wall, absorption and desorption of unburned hydrocarbon in the liquid film and radical recombination are common phenomena (Heywood (1988)). Bilger (2001) analyzed the case of autoignition close to a solid cold wall. It was demonstrated that in case of no material flux through the wall, no flux (neither convective nor diffusive) perpendicular to the wall should be considered. Hence, zero gradient Von Neumann boundary conditions was imposed for all species except radicals. It was postulated that radicals must be set to zero at the walls and then the fluxes of some of the major species must be adjusted to account for the recombination reactions. The wall temperature was then assumed as independent of the state of mixing with a condition, which implies the Dirichlet boundary condition $\langle T|\eta\rangle = \widetilde{T}_{wall}$.

In the present work the unconditional heat flux to the wall is known from the CFD code and hence, the distribution thereof in conserved scalar space can be evaluated as in Hergart and Peters (2001):

$$\begin{aligned} \langle w_{wall}|\eta\rangle &= \alpha(\langle T|\eta\rangle - \widetilde{T}_{wall}) \\ \alpha &= \frac{\widetilde{w}_{wall}}{\int_0^1 \langle T|\eta\rangle - \widetilde{T}_{wall})\widetilde{P}(\eta)d\eta} \end{aligned} \tag{2.76}$$

This conditional wall heat flux is accounted for in the CMC nodes located at the wall boundaries and makes the enthalpy equation fully consistent with the enthalpy equation in the CFD code (if gaseous fuel is considered). Radical recombination has not been considered yet, therefore, Von Neumann zero gradient boundary conditions were used for all reactive species. Further work is needed to validate the treatment of CMC boundary at the wall, effort in this direction was demonstrated by Wright (2005).

2.5 Second-order closure

In presence of localized phenomena of extinction/re-ignition, the fluctuations above the conditional mean are not negligible. A first-order closure for the reaction rate (equation 2.57) may produce erroneous results and a most sophisticated formulation including the conditional fluctuations should be considered. Second-order closure extends the previous developments of first order closure to transports equation for the scalar conditional second moments.

2.5.1 Conditional species covariance equations

Conditional second moments are variances and covariances about the conditional mean. The conditional fluctuation as Y'' was defined in equation 2.22. The conditional covariance G_{ij} of species i and j is defined as $G_{ij} \equiv \langle K_{ij}|\eta\rangle$, where $K_{ij} \equiv Y_i''Y_j''$. Repeated indexes $G_{ii} \equiv \langle Y_i''Y_i''|\eta\rangle \equiv \langle Y_i''^2|\eta\rangle$ identify the conditional variance.

In the following Bilger's derivation using the decomposition method has been rigorously applied (Klimenko and Bilger (1999)). Transport equations for the G_{ij} can be derived through the conditional average of the instantaneous transport equation of the K_{ij}. For simplicity the case of equal diffusivity of the species and temperature is treated. Equation 2.26 associates the conditional mean of a scalar to its fluctuation and it is valid for all reactive scalars. Writing equation 2.26 for scalar i and j, multiplied respectively by Y_j'' and Y_i'' and adding one to the other we obtain

$$\begin{aligned} \rho\frac{\partial K_{ij}}{\partial t} &+ \rho\mathbf{v}\cdot\nabla K_{ij} - \nabla\cdot(\rho D\nabla K_{ij}) + 2\rho D(\nabla Y_i''\cdot\nabla Y_j'') \\ &= \rho(W_iY_j'' + W_jY_i'') + E_{Dij} + E_{Dji} - E_{Qij} - E_{Qji} \end{aligned} \tag{2.77}$$

where

$$E_{Dij} \equiv Y_i''\rho D\nabla\xi\cdot\nabla\left(\frac{\partial Q_j}{\partial\eta}\right) + Y_i''\nabla\cdot(\rho D\nabla Q_j)) \tag{2.78}$$

$$E_{Qij} \equiv Y_i''\left(\rho\frac{\partial Q_j}{\partial t} + \rho\mathbf{v}\cdot\nabla Q_j - \rho N\frac{\partial^2 Q_j}{\partial\eta^2}\right) \tag{2.79}$$

In the derivation of equation 2.77 the following transformations were used

$$\begin{aligned}
\partial(Y_i''Y_j'')/\partial t &= Y_i''(\partial Y_j''/\partial t) + Y_j''(\partial Y_i''/\partial t) && (2.80)\\
\nabla(Y_i''Y_j'') &= Y_i''\nabla Y_j'' + Y_j''\nabla Y_i'' && (2.81)\\
\nabla\cdot(\rho D\nabla(Y_i''Y_j'')) &= Y_i''(\nabla\cdot(\rho D\nabla Y_j'')) + Y_j''(\nabla\cdot(\rho D\nabla Y_i'')) && (2.82)\\
&+ 2\rho D(\nabla Y_i''\nabla Y_j'')
\end{aligned}$$

The decomposition method applied to K_{ij}, reads

$$K_{ij}(\mathbf{x},t) = G_{ij}(\xi(\mathbf{x},t),\mathbf{x},t) + K_{ij}''(\mathbf{x},t) \tag{2.83}$$

note that by definition $\langle K_{ij}''|\eta\rangle = 0$. Differentiating equation 2.83 with respect to time and space we obtain

$$\frac{\partial K_{ij}}{\partial t} = \frac{\partial G_{ij}}{\partial t} + \frac{\partial G_{ij}}{\partial \eta}\frac{\partial \xi}{\partial t} + \frac{\partial K_{ij}''}{\partial t} \tag{2.84}$$

$$\nabla K_{ij} = \nabla G_{ij} + \frac{\partial G_{ij}}{\partial \eta}\nabla\xi + \nabla K_{ij}'' \tag{2.85}$$

The molecular diffusion term in equation 2.77 can be expanded as

$$\begin{aligned}
\nabla\cdot(\rho D\nabla K_{ij}) &= \nabla\cdot(\rho D\nabla G_{ij}) + \frac{\partial G_{ij}}{\partial\eta}\nabla\cdot(\rho D\nabla\xi)\\
&\quad +\rho D(\nabla\xi)^2\frac{\partial^2 G_{ij}}{\partial\eta^2} + \rho D\nabla\xi\cdot\nabla\frac{\partial G_{ij}}{\partial\eta}\\
&\quad +\nabla\cdot(\rho D\nabla K_{ij}'') && (2.86)
\end{aligned}$$

Substituting equations 2.84, 2.85 and 2.86 into equation 2.77, we get

$$\begin{aligned}
\rho\frac{\partial G_{ij}}{\partial t} &+ \rho\mathbf{v}\cdot\nabla G_{ij} - \rho N\frac{\partial^2 G_{ij}}{\partial\eta^2} + 2\rho(\nabla Y_i''\cdot\nabla Y_j'')\\
&= \rho(W_iY_j'' + W_jY_i'') + E_{Dij} + E_{Dji} - E_{Qij} - E_{Qji}\\
&+ E_G - E_K && (2.87)
\end{aligned}$$

where

$$E_G \equiv \nabla\cdot(\rho D\nabla G_{ij}) + \rho D\nabla\xi\cdot\nabla\frac{\partial G_{ij}}{\partial\eta} \tag{2.88}$$

$$E_K \equiv \rho\frac{\partial K_{ij}''}{\partial t} + \rho\mathbf{v}\cdot\nabla K_{ij}'' - \nabla\cdot(\rho D\nabla K_{ij}'') \tag{2.89}$$

Taking the conditional average of equation 2.87, conditional to $\xi(\mathbf{x},t)=\eta$, gives

$$\begin{aligned}\rho_\eta\frac{\partial G_{ij}}{\partial t} &+ \rho_\eta\langle\mathbf{v}|\eta\rangle\cdot\nabla G_{ij}-\rho_\eta\langle N|\eta\rangle\frac{\partial^2 G_{ij}}{\partial\eta^2}\\ &= \rho_\eta\langle W_iY_j''+W_jY_i''\rangle-2\rho_\eta\langle D(\nabla Y_i''\cdot\nabla Y_j'')\rangle\\ &- e_{Qij}-e_{Qji}-e_K\end{aligned}\tag{2.90}$$

In analogy with the analysis in section 2.4.2, the terms $e_{Dij}\equiv\langle E_{Dij}|\eta\rangle$, $e_{Gij}\equiv\langle E_{Gij}|\eta\rangle$ have been neglected in the condition of high Reynolds number and the term $e_K\equiv\langle E_K|\eta\rangle$ can be manipulated similarly to equation 2.35 as follows

$$\begin{aligned}&\int e_K P(\eta)d\eta=\left\langle\frac{\partial\rho K_{ij}''}{\partial t}+\nabla\cdot(\rho\mathbf{v}K_{ij}'')-\nabla\cdot(\rho D\nabla K_{ij}'')\right\rangle\\ &=\frac{\partial\langle\rho K_{ij}''\rangle}{\partial t}+\nabla\cdot(\langle\rho\mathbf{v}K_{ij}''\rangle)-\nabla\cdot(\langle\rho D\nabla K_{ij}''\rangle)\\ &=\nabla\cdot(\langle\rho\mathbf{v}''K_{ij}''\rangle)=\nabla\cdot\left(\int\rho_\eta\langle\mathbf{v}''K_{ij}''|\eta\rangle P(\eta)d\eta\right)\\ &=\int\nabla\cdot(\rho_\eta\langle\mathbf{v}''K_{ij}''|\eta\rangle P(\eta)d\eta)\end{aligned}\tag{2.91}$$

Assuming equal integrand function for equal integral, the closure for e_K can be written as

$$e_K P(\eta)=\nabla\cdot(\rho_\eta\langle\mathbf{v}''K_{ij}''|\eta\rangle P(\eta))\tag{2.92}$$

As was commented in section 2.4.2, the above assumption is not necessarily an equality. According to Kim (2002), the e_K term can be more rigorously written as

$$e_K P(\eta)=\nabla\cdot(\rho_\eta\langle\mathbf{v}''K_{ij}''|\eta\rangle P(\eta))+F_{K_{ij}''}\tag{2.93}$$

so that

$$\int\rho_\eta F_{K_{ij}''}P(\eta)d\eta=0\tag{2.94}$$

where

$$F_{Y''}=\frac{1}{\rho_\eta P(\eta)}\frac{\partial J_{K_{ij}''}}{\partial\eta}\tag{2.95}$$

The term $J_{K''_{ij}}$ was derived using the joint PDF method having the form

$$J_{K''_{ij}} \equiv -\frac{\partial \rho_\eta \langle N'' K''_{ij} | \eta \rangle P(\eta)}{\partial \eta} + 2\rho_\eta \langle D \nabla K''_{ij} \cdot \nabla \xi | \eta \rangle P(\eta) \tag{2.96}$$

Validation with DNS in Kim (2002) showed that this last term is Damköhler number dependent. It is negligible for high Damköhler numbers and becomes more important when it gets low, therefore exactly when it is interesting to solve for second moments.

A last manipulation concerns the term $e_{Qij} \equiv \langle E_{Qij} | \eta \rangle$ that can be rewritten

$$e_{Qij} = \rho_\eta \left(\nabla Q_j \cdot \langle \mathbf{v}'' Y''_i | \eta \rangle - \frac{\partial^2 Q_j}{\partial \eta^2} \langle Y''_i N'' | \eta \rangle \right) \tag{2.97}$$

where the decompositions $\mathbf{v} \equiv \langle \mathbf{v} | \eta \rangle + \mathbf{v}''$ for the velocity and $N \equiv \langle N | \eta \rangle + N''$ for the scalar dissipation rate have been used.

The final expression for the conditional covariance G_{ij} equation reads

$$\begin{aligned} \frac{\partial G_{ij}}{\partial t} &+ \langle \mathbf{v} | \eta \rangle \cdot \nabla G_{ij} - \langle N | \eta \rangle \frac{\partial^2 G_{ij}}{\partial \eta^2} + \frac{\nabla \cdot \left(\rho_\eta P(\eta) \langle \mathbf{v}'' K''_{ij} | \eta \rangle \right)}{\rho_\eta P(\eta)} \\ &= \langle W''_i Y''_j + W''_j Y''_i | \eta \rangle - 2 \langle D (\nabla Y''_i \cdot \nabla Y''_j) | \eta \rangle \\ &- \nabla Q_i \cdot \langle Y''_j \mathbf{v}'' | \eta \rangle - \nabla Q_j \cdot \langle Y''_i \mathbf{v}'' | \eta \rangle \\ &+ \frac{\partial^2 Q_i}{\partial \eta^2} \langle Y''_j N'' | \eta \rangle + \frac{\partial^2 Q_j}{\partial \eta^2} \langle Y''_i N'' | \eta \rangle \\ &+ \frac{1}{\rho_\eta P(\eta)} \frac{\partial J_{G_{ij}}}{\partial \eta} \end{aligned} \tag{2.98}$$

The equation for the conditional variance G_{ii} is given writing equation 2.98 for $i = j$, for completeness

$$\begin{aligned} \frac{\partial G_{ii}}{\partial t} &+ \langle \mathbf{v} | \eta \rangle \cdot \nabla G_{ii} - \langle N | \eta \rangle \frac{\partial^2 G_{ii}}{\partial \eta^2} + \frac{\nabla \cdot \left(\rho_\eta P(\eta) \langle \mathbf{v}'' K''_{ii} | \eta \rangle \right)}{\rho_\eta P(\eta)} \\ &= 2 \langle W''_i Y''_i | \eta \rangle - 2 \langle D (\nabla Y''_i)^2 | \eta \rangle - 2 \nabla Q_i \cdot \langle Y''_i \mathbf{v}'' | \eta \rangle \\ &+ 2 \frac{\partial^2 Q_i}{\partial \eta^2} \langle Y''_i N'' | \eta \rangle + \frac{1}{\rho_\eta P(\eta)} \frac{\partial J_{G_{ii}}}{\partial \eta} \end{aligned} \tag{2.99}$$

Equation 2.98 has a similar structure to equation (2.37). The first term on the left-hand side is the accumulation term, the second is the transport by convection, the third is the diffusion in conserved scalar space followed by the transport by

conditional fluctuations of K_{ij} in physical space closed as turbulent flux. On the right-hand side, the first term represents the generation of covariance due to the chemistry and the second is a dissipative term. The generation term due to the conditional velocity fluctuations and the conditional scalar dissipation rate fluctuations follows. The last term is the effect that the fluctuation of K_{ij} has in conserved scalar space.

Sub-models are still required to close the different terms in equation 2.98 and will be described in section 2.5.3.

2.5.2 Conditional energy covariance equations

In section 2.4.4 we stated the importance that conditional turbulent fluctuations have in the evaluation of the conditional reaction rate. From equation (2.66) we can see how crucial is an accurate prediction of $\langle Y_i'' T'' | \eta \rangle$ and $\langle T''^2 | \eta \rangle$. As was done in section 2.4.3 either enthalpy or temperature can be considered as possible energy related variables to evaluate the conditional covariances.

The use of total enthalpy $\langle h | \eta \rangle$, from the similarity between equation 2.13 and 2.16, would not change equation 2.98. It is important to remind that enthalpy is conserved during the reaction so the term $W_i \equiv W_h$ that appears in equation 2.98 would need a different closure based on the problem studied. Local variation of total enthalpy can be caused by radiation, boundary effects (i.e. wall heat transfer, localized source of energy), droplet evaporation and pressure. In absence of sources $\langle h'' | \eta \rangle = 0$, hence the transport equations for the covariance of enthalpy would vanish. Although this formulation would allow a smaller set of equation to be solved, solving using a Taylor expansion method, it is not trivial from the knowledge of enthalpy and composition to estimate the conditional temperature fluctuations. However, closure using the joint-PDF method remains feasible.

If a temperature formulation is used, then the covariances of species and temperature are explicitly calculated. To the author knowledge, the temperature species covariance has always been considered analogous to equation 2.98 (Sreedhara and Huh (2005b)), whereas it is expected from the results of section 2.4.3, equation 2.98 to be modified in case of variable $c_{p,i}$. In the following the transport equation for $G_{iT} \equiv \langle Y_i'' T'' | \eta \rangle$ has been derived following Bilger's decomposition

method. The derivation is new and aims to accurately identify the transport equation to be solved for a full second-order closure.

Following the procedure described in section 2.5 we can add equation 2.26 multiplied by $c_p T''$ to equation 2.49 multiplied by Y''. Using the transformations (2.80) and rearranging we can write an equation for $K_{iT} \equiv Y_i'' T''$:

$$\begin{aligned}\rho c_p \frac{\partial K_{iT}}{\partial t} &+ \rho c_p \mathbf{v} \cdot \nabla K_{ij} - c_p \nabla \cdot (\rho D \nabla K_{iT}) + 2\rho c_p D(\nabla Y_i'' \cdot \nabla Y_T'') \\ &= \rho(c_p W_i T'' + W_T Y_i'') + E_{DiT} + E_{DTi} \\ &- E_{QiT} - E_{QTi} + E_{c_p iT} \end{aligned} \tag{2.100}$$

where

$$E_{DiT} \equiv c_p Y_i'' \rho D \nabla\xi \cdot \nabla \left(\frac{\partial Q_T}{\partial \eta} \right) + c_p Y_i'' \nabla \cdot (\rho D \nabla Q_T)) \tag{2.101}$$

$$E_{DTi} \equiv c_p T'' \rho D \nabla\xi \cdot \nabla \left(\frac{\partial Q_i}{\partial \eta} \right) + c_p T'' \nabla \cdot (\rho D \nabla Q_i)) \tag{2.102}$$

$$\begin{aligned} E_{QiT} \equiv\ & Y_i'' \left(\rho \frac{\partial Q_T}{\partial t} + \rho \mathbf{v} \cdot \nabla Q_T - \rho N \frac{\partial^2 Q_T}{\partial \eta^2} \right) \\ &- \rho N \frac{\partial \langle c_p | \eta \rangle}{\partial \eta} \frac{\partial Q_T}{\partial \eta} - \rho N \sum_{i=1}^{n} c_{p,i} \frac{\partial Q_i}{\partial \eta} \frac{\partial Q_T}{\partial \eta} \Bigg) \end{aligned} \tag{2.103}$$

$$E_{QTi} \equiv T'' \left(\rho \frac{\partial Q_i}{\partial t} + \rho \mathbf{v} \cdot \nabla Q_i - \rho N \frac{\partial^2 Q_i}{\partial \eta^2} \right) \tag{2.104}$$

$$\begin{aligned} E_{c_p,iT} \equiv\ & Y_i'' \left(\frac{\partial Q_T}{\partial \eta} \rho D \nabla\xi \cdot (\nabla c_{p_\eta} + \nabla c_p'') \right. \\ &+ \rho D \sum_{i=1}^{n} c_{p,i}\ (\nabla Q_i + \nabla Y_i'') \cdot \nabla\xi \frac{\partial Q_T}{\partial \eta} \\ &+ \rho D \sum_{i=1}^{n} c_{p,i} \frac{\partial Q_i}{\partial \eta} \nabla\xi \cdot (\nabla Q_T + \nabla T'') \\ &+ \rho D \sum_{i=1}^{n} c_{p,i}\ (\nabla Q_i + \nabla Y_i'') \cdot (\nabla Q_T + \nabla T'') \\ &+ \left. \rho D \left(\nabla c_{p_\eta} + \frac{\partial c_{p_\eta}}{\partial \eta} \nabla\xi + \nabla c_p'' \right) \cdot (\nabla Q_T + \nabla T'') \right) \end{aligned} \tag{2.105}$$

substituting equations 2.84, 2.85 and 2.86 into equation 2.100. We obtain

$$\begin{aligned}\rho c_p \frac{\partial G_{iT}}{\partial t} &+ \rho c_p \mathbf{v}\cdot\nabla G_{iT} - \rho c_p N \frac{\partial^2 G_{iT}}{\partial \eta^2} + 2\rho c_p (\nabla Y_i'' \cdot \nabla T'') \\ &= \rho(c_p W_i T'' + W_T Y_i'') + E_{DiT} + E_{DTi} - c_p E_K + c_p E_G \\ &- E_{QiT} - E_{QTi} + E_{c_p iT} \end{aligned} \tag{2.106}$$

where the definition of E_G and E_K are the same as equation (2.88) and (2.89) respectively. Taking the conditional average of equation 2.106, conditional to $\xi(\mathbf{x},t)=\eta$ and neglecting the fluctuation of density, we can write

$$\begin{aligned}\rho_\eta c_{p_\eta} \frac{\partial G_{iT}}{\partial t} &+ \rho_\eta c_{p_\eta}\langle \mathbf{v}|\eta\rangle\cdot\nabla G_{iT} - \rho_\eta c_{p_\eta}\langle N|\eta\rangle \frac{\partial^2 G_{iT}}{\partial \eta^2} \\ &= \rho_\eta \langle c_{p_\eta} W_i T'' + W_T Y_i''|\eta\rangle - 2\rho_\eta c_{p_\eta}\langle D(\nabla Y_i''\cdot\nabla T'')|\eta\rangle \\ &- e_{QiT} - e_{QTi} - c_{p_\eta} e_K + e_{c_p iT} \end{aligned} \tag{2.107}$$

The terms $\langle E_{DiT}|\eta\rangle$ and $\langle E_{DTi}|\eta\rangle$ have been neglected in the hypothesis of high Reynolds number. In analogy with the derivation in section 2.5 we can rewrite the term $c_{p_\eta} e_K$ using the primary closure hypothesis as

$$c_{p_\eta} e_K P(\eta) = c_{p_\eta} \nabla\cdot(\rho_\eta \langle \mathbf{v}'' K_{ij}''|\eta\rangle P(\eta)) \tag{2.108}$$

Reminding that, by definition, $\langle Y''|\eta\rangle \equiv 0$ and decomposing velocity and scalar dissipation rate in conditional mean and fluctuation, we can transform the last three terms in equation (2.107) as

$$e_{QiT} = \rho_\eta c_{p_\eta}\left(\langle \mathbf{v}'' T''|\eta\rangle\cdot\nabla Q_i - \langle T'' N''|\eta\rangle \frac{\partial^2 Q_i}{\partial \eta^2}\right) \tag{2.109}$$

$$\begin{aligned} e_{QTi} &= \rho_\eta c_{p_\eta}\left(\langle \mathbf{v}'' Y_i''|\eta\rangle\cdot\nabla Q_T - \langle Y_i'' N''|\eta\rangle \frac{\partial^2 Q_T}{\partial \eta^2}\right. \\ &- \langle Y_i'' N''|\eta\rangle \frac{1}{c_{p_\eta}}\left(\frac{\partial c_{p_\eta}}{\partial \eta} + \sum_{i=1}^{n} c_{p,i_\eta}\frac{\partial Q_i}{\partial \eta}\right)\left.\frac{\partial Q_T}{\partial \eta}\right) \\ &- \rho_\eta \langle N|\eta\rangle \left\langle Y_i''\left(\sum_{i=1}^{n} c_{p,i}''\frac{\partial Q_i}{\partial \eta}\right)\middle|\eta\right\rangle \frac{\partial Q_T}{\partial \eta} \\ &- \rho_\eta \left\langle Y_i'' N''\left(\sum_{i=1}^{n} c_{p,i}''\frac{\partial Q_i}{\partial \eta}\right)\middle|\eta\right\rangle \frac{\partial Q_T}{\partial \eta} \end{aligned} \tag{2.110}$$

The term e_{QTi} has four additional terms with respect to e_{QiT}. Those act as to correct the term $\langle Y_i'' N''|\eta\rangle \partial Q_T/\partial\eta$ to take into account the $\langle N|\eta\rangle$ curvature due to the effect of the different species c_p (we notice that the first two have the same structure as in equation 2.50. The last two terms in equation 2.110 can be neglected under the assumption of negligible $c_{p,i}''$. The last term in equation (2.107), $e_{c_piT} \equiv \langle E_{c_piT}|\eta\rangle$ is of difficult evaluation. It is proportional to the scalar product of scalar gradients thus, even under the assumption of high Reynolds number can not be neglected. The relevance of this term has not been yet examined in the literature and consistently with the treatment done at first order closure it will be neglected.

The resulting equation for the covariance of temperature and species is

$$\begin{aligned}
\frac{\partial G_{iT}}{\partial t} &+ \langle \mathbf{v}|\eta\rangle \cdot \nabla G_{iT} - \langle N|\eta\rangle \frac{\partial^2 G_{iT}}{\partial \eta^2} + \frac{\nabla \cdot (\rho_\eta P(\eta) \langle \mathbf{v}'' K_{iT}''|\eta\rangle)}{\rho_\eta P(\eta)} \\
&= \langle W_i'' T'' + (W_T'' Y_i''/c_{p_\eta})|\eta\rangle - 2\langle D(\nabla Y_i'' \cdot \nabla T'')|\eta\rangle \\
&- \langle T''\mathbf{v}''|\eta\rangle \cdot \nabla Q_i - \langle Y_i''\mathbf{v}''|\eta\rangle \cdot \nabla Q_T \\
&+ \langle T'' N''|\eta\rangle \frac{\partial^2 Q_i}{\partial \eta^2} + \langle Y_i'' N''|\eta\rangle \frac{\partial^2 Q_T}{\partial \eta^2} \\
&- \langle Y_i'' N''|\eta\rangle \frac{1}{c_{p_\eta}} \left(\frac{\partial c_{p_\eta}}{\partial \eta} + \sum_{i=1}^{n} c_{p,i_\eta} \frac{\partial Q_i}{\partial \eta} \right) \frac{\partial Q_T}{\partial \eta} \\
&+ \frac{1}{\rho_\eta P(\eta)} \frac{\partial J_{G_{iT}}}{\partial \eta}
\end{aligned} \tag{2.111}$$

2.5.3 Sub-models

Equation 2.99 is the unclosed form of the conditional covariance transport equation. A very comprehensive analysis of different closure strategies have been reported in Swaminathan and Bilger (1999). More recently, additional work has been presented in Sreedhara and Huh (2005a). Closures for first and second moments need to be consistent, therefore the same models used in section 2.4.5 still apply here. To summarize, the linear model was used to close the conditional velocity and the AMC or Girimaji to model the conditional scalar dissipation rate.

The gradient diffusion approximation has been applied to model the conditional turbulent flux.

$$\langle \mathbf{v}'' K_{ij}'' | \eta \rangle = -D_t \nabla G_{ij} \tag{2.112}$$

Nothing can be said regarding the inaccuracy of this model in the context of a second-order closure and further validation are needed. This term has been neglected in turbulent shear flow (Li and Bilger (1993a)) and in parabolic formulations (Kronenburg et al. (1998)). Closure of the conditional turbulent flux

$$\langle Y_i'' \mathbf{v}'' | \eta \rangle = -D_t \nabla Q_i \tag{2.113}$$

shows that a generation term appears due to the conditional mean scalar gradient. It is not clear if additional models, which may include counter gradient diffusion, can be applied here.

The terms involving the conditional reaction rate fluctuations have to be modeled consistent with the mean conditional chemical source term closure. Therefore, using a Taylor expansion method, we can write (Kim et al. (2002))

$$\langle W_i'' Y_j'' | \eta \rangle \approx \left. \frac{\partial W_i}{\partial Y_k} \right|_{\mathbf{Y}=\mathbf{Q}} G_{kj} \tag{2.114}$$

Alternatively using the joint-PDF method following the approach of Swaminathan and Bilger (1999), we get

$$\langle W_i'' Y_j'' | \eta \rangle = \int_\infty Y_j W_i(\mathbf{Y}^*) P(\mathbf{Y}^* | \eta) d\mathbf{Y}^* - \langle W_i | \eta \rangle \langle Y_j | \eta \rangle \tag{2.115}$$

where the nomenclature used in section 2.4.4 has been applied.

The second term on the left-hand side in equation (2.99) is a dissipative term. It has been modeled according to Li and Bilger (1993a) as

$$\langle D(\nabla Y_i'' \cdot \nabla Y_j'') | \eta \rangle = \sqrt{C_i C_j} \frac{G_{ij}}{\tau_Y} \qquad \text{with} \qquad \tau_Y = C_{\tau_Y} \frac{\widetilde{\xi''^2}^{1/2}}{\tilde{\chi}} \tag{2.116}$$

τ_Y represent a mixing timescale. Standard values have been used for the model constants $C_i = C_j = C_{\tau_Y} = 1$ and following Li and Bilger (1993a). Swaminathan and Bilger (1999) in their DNS showed poor agreement of the present model showing dependence of the 'constants' on η and Da. It was proposed a new

closure based on the steady laminar flamelet theory that may be implemented in the future.

The term involving scalar dissipation-scalar fluctuation correlation, has been closed with the model presented by Li and Bilger (1993a).

$$\begin{aligned} \langle Y_i'' N''|\eta\rangle &= C_{N''Y''}\langle N|\eta\rangle G_{ii}^{1/2} \\ C_{N''Y''} &= R_{N''Y''}F \qquad \text{with} \qquad F = \frac{\langle N''^2|\eta\rangle^{1/2}}{\langle N|\eta\rangle} \end{aligned} \tag{2.117}$$

Further work by Mastorakos et al. (1997a), analysing a DNS database of autoignition for a one-step chemistry, showed that the correlation coefficient between the two fluctuating quantities $R_{N''Y''}$, is a function of η but does not vary much with Re. The correlation coefficient between conditional temperature and conditional scalar dissipation was shown to be a sinusoidal-like function. Sreedhara (2002) found similar results using four step chemical mechanism and estimated the coefficient using the mathematical shape

$$R_{N''Y''} = -4.2 * (1-\eta)^6 exp(-0.08/\eta) \tag{2.118}$$

The model predicts a minimum in the region of stoichiometry and zero-correlation at the rich mixture fractions. The zero correlation was mostly to account the small influence in the N'' fluctuations far from the reaction zone (Sreedhara (2002)). Additional work was performed in Swaminathan and Bilger (1999), who analyzed a DNS database based two-step chemical mechanism with arbitrarily varying Damköhler number (Da). They found that for low Da the product was following the same shape as Mastorakos et al. (1997a) whereas for high values was close to constant function of η. The sign of function was found positive or negative respectively for products or reactants.

In this thesis, equation 2.118 have been used to model the correlation coefficient $R_{N''Y''}$. The stoichiometry and the most reactive mixture fraction of the test case modeled is similar to what reported in Sreedhara (2002). It is opinion of the author that the model, used in an autoignition case, could give a reasonable representation of the physics. However, it can not be considered as 'universal' for all species without a proper validation.

The coefficient F appearing in equation 2.117 was investigated experimentally and numerically in Markides and Mastorakos (2006b). It was found to increase

with the Reynolds number stabilizing to a constant value between $F \in [1-2]$, relatively constant in η-space.

The last term in equation 2.99 has been modeled as (Kim (2002))

$$J_{G_{ij}} = C_J \rho_\eta P(\eta) \langle N|\eta \rangle \frac{\partial G_{ij}}{\partial \eta} \tag{2.119}$$

using the suggested of $C_J = 1$ for the constant.

A comprehensive validation of the different sub-models for second-order closure have been recently presented by Sreedhara and Huh (2005a). Models have been presented for equation (2.117) and (2.116) based on laminar flamelet tabulation. Even if an apparent inconsistency is present using laminar flamelets in the context of second-order closure, the agreement of the results in various test cases (Kronenburg and Kostka (2005); Sreedhara and Huh (2005b)) is promising.

2.5.4 Boundary conditions

In problems involving second-order closure, boundary conditions are needed for the conditional variances and co-variances. In analogy with the first-moment treatment, boundary conditions have to be imposed at the isosurface containing the finite $P(\eta)$ as well as at the physical boundaries.

At the inlet, where unreacted mixing is generally prescribed, a finite variance may be considered to mimic the fluctuations in temperature and reactant concentrations due to the inherent tolerances in the experimental setup. At the outflow, Von Neuman conditions of zero gradient are imposed consistently with the first-order treatment.

In presence of solid inert boundaries two different treatments are possible. For those second moments involving temperature and the unstable species obeying to Dirichlet conditions for first moments, it is reasonable to assume that second moments will be zero at the wall since there will be no fluctuations. For those involving only stable species or enthalpy, fluctuations about the conditional average are possible and no sure answer can be given without reference to experiment.

2.6 Summary

In this chapter the CMC transport equations that will be used throughout this thesis have been derived. Bilger's decomposition method (Bilger (1993)) has been used in the derivation. The assumption of high Reynolds number flows and equal species diffusivities allowed the closures at first and second-order. Only the case of gaseous fuel has been considered.

Different models for the conditional reaction rate closure have been discussed. Two methods have been selected for higher-order closures: a Taylor expansion method with a numerical evaluation of the Hessian and the Jacobian of the reaction rate (Kim et al. (2002)) and the conditional joint-PDF limited to the only conditional temperature PDF (Pitsch et al. (2003)).

The application of the CMC equation to a transient calculation, needs the definition of appropriate boundary and initial conditions in physical and mixture fraction space. A discussion is presented on the limit of realizability for the mixture fraction PDF. Appropriate re-initialization of η-domain portions that in time get reincorporated in the domain, is needed. A non reacting mixing (straight line in η-space) between the last realizable point, $\eta_{min,max}$, and respectively $[0, 1]$, has been proposed. The boundary conditions in case of confined flows, were defined in case of no material flux and no recombination reactions (Bilger (2001)), with the wall heat transfer modeled according to Hergart and Peters (2001).

Transport equations for temperature and temperature convariance have been newly derived in this chapter following the decomposition method starting from the instantaneous temperature equation rather than from the enthalpy equation. Additional term are found that may be significant in particular in second-order closure.

Chapter 3

Numerical method

3.1 Chapter objective

The aim of the present chapter is to describe the implementation and the coupling of the CMC model with a fluid mechanics solver for unsteady turbulent combustion simulation.

Autoignition, flame propagation, variable geometry, wall quenching, are all different aspects of the unsteady combustion as it occurs in diesel engine modelling. A two-way coupling between the fluid mechanics and the combustion solver is, therefore, needed since the change in the flow field may be determined by the changes in density due to combustion.

CMC solves transport equations in five independent variables (time, three coordinate in physical space and conserved scalar space). The numerical efficiency becomes an important requirement, together with accuracy and stability, in particular when the code is solving for complex chemistry involving several species.

After a description of the discretization method, this chapter presents various integration procedures, each of them with a different requirement in terms of memory allocated, numerical efficiency and accuracy. In en effort to speed up the computational time, the CMC solver has been parallelized and an algorithm of node balancing have been proposed. Finally the description of the interface between the CFD and the CMC solver has been presented.

3.2 Discretisation

The CMC transport equations using density weighted conditioning can be written, using the gradient diffusion hypothesis to close the conditional turbulent flux term (being D_t the turbulent diffusivity), as

$$\begin{aligned} \frac{\partial Q_i}{\partial t} &+ \langle \mathbf{v}|\eta\rangle \cdot \nabla Q_i \\ &= \frac{\nabla \cdot (\bar{\rho}\tilde{P}(\eta) D_t \nabla Q_i)}{\bar{\rho}\tilde{P}(\eta)} + \langle N|\eta\rangle \frac{\partial^2 Q_i}{\partial \eta^2} + \langle W_i|\eta\rangle \end{aligned} \tag{3.1}$$

or, decomposing further the diffusion term, as

$$\begin{aligned} \frac{\partial Q_i}{\partial t} &+ \left[\langle \mathbf{v}|\eta\rangle - D_t \nabla \left(\ln(\bar{\rho}\tilde{P}(\eta))\right)\right] \cdot \nabla Q_i \\ &= \nabla \cdot (D_t \nabla Q_i) + \langle N|\eta\rangle \frac{\partial^2 Q_i}{\partial \eta^2} + \langle W_i|\eta\rangle \end{aligned} \tag{3.2}$$

The CMC transport equations have been discretized using a finite difference approach. Second order central differences for second derivatives and first order upwind for the first derivatives have been implemented. Both formulations as in equation (3.1) and (3.2) are available. While the first respects the diffusion aspect of the term involving the PDF contribution, the second one is by discretization more stable when strong PDF gradients are present. For fine resolutions in physical space a fully second order formulation using central differencing for the convection term is also available.

If we compare with a standard unconditional scalar approach, the use of a conserved scalar formulation increases the solution domain by one dimension so that an unsteady calculation becomes a function of five independent variables (i.e. t-time, x, y, z-physical coordinates and η-conserved scalar space). The computational domain consists in general of a three-dimensional structured grid, in which both cartesian or cylindrical formulation can be selected to discretize physical space, and a one-dimensional grid in η-space.

The dimensionality of the CMC domain and its resolution is often dependent on the problem considered. Simplifying hypothesis can be made for turbulent shear flows (Klimenko (1995)) for which the conditional scalars are not strong functions of the cross-stream direction that and can, therefore, be simplified. The

conditional averages have a different dependence on space than the unconditional ones since the macro-mixing effect is resolved in the conserved scalar field. It is often possible to use a CMC grid coarser then the CFD one saving computational time without losing in accuracy. However, in regions of flame development, the edge flame need to be resolved and higher density is required. A procedure for data transfer from the CFD to the CMC grid has to be considered and will be treated in section 3.5.

3.3 Solvers and integration methods

The use of complex chemical mechanisms can be computationally expensive since the systems of Ordinary Differential Equations (ODEs) become stiff. Stiffness occurs when the rate of change of the different scalars spans at a particular time several orders of magnitudes. The use of a complex chemistry furthermore, implies that the size of the system to be integrated can be very large so the use of an ODE stiff solver with adaptive timestep and designed for large system is necessary. In the present work two solvers have been implemented: VODPK (Brown et al. (1989); Brown and Hindmarsh (1989); Byrne (1992)) and CHEMEQII (Mott et al. (2000)). VODPK is based on a linear multistep method using the Backward Differentiation Formula (BDF). It is implicit with good stability properties and can be used for stiff and non-stiff system with large number of ODEs. CHEMEQII is based on a one-step method using an asymptotic integration method working with a predictor-corrector technique. The solver is second order accurate but, opposite to VODPK, does not rely on the evaluation of the Jacobian of the right-hand side term and can be faster in particular for problem involving high solver restart costs.

The increased dimensionality of the CMC PDEs due to the use of the conserved scalar as independent variable, raises the number of ODEs to integrate. For a typical 2D simulation for example, using a complex chemistry of 32 scalars, the number of ODEs to solve are $30 \times 40 \times 100 \times 32 = 3840000$ that represent respectively the number of nodes in radial, axial, η-direction. The memory storage needed for this large system and the computational time required for the linear

algebra involved in the resolution algorithm makes this system improbable for a single work station.

In the present work, three different methodologies have been considered to improve the numerical efficiency of the combustion code. Comparison in terms of computational efficiency and accuracy have been made using (i) a simultaneous resolution of the set of ODEs, therefore, using the so-called Method of Lines (MOL) (ii) a sequential integration of physical-space and η-space using an Operator Splitting Method (OS) (iii) a sequential integration of physical-space, diffusion in η-space and the conditional reaction rate. In the following cases (ii) and (iii) will be referenced respectively as OS1 and OS2. Validation of the integration procedure can be found in chapter 5.

Numerically, equation 3.1 can be implemented for OS1 as

$$\begin{aligned}
\frac{\partial Q_i^{(1)}}{\partial t} &= -\langle \mathbf{v}|\eta\rangle \cdot \nabla Q_i^{(1)} + \frac{\nabla \cdot (\bar{\rho}\tilde{P}(\eta) D_t \nabla Q_i^{(1)})}{\bar{\rho}\tilde{P}(\eta)} \\
&\quad t \in [t_0, t_0 + \alpha_{OSxyz}\Delta t] \\
\frac{\partial Q_i^{(2)}}{\partial t} &= \langle N|\eta\rangle \frac{\partial^2 Q_i^{(2)}}{\partial \eta^2} + \langle W_i|\eta\rangle \\
&\quad t \in [t_0, t_0 + \Delta t] \\
\frac{\partial Q_i^{(3)}}{\partial t} &= -\langle \mathbf{v}|\eta\rangle \cdot \nabla Q_i^{(3)} + \frac{\nabla \cdot (\bar{\rho}\tilde{P}(\eta) D_t \nabla Q_i^{(3)})}{\bar{\rho}\tilde{P}(\eta)} \\
&\quad t \in [t_0 + \alpha_{OSxyz}\Delta t, t_0 + \Delta t]
\end{aligned} \tag{3.3}$$

where equations 3.3 are solved sequentially in the time interval $t \in [t_0, t_0 + \Delta t]$ where Δt is the CMC timestep. $Q_i^{(i)} = Q_i^{(i-1)}$ is used to initialize each inner timestep. All thermodynamic properties and boundary conditions are updated at every inner timestep. $\alpha_{OSxyz} \in [0, 1]$ is a weight coefficient that defines how much of the physical transport inner iteration has to be performed prior the η-space timestep. Solving equation 3.3 step (2) is similar to the transient flamelet equation and will be denoted as '0DCMC'

Analogously the OS2 is formulated as

$$\begin{aligned}
\frac{\partial Q_i^{(1)}}{\partial t} &= -\langle \mathbf{v}|\eta\rangle \cdot \nabla Q_i^{(1)} + \frac{\nabla \cdot (\bar{\rho}\tilde{P}(\eta) D_t \nabla Q_i^{(1)})}{\bar{\rho}\tilde{P}(\eta)} \\
&\quad t \in [t_0, t_0 + \alpha_{OSxyz}\Delta t]
\end{aligned}$$

$$
\begin{aligned}
\frac{\partial Q_i^{(2)}}{\partial t} &= \langle N|\eta\rangle \frac{\partial^2 Q_i^{(2)}}{\partial \eta^2} \\
& \quad t \in \left[t_0 + \Delta t \frac{(i_{NW}-1)}{n_{NW}}, t_0 + \Delta t \frac{(i_{NW}-1+\alpha_{OS\eta})}{n_{NW}} \right] \\
\frac{\partial Q_i^{(3)}}{\partial t} &= \langle W_i|\eta\rangle \\
& \quad t \in \left[t_0 + \Delta t \frac{(i_{NW}-1)}{n_{NW}}, t_0 + \Delta t \frac{i_{NW}}{n_{NW}} \right] \\
\frac{\partial Q_i^{(4)}}{\partial t} &= \langle N|\eta\rangle \frac{\partial^2 Q_i^{(4)}}{\partial \eta^2} \\
& \quad t \in \left[t_0 + \Delta t \frac{(i_{NW}-1+\alpha_{OS\eta})}{n_{NW}}, t_0 + \Delta t \frac{i_{NW}}{n_{NW}} \right] \\
\frac{\partial Q_i^{(5)}}{\partial t} &= -\langle \mathbf{v}|\eta\rangle \cdot \nabla Q_i^{(5)} + \frac{\nabla \cdot (\bar{\rho}\tilde{P}(\eta) D_t \nabla Q_i^{(5)})}{\bar{\rho}\tilde{P}(\eta)} \\
& \quad t \in [t_0 + \alpha_{OSxyz}\Delta t, t_0 + \Delta t]
\end{aligned}
\tag{3.4}
$$

where the additional symbols n_{NW}, i_{NW} represent respectively the number of internal iteration between diffusion in η-space and chemistry and its counter. $\alpha_{OS\eta} \in [0,1]$ is a weight coefficient that defines how much of the diffusion in η-space inner iteration has to be performed prior the chemical timestep. The superscripts (1-5) can be misleading: they state the different type of splitting more than a proper sequence.

It can be seen from equations 3.3 and 3.4, that the OS has the characteristic of reducing the ODEs system size the solver has to solve simultaneously. In OS1 this advantage is partially balanced by the restarting costs that the solver has in case the Jacobian of the right-hand side term has to be re-evaluated at each call. The use of a solver like CHEMEQII can avoid this inconvenience. It was found, furthermore, that using the OS2 methodology, the restarting costs for VODPK are negligible since the system is of much smaller size than OS1. The OS2 using VODPK is therefore the method of choice for CMC unsteady calculation. In equation 3.4, furthermore, we notice that the conditional chemical source term is evaluated on his own leaving room to the use of look-up tables instead of a direct integration method. This can improve the numerical efficiency of the code in case of very large chemical mechanisms, but was not the aim of the present work.

The use of an OS methodology needs a careful analysis on the accuracy of the solution obtained. Numerically the OS solves sequentially phenomena that are coupled in nature. A detailed analysis of the effect of the OS in case of stiff problem can be found in Strang (1968) and Sportisse (2000). In the latter the effect of the order of integration between a stiff and a non stiff operator is treated as a function of the splitting time. It was shown that the non-stiff operator should always come first and the accuracy depends on the order of integration and the splitting time. For $\alpha_{OS\eta} = 0.5$ and $\alpha_{OSxyz} = 0.5$, Strang (1968) claimed second order accuracy. The fact that no distinction is done in OS between slow and fast-variable, the error committed can be large for fast species with small timescales (Sportisse (2000)). Future development might consider a system reduction based on a single perturbation analysis rather then based on the external timestep. Examples of OS method in the CMC can be found in Kim et al. (2000b), Kim and Huh (2002), Devaud and Bray (2003), and in Wright et al. (2005).

3.4 Parallelization

A natural improvement in the computational efficiency for large scale calculations can be achieved by making the code compliant for parallel calculation and using a multiprocessor machine. Two different methodologies can be pursued: (i) splitting the computational domain in multiple zones (sets) that can be solved in parallel allowing the boundaries to exchange information (halo cells), (ii) taking advantage of the OS methodology and solving in parallel only the η-space part of the calculation (0DCMC), the most computationally expensive. The first methodology has the advantage of a better use of the machine memory since only information on the local set has to be stored and is the one usually implemented in the CFD software. The second has in general better parallel efficiency, takes advantage that each 0DCMC can be treated as a separate entity and uses an algorithm to automatic balance the load on each CPU. The memory requirements are normally higher in the latter case since the full matrix of solution has to be stored on each of the processors. Since in combustion modelling not all the domain is involved in computational expensive calculations (normally only the

high temperature cells require high CPU time), methodology (ii) allows better parallel efficiency and has been implemented in the present work.

The algorithm implemented can be explained for OS1, equation 3.3, as follows. At first, step (1) is computed on the master node, which results in an array of conditional scalars that is the initial condition for step (2) that is sent to all processors. The cells are sorted according to the computational time that had on step (2) in the previous timestep and redistributed such that the most numerically-expensive cells fall on different CPUs. Once step (2) is completed, the array with the newly calculated conditional scalars is retrieved by the main node as well as the CPU time per cell that each CPU took. Step (3) is performed on the master node and the cycle can start again for the next timestep.

3.5 CFD/CMC interface

In this section the interface between the CFD solver STAR-CD (2004) and the combustion code is described in case of fixed and moving grid. Figure 3.1 shows the coupling between the two codes.

Star-CD solves transport equations for velocity field ($\bar{\rho}$, $\widetilde{u}$, $\widetilde{v}$, $\widetilde{w}$), turbulent quantities ($\widetilde{k}$, $\widetilde{\epsilon}$), enthalpy ($\widetilde{h}$), mixture fraction mean ($\widetilde{\xi}$) and variance ($\widetilde{\xi''^2}$). All scalars computed are Favre average quantities. Three different methods can be used to couple the combustion to the CFD code depending on the type of simulation to perform: (i) only density is passed from the CMC to the CFD code. Since conditional Favre averages are calculated, the mean density can be obtained as Klimenko and Bilger (1999)

$$\bar{\rho} = \left(\int \langle \rho | \eta \rangle^{-1} \tilde{P}(\eta) d\eta \right)^{-1} \tag{3.5}$$

Knowing the density, the flow field can be updated without the need for solving an extra equation for enthalpy. It is the most simple coupling but can not be used in case of confined flows in presence of heat transferred to the wall or in case of evaporating multiphase flows in which the droplet properties as function of temperature require the enthalpy equation to be solved. In these cases, the thermodynamic properties of the fluid have to be known, hence, two procedure

are possible: (ii) the unconditional mean molecular weight MW_{mix} and specific heat capacity $c_{p_{mix}}$ may be passed as calculated from the conditional value or (iii) the whole composition can be used so that the CFD software even without solving transport equations for all species is able to iteratively find temperature from enthalpy. Method (iii) is probably the most computationally costly since it implies the convolution of all the scalars for all the CFD cells but it is tested as the most stable.

We remind that the unconditional mean for any scalar can be calculated from the conditional mean using

$$\tilde{\phi} = \int \langle \phi | \eta \rangle \tilde{P}(\eta) d\eta \tag{3.6}$$

To compute the coefficients of the CMC equations an averaging procedure has to be set to allow the data transfer from conditional to unconditional quantities. Two procedures are available (i) mass averaging of the unconditional quantity from where the conditional coefficient can be calculated and (ii) a mass averaging weighted by the PDF of mixture fraction (shortly referred as PDF-averaging in the following) of the conditional coefficients calculated at the CFD resolution. Given $\tilde{\psi}$ scalar calculated by the CFD solver, the volume average $\tilde{\psi}^*$ can be expressed as

$$\tilde{\psi}^*_{CMC} = \left. \frac{\int \tilde{\psi} \bar{\rho} dv}{\int \bar{\rho} dv} \right|_{CFD \in CMC} \tag{3.7}$$

while the PDF-averaging $\langle \tilde{\psi} | \eta \rangle^*$ can be written has

$$\langle \psi | \eta \rangle^*_{CMC} = \left. \frac{\int \langle \psi | \eta \rangle \bar{\rho} \tilde{P}(\eta) dv}{\int \bar{\rho} \tilde{P}(\eta) dv} \right|_{CFD \in CMC} \tag{3.8}$$

The integral on the right-hand side is calculated over all CFD cells belonging to a CMC cell. The PDF-averaging should be in general preferred especially for coarse CMC grid. For very fine grid in which the there is a one to one correspondence between the CFD and CMC grids, the two formulations are equivalent. The mass averaging procedure is generally computationally more efficient and can be useful in cases in which the CFD grid can not resolve properly the PDF field.

The coupling is realized using user-defined subroutines available into STAR-CD. The CFD properties are obtained from posdat.f which is called at the beginning and at the end of each timestep whereas the unconditional scalars are transferred using densit.f if only $\bar{\rho}$ is passed (case (i)), densit.f and coteet.f if $\bar{\rho}$, MW_{mix} and $c_{p_{mix}}$ are used (case (ii)) or through scalfn.f if all scalars are transferred (case (iii)).

Further developments in the interface concerns the automatic meshing and the application of the combustion code for moving grid in reciprocating engine calculation. STAR-CD uses a formulation of cell addition/removal to keep the cell aspect ratio almost constant during the expansion and compression strokes in the engine, and a similar formulation has been implemented for the CMC grid.

The CMC/CFD interface manages both static and moving grids. An algorithm is capable to screen and work with the only active cells present in the domain. At a first stage, the active cells are recognized and their cell centers stored. The cell coordinates and the Favre-averaged velocities are translated in the CMC coordinate system that can be either cartesian or cylindrical and oriented arbitrarily compared to the CFD one (the origin is usually set at the inlet of the scalar or at the injector). Based on the CFD domain extremes, the CMC grid is built and a mapping between CFD and CMC cells is performed. The CMC cells that do not have at least one correspondent CFD cell are deleted so that the resulting boundaries are approximated as a stepwise function. For a static grid, this occurs once whereas for a moving grid this is done at every timestep.

For the compression and expansion processes, a moving and variable CMC grid has been implemented. The user is able to define two parts of the CMC domain, a purely translating one, corresponding to the piston bowl, and a variable one which corresponds to the sweep volume. An important feature of this latter part is that the grid size is automatically managed based on a cell maximum number and a minimum size the user defines. Hence the cells are squeezed/stretched during the compression/expansion far from the Top Dead Center (TDC). When the minimum grid size is reached, the grid is kept constant and layers are added or removed. During the layer addition, the solution from the previous timestep is mapped into the new grid using a linear interpolation. The grid sliding is modeled with an additional convection term, based on the grid relative velocity,

introduced into the conditional velocity formulation. Defining $\mathbf{x}_P^i$ the location of the point **P** in CMC coordinate system at iteration i, the relative velocity can be written as $\tilde{\mathbf{v}}_{REL} = (\mathbf{x}_P^i - \mathbf{x}_P^{i-1})/\Delta t_{CFD}$. Using the linear model for the conditional velocity (equation 2.71), the moving grid conditional velocity is

$$\langle \mathbf{v}|\eta\rangle = \tilde{\mathbf{v}} - \tilde{\mathbf{v}}_{REL} - \frac{D_t}{\widetilde{\xi'^2}}\nabla\tilde{\xi}(\eta - \tilde{\xi}) \tag{3.9}$$

The model can be applied for any kind of grid sliding including grid refinement.

A remark is needed to understand the CMC gridding. Since the CMC is a conserved scalar based approach, the needs of grid refinement of the CMC grid are not necessarily the same than the CFD one. In some cases (i.e. to resolve the flame brush or in a structured cylindrical mesh the region close to the axis) the CMC grid is better resolved than the CFD grid. An algorithm of interpolation of the CFD solution has been implemented to transfer the flowfield values to CMC nodes that does not have direct correspondence with any CFD ones.

3.6 Conclusion

In this chapter a numerical code solving the CMC equatoins has been interfaced with the CFD software STAR-CD to allow fully coupled transient combustion calculation.

The numerical efficiency of the code has been improved using an Operator Splitting (OS) procedure. The OS consists in the sequential integration of transport in physical space, transport and chemistry in conserved scalar space, allowing the user to decide whether integrating the last two simultaneously or sequentially. The solution of a smaller system of ODEs (i.e. smaller array to solve) allows better solver efficiency reducing the computational time as the requirement in memory usage. However, the OS introduces a numerical error due to the decoupling of physical processes physically interacting, a careful selection of the splitting timestep can give a good compromise of numerical efficiency and accuracy. A comparison of results obtained with the various splitting strategies is given in chapter 5.

The splitting procedure allows an easy parallelization of the code. The physical transport (non stiff) is integrated on the main node, whereas the conserved

scalar space (stiff), split on different machines as for parallel homogeneous CMC calculations. An automatic node balancing algorithm has been proposed to allow an optimal scalability of the code.

The coupling between the CFD and the CMC codes is performed using an automatic CFD mesh mapping. This procedure allows the file transfer between a generally unstructured CFD mesh to the structured CMC grid. Sliding and moving CMC grid typical of diesel engine modelling can be accounted for. In this purpose a modification of the CMC equations have been proposed with the addition of an extra convection term that takes into account the relative velocity of the CMC nodes. An algorithm, furthermore, of cell addition/removal has been implemented to maintain the CMC cell density within user definition in case of engine calculation during the compression and expansion stroke. Results from this code will be given in chapters 5 and 6.

3.7 Figures

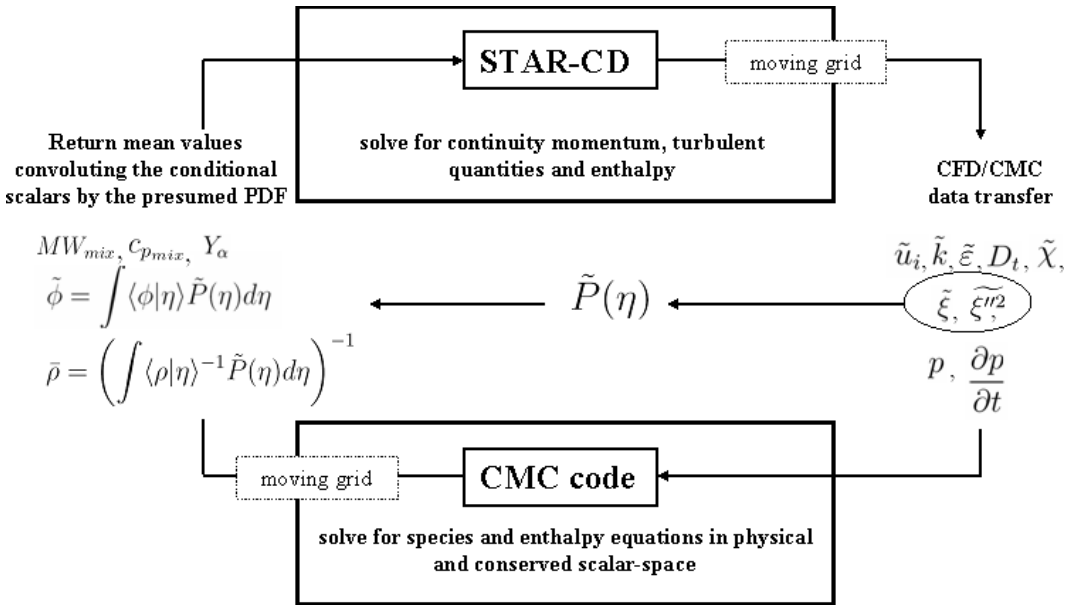

Figure 3.1: Schematic of the interfacing of the CFD and the CMC codes.

Chapter 4

Results - I Autoignition in a turbulent n-heptane plume

Autoignition of a pre-vaporized n-heptane plume in a confined coflow of heated air has been studied with first- and second-order CMC. The aim of this chapter is to investigate how turbulent mixing and chemistry interact in the turbulent autoignition event for a gaseous fuel. At first, an *a priori* study with a homogeneous CMC formulation will be used to assess the dependence of autoignition on mixture composition and conditional scalar dissipation rate at the conditions for which experimental data are available. Subsequently, the mixing in the plume will be presented and a CMC space-marching formulation has been considered. The effects of the initial velocity (i.e. turbulence level) and temperature (i.e. chemistry) will be investigated using first-order CMC closure. Second order-closure using the same parabolic formulation has been implemented. At first a Taylor expansion methodology has been used to solve for the conditional covariances of the full mechanism. First and second-order predictions will then be compared to assess the effects of conditional fluctuations. A computationally efficient closure based only on the temperature variance has then been considered with two different closures strategies for the conditional reaction rate: (i) the Taylor expansion, (ii) the joint-PDF method. The chapter closes with various conclusions.

4.1 Background and objectives

In the present section some key concepts regarding turbulent autoignition are revisited to motivate the modelling assumptions and better interpret the results. Study of turbulent autoignition in a mixing layer using Direct Numerical Simulation (DNS) has been conducted initially by Mastorakos et al. (1997a) using a two-dimensional flow field and a one-step chemistry for the reaction rate. In this work, the topology of the autoignition spot was described based on the local concentration (mixture fraction ξ) and its spacial gradient (scalar dissipation rate χ). It was stated that inhomogeneous mixtures autoignite at a well-defined mixture composition defined as 'most-reactive' mixture fraction ξ_{MR}, dependent on the reaction kinetics, the initial composition and the initial temperature of the reactants. Among the different possible autoignition locations the one with lower scalar dissipation rate $\chi|\xi_{MR}$ ignites first due to the smaller heat losses.

The effect of turbulence was also investigated. It was concluded that autoignition is enhanced by turbulence so that increasing the velocity fluctuations u' will shorten the autoignition delay τ_{IGN}. This was explained as an indirect effect that turbulence has on the mixing field, rather than as a direct relation between the turbulent timescale τ_{TURB} and τ_{IGN}. High initial value of u' enhances the appearance of ξ_{MR} and eventually creates well-mixed spots with reduced gradient ($\chi|\xi_{MR}$), with the overall effect of increasing the probability of autoignition. It was also found that the statistical spread of τ_{IGN} for different calculations at the same condition increased by reducing τ_{TURB}. This was attributed to the limited sample of ξ_{MR} and $\chi|\xi_{MR}$ within the solution domain advancing the hypothesis that for an infinite domain the statistic of τ_{IGN} would be narrow. Additional work was carried in Mastorakos et al. (1997b) to evaluate the effect of mixing on autoignition. The results for laminar autoignition from Liñan and Crespo (1976) and Thevenin and Candel (1995) were extended to turbulent flows. Autoignition is inhibited by high value of $\chi|\xi_{MR}$. A critical value can be observed, χ_{CR}, so that for $\chi|\xi_{MR} > \chi_{CR}$ autoignition can not occur. In a turbulent flow the fluctuations of scalar dissipation rate above its conditional mean can be significant, $\chi''|\xi_{MR}$, hence even if its average value $\langle\chi|\xi_{MR}\rangle$ is above χ_{CR} instantaneously reaction can proceed leading to ignition. The implication that these studies have on the

modelling approach to autoignition is that a conserved scalar approach need to be used to explicitly account for the effect of ξ_{MR} and $\chi|\xi_{MR}$. The conclusions by Mastorakos et al. (1997a) were confirmed in later work by Im et al. (1998), Sreedhara and Lakshmisha (2002b) and Echekki and Chen (2003) using a more realistic chemistry for a three-dimensional flow field.

CMC inherently resolves the effects of inhomogeneities solving for scalars conditioned to mixture fraction and explicitly includes the effect of the scalar dissipation rate in its equations. Hence, it represents an appropriate approach to model turbulent autoignition. DNS plots of conditional temperature during the thermal 'run-away' at ignition show large scatter of the igniting particles, highlighting that the common assumption of negligible conditional fluctuations necessary for a first-order closure is too restrictive. A more complete formulation based on higher-order closure for the reaction rate or doubly conditioning can be necessary when the effects of conditional fluctuation is significant. Mastorakos and Bilger (1998) compared the results of CMC using first- and second-order closure with the prediction of autoigniting DNS. The reaction rate was calculated in all cases based on a one-step reaction and a Taylor expansion series truncated at second-order was used to approximate the exponential in the conditional chemical source term in the second-order closure. The second-order correction was closed solving for the conditional temperature variance equation. DNS and second-order predictions compared favorably. It was also shown that CMC predictions with first and second-order closure were similar at low χ, while they diverged for higher values and, in particular for $\chi > \chi_{CRIT}$, first-order closure failed to predict ignition. At this later condition, the process is driven by the fluctuations of the conditional scalar dissipation rate so that only second-order closure could reproduce the DNS results.

Sreedhara and Lakshmisha (2002a) revisited the above analysis using a 3D DNS database of autoignition and using a reaction mechanism with four reactions. The use of a more complex chemistry introduced the effect of the scalar conditional covariances in the autoignition prediction. It was shown that for complex chemistry the modelling of species and temperature covariances is also important. In this paper the influence of the species conditional fluctuations was

included as a correction term rather than extra transport equations. Nevertheless, a selection of the most critical species and reactions was advanced. In both cases presented, the model was able to predict the autoignition time, but the linear approximation of the exponential in the reaction rate, due to the Taylor series expansion, could not proceed after autoignition. CMC modelling for autoignition is yet limited either to higher-order closure with very simple chemical kinetics (Mastorakos and Bilger (1998), Sreedhara and Lakshmisha (2002a)) or to more complex mechanism using a first-order closure (Kim and Huh (2002) Wright et al. (2005)). To the author's knowledge, a study on the limit of applicability of first and second-order closure to model turbulent autoignition with detailed chemistry has not been done before. The effect of conditional reactive scalar fluctuations on the autoignition prediction has not been investigated yet. Furthermore, a numerical methodology able to predict the influence of conditional fluctuations on autoignition and its transition to the subsequent flame kernel development has not been realized in the past, but can prove useful to model the 'premix' phase of diesel engine combustion as well as HCCI combustion.

The experiment investigated in the present chapter has been analyzed in terms of mixing and autoignition statistics in Markides (2005), Markides and Mastorakos (2005) and Markides and Mastorakos (2006a)). Numerical modelling of autoignition for the present configuration using hydrogen as fuel can be found in Jones et al. (2007) where an LES fluid mechanics solver was coupled with a stochastic field method to treat combustion. The present work has been partially published as Markides et al. (2007).

4.2 Experimental configuration

The experiment modeled in this chapter was performed in the Cambridge University Engineering Department. Details on the configuration, the measurement and the set of experiments performed can be found in Markides (2005).

The experiment consisted of an axi-symmetric injection of gaseous fuel into a stream of pre-heated turbulent coflowing air. With the aim of reducing the heat losses, the burner was confined into a vacuum-insulated quartz tube that allowed the full optical access. Autoignition, under certain conditions, occurred

at a location depending on the fuel (i.e. type, dilution), the initial temperature and the flow velocity. The advantage of this configuration is that it involves a uniform turbulent air stream, which allows an estimate of the mean autoignition delay time from the measurement of the mean autoignition location. Another characteristic is that the full optical access allows an accurate measurement of the mixing pattern for an optimal description of autoignition. A sketch of the experimental apparatus can be seen in figure 4.1.

For a certain range of T_{AIR}, U_{AIR} and U_{FU}, individual autoignition events manifested in the form of localized 'flashes'. Each event was associated with an ignition kernel that ignited successfully, propagated and extinguished. Autoignition behaviour was statistically steady. Random autoignition events occurred continuously at a well defined mean frequency and location. Markides (2005) referred to this regime as 'Random Spots'. It was identified as an intermediate and well defined regime between a 'no ignition' and an intermediate pre-ignition regime in which no proper autoignition took place; and the 'flash-back regime' in which the autoignition spot instead of quenching gave rise to an attached or lifted flame.

Experimentally, autoignition was detected by chemiluminescence radiated from of the hydroxyl radical (OH^*) in the reacting regions. Measurement of autoignition length (L_{IGN}), specified as the axial distance from the injector to the autoigniting region, was determined based on the PDFs of the axial positions of the emitting light. Two definitions were used: L_{MIN} corresponding to the axial location of a 3% rise in the mean signal intensity among many realizations and L_{MODE} its maximum. Typical plots of autoignition location are shown in figure 4.2, taken from Markides (2005).

For the set of experiments considered in this chapter, air was electrically preheated to a T_{AIR} of 1100-1140 K and flowed with bulk velocities U_{AIR} ranging between 10 and 20 m/s through the quartz tube of an inner diameter (D_{IN}) of 24.8 mm open to atmosphere. Turbulence were generated by a grid with 3.0 mm holes and 44% solidity. Pre-vaporized nitrogen diluted n-heptane (C_7H_{16}) was used as fuel, with the mass fraction of C_7H_{16} kept constant at $Y_{C_7H_{16}} = 0.95$. The fuel injector with inner (d) and outer diameters of 2.27 and 2.96 mm, was placed aligned in the centerline of the quartz tube and at a distance of 63 mm

from the turbulence-generating grid. The average fuel bulk velocities (U_{FUEL}) ranged from 10 to 30 m/s with values for the non-dimensional velocity ratio $\upsilon = U_{FUEL}/U_{AIR}$ between 1.05 and 1.20. The nitrogen-diluted fuel was injected at temperatures (T_{FUEL}) that were measured to be in the range 1020-1050 K, with the difference between T_{FUEL} and T_{AIR} within 70-100 K.

4.3 Numerical method

4.3.1 CFD

As the heat release before autoignition in negligible, the density changes in the flow field in the phase prior to autoignition can be neglected allowing the assumption of frozen mixing and the decoupling between the CFD and the CMC solver. The flow and the mixing field were predicted by the solution of a two dimensional axi-symmetric problem using the commercial CFD software FLUENT (2003). The CFD mesh, highly refined along the axis and close to the injector-exit with a radial size at the injector exit of $d/20$, extended for the full length of the quartz-tube and incorporated a total of 64500 cells giving a grid independent solution. The flow field was computed using a Reynolds Stress turbulence model (RSM). Three different methodologies have been compared to achieve the best prediction of the mixture fraction ($\widetilde{\xi}$), its variance ($\widetilde{\xi''^2}$) and dissipation rate ($\widetilde{\chi}$).(i) Standard transport equations using a gradient diffusion model for the turbulent flux have been used for $\widetilde{\xi}$ and $\widetilde{\xi''^2}$ with an algebraic closure for $\widetilde{\chi}$; (ii) the scalar flux transport equations Craft and Launder (2002) have been applied and an extra equation for $\widetilde{\chi}$ (Jones and Musonge (1988)) implemented; finally (iii) as in (ii) using the closure developed by Thielen et al. (2005) and Suga (1995) as explained by Kim and Mastorakos (2006). The calculation of the flow field have been performed by Dr. I.S. Kim. The use of these extra equations is motivated by the need to capture well the early mixing region, close to the injector, where the rapid decay of the scalar dissipation rate and mixture fraction variance was not possible to capture with a simple algebraic closure. Details on the validity of the C_D constant in the algebraic closure of $\widetilde{\chi}$ can be found in Markides and

Mastorakos (2006a). Boundary conditions based on the measured turbulent intensity and length scale at the nozzle plane were imposed at the inlet. Outflow boundary conditions were used for the downstream exit.

4.3.2 CMC

First and second-order CMC has been applied, denoted respectively as CMCI and CMCII. The flow field and the phenomena analyzed have been considered, in first approximation, as parabolic. A space-marching formulation has been applied, hence neglecting the effect of axial diffusion. Under the hypothesis of thin boundary-layer flows, furthermore, it is assumed that the conditional statistics vary little over the width of the flow (Klimenko (1995)) so that the system of equation to integrate (equations 2.37 and 2.98) could be reduced to:

$$\langle v_Z|\eta\rangle^* \frac{\partial Q}{\partial z} = \langle N|\eta\rangle^* \frac{\partial^2 Q}{\partial \eta^2} + \langle W|\eta\rangle \tag{4.1}$$

$$\begin{aligned}
\langle v_Z|\eta\rangle^* \frac{\partial G_{ij}}{\partial z} &= \langle N|\eta\rangle^* \frac{\partial^2 G_{ij}}{\partial \eta^2} && (T1)\\
&+ \langle W_i'' Y_j'' + W_j'' Y_i''|\eta\rangle && (T2)\\
&- 2\langle D(\nabla Y_i'' \cdot \nabla Y_j'')|\eta\rangle && (T3)\\
&+ \langle Y_j'' N''|\eta\rangle \frac{\partial^2 Q_i}{\partial \eta^2} + \langle Y_i'' N''|\eta\rangle \frac{\partial^2 Q_j}{\partial \eta^2} && (T4)\\
&+ \frac{1}{\rho_\eta P(\eta)} \frac{\partial J_{G_{ij}}}{\partial \eta} && (T5)\\
&- \langle Y_j'' v_Z''|\eta\rangle \frac{\partial Q_i}{\partial z} - \langle Y_i'' v_Z''|\eta\rangle \frac{\partial Q_j}{\partial z} && (T6)
\end{aligned} \tag{4.2}$$

The energy equation can be rewritten analogously under the assumption of adiabatic wall, constant pressure and no heat loss of radiation from equation 2.50 and (2.111). The terms on the right-hand side of the variance equation have been grouped (T_i) as it will be referred to later. The term $T6$ that appears in equation (4.2) has been retained even if on a dimensional analysis its magnitude is comparable to the spatial diffusion term that has been neglected. This source term is not directly dependant on the G_{ij} and can be estimated from equation 4.1, its magnitude will be assessed in section 4.4.4.

$\langle\cdot|\eta\rangle^*$ is a cross-stream averaging operator. Following equation 3.8, the operator for the generic variable ψ can be written:

$$\langle\psi|\eta\rangle^* = \frac{\int_0^{D_{IN}} \langle\psi|\eta\rangle \bar{\rho}\tilde{P}(\eta)\pi r dr}{\int_0^{D_{IN}} \bar{\rho}\tilde{P}(\eta)2\pi r dr} \tag{4.3}$$

where $\langle\psi|\eta\rangle$ and $\tilde{P}(\eta)$ are evaluated locally in the CFD cells. $\tilde{P}(\eta)$ is the probability density function and it is assumed to obey a β-function. As discussed in section 2.4.6, the finite probability region was set under the condition $\tilde{P}(\eta) > 1\times10^{-50}$ in order to define $[\eta_{MIN}, \eta_{MAX}]$; a sensitivity analysis on the threshold is discussed in section 4.4.3. The linear model was used for the conditional velocity $\langle u_Z|\eta\rangle$ (equation 2.71) and the AMC and the Girimaji model have been both assessed to model the conditional scalar dissipation rate $\langle N|\eta\rangle$ (equations 2.69 and 2.70). Validation of $\tilde{P}(\eta)$ and $\langle N|\eta\rangle$ sub-models against experiment can be found in section 4.4.2.

The non-linear chemical source term was obtained using a reduced n-heptane mechanism Bikas (2001) based on the detailed n-heptane mechanism of Hewson (1997) and additionally validated for both low-temperature and high-temperature autoignition in section 4.4.1. This mechanism contains 31 species for which equations 4.1 and 4.2 are being solved and another 28 which are put in steady-state, selected using computational singular perturbation (CSP) concepts (Massias et al. (1999)). The conditional reaction rate has been solved at first-order (CMCI) using equation 2.57.

Two methodologies have been considered for the higher-order closure (CMCII): the Taylor expansion (equation 2.65) and the joint-PDF (equation (2.58)) method. In the first, the second-order correction has been calculated using the Hessian of the reaction rate numerically evaluated as explained in chapter 3. The full set of conditional variances and covariances of the species in the mechanism have been considered for a total of $n\times(n+1)/2$ additional equations, where n is the number of the reactive species in the chemical mechanism and temperature.

The closure for the terms in equations 4.1 and 4.2 involving the reaction rate can be closed as

$$\langle W(\mathbf{Y})|\eta\rangle = \underbrace{\langle W(\mathbf{Q})|\eta\rangle}_{\langle W_T^I|\eta\rangle} + \underbrace{\frac{1}{2}\frac{\partial^2 W}{\partial Y_i \partial Y_j}\bigg|_{\mathbf{Y}=\mathbf{Q}} \langle Y_i'' Y_j''|\eta\rangle}_{\langle W_T^{II}|\eta\rangle} \tag{4.4}$$

in which the first and second order term have been highlighted as it will be referred to later, and as

$$\langle W_i'' Y_j'' | \eta \rangle = \left. \frac{\partial W_i}{\partial Y_k} \right|_{\mathbf{Y}=\mathbf{Q}} G_{kj} \tag{4.5}$$

In the second method, a presumed shape for the conditional joint-PDF of the scalars and temperature ($\tilde{P}(\mathbf{Y}, T|\eta)$) has to be prescribed. Because no clear indication is given in the literature on the shape of $\tilde{P}(\mathbf{Y}, T|\eta)$ during autoignition and justified by the strong dependence on temperature of the reaction rate, in the present work the implementation of the joint-PDF method has been limited to only the conditional statistic of temperature so that $\tilde{P}(\mathbf{Y}, T|\eta) \approx \tilde{P}(T|\eta)$. The shape of $\tilde{P}(T|\eta)$ during autoignition can be inferred by the plot of reactedness in Mastorakos et al. (1997a) where it can be noticed that $\langle T|\eta \rangle$ is a bounded scalar between its value at cold mixing between fuel and oxidizer ($\langle T|\eta \rangle_{MIX}$) and at equilibrium. Here it can be calculated using a separate run of the 0DCMC code at the same initial temperatures but with low scalar dissipation rate ($\langle T|\eta \rangle_{EQ}$). A presumed two-parameter β-function has been used to model $\tilde{P}(T|\eta)$, function of the reduced conditional mean and the reduced conditional variance of temperature respectively defined as

$$\widehat{Q}_T = \frac{Q_T - \langle T|\eta \rangle_{MIX}}{\langle T|\eta \rangle_{EQ} - \langle T|\eta \rangle_{MIX}} \tag{4.6}$$

$$\widehat{G}_{TT} = \frac{G_{TT}}{(\langle T|\eta \rangle_{EQ} - \langle T|\eta \rangle_{MIX})^2} \tag{4.7}$$

Using this formulation only one extra equation for the temperature variance had to be added to CMCI and the closure for the reaction rate terms in equations 4.1 and 4.2 can be rewritten as

$$\langle W_i(\mathbf{Y}, T)|\eta \rangle \equiv \int_{\langle T|\eta \rangle_{MIX}}^{\langle T|\eta \rangle_{EQ}} W_i(\mathbf{Q}, T) P(T|\eta) dT \tag{4.8}$$

$$\langle W_T'' T'' | \eta \rangle = \int_{\langle T|\eta \rangle_{MIX}}^{\langle T|\eta \rangle_{EQ}} W_T(\mathbf{Q}, T) P(T|\eta) dT - \langle W_T|\eta \rangle Q_T \tag{4.9}$$

For the clarity reasons, in equations 4.8 and 4.9 the temperature dependence of the reaction rate has been explicitly stated. To simplify the nomenclature the

same symbol, T, will be used for temperature and its sample space. From the S-shape curve describing the ignition/exctintion limit in a laminar counterflow configuration (Liñan and Crespo (1976)), the autoignition limit it is not exactly defined at the frozen temperature so a normalization based on a higher value may be needed, but this has not been attempted here. The use of a β-function to model $\tilde{P}(T|\eta)$ has already been used in the literature by Cha and Pitsch (2002) and Kronenburg and Kostka (2005) in the context of extinction/reignition problems. In the present work the validity of this presumed shape has not been questioned, assuming implicitly that some similarity between the two phenomena may exist due to their low Damköhler number dependence. Useful comments on the shape of the conditional joint-PDF for a two-reaction DNS database can be found for extinction/reignition phenomena in Swaminathan and Bilger (1999). Further studies on the conditional joint-PDF of the different scalars during the autoignition phase using more complex chemistry might clarify this issue.

The closure of the unclosed terms in equation (4.2) has been done according to section 2.5.3. It is worth to notice that conditional second-moment equations require the prescription of a number of constants that appear in the closure models for terms $T3$, $T4$, $T5$. Unfortunately, no DNS data were available to clarify this issue and the suggested values proposed in the literature were used. Additional sensitivity analysis has been carried to state the importance that the scalar dissipation conditional fluctuation term ($T4$) has on the autoignition, as reported in section 4.4.4.

Details on the numerical implementation of the CMC equations can be found in chapter 3. The parabolic CMC (CMCI and CMCII) have been discretized using the Method of Lines in a system of ODEs that has been implicitly integrated by the package VODPK (Brown et al. (1989)). A finite difference grid of 101 nodes clustered around $\xi_{ST} = 0.065$ have been used in η-space. The space-marching step was defined by the same stiff solver while the flow field were updated in intervals corresponding to the size of the fine CFD mesh. All thermodynamic properties including the Jacobian and the Hessian of the reaction rate in the Taylor expansion and the $\tilde{P}(T|\eta)$ in the Joint-PDF method have been calculated implicitly. The boundary conditions have been set according to section 2.4.6. In η-space only the region $[\eta_{MIN}, \eta_{MAX}]$ has been solved and equation (2.75) is

applied at the boundaries. $\tilde{P}(T|\eta)$ is evaluated at every η on a 51 node adaptive grid, which is a function of $\widehat{Q}_T$ and $\widehat{G}_{TT}$ to resolve all β-function shapes from the gaussian to the J-shape. A δ-function is used instead of the β-function at low conditional temperature variance for conditions $\widehat{G}_{TT} < 1 \times 10^{-8}$. Equation (4.2), in the absence of the term $T6$, requires the initial covariance to be initialized with a very small but finite value to start the second moment calculation. $G_{TT} = 1 \times 10^{-50}$ has been enforced to all initial reactant covariances whose both conditional mean mass fraction were finite.

4.4 Results and discussion

The simulation results obtained for the autoignition experiment are analyzed and discussed in the following. Section 4.4.1 reports an *a priori* study of the chemical mechanism and the definition at the present conditions of important parameters such as η_{MR} and χ_{CR} that will help the interpretation of the subsequent results. Section 4.4.2 follows where the calculated flow field is validated against experiments and the sub-models for $P(\eta)$ and $\langle N|\eta\rangle$ are also investigated. Section 4.4.3 presents the autoignition predictions for first-order closure using the parabolic formulation (CMCI). A discussion on the autoignition location, the role of the conditional scalar dissipation rate and the mixture fraction statistic is considered. Section 4.4.4 using the same parabolic formulation present the results for the second-order closure (CMCII). An analysis aiming to assess the influence of the scalar dissipation fluctuations is carried. Results for the Taylor expansion and the joint-PDF method are presented and discussed.

4.4.1 Autoignition *a priori* analysis

The oxidation mechanism for n-heptane (Bikas (2001)) has been tested for homogeneous autoignition under different pressure and temperature conditions. Figure 4.3 show a validation of the predicted autoignition delay against the shock-tube experiments performed by Ciezky and Adomeit (1993). In the simulations the autoignition delay is defined based on the maximum temperature gradient in time. The mechanism adequately reproduces the region of Negative Temperature

Coefficients (NTC) and performs well in the hight temperature region where the autoignition experiment is situated. The mechanism validated here will be used throughout the present work.

As seen in Markides (2005), the autoignition of the non-premixed fuel may occur at various distances, and hence mixing states, from the nozzle. Before embarking on the full analysis by the CMC method, here we discuss three *a priori* methods that could possibly be used for analysing this bounded mixing problem.

First, autoignition of homogeneous mixtures of various initial conditions. The effect of mixture composition, can be assessed through plotting the autoignition delay time as a function of initial mass fractions and temperature given by the mixture fraction η for homogeneous reactor calculation. η represents the level of mixing between two different reactant streams, each of them characterized by an initial composition temperature. Using the above validated mechanism, figure 4.4 shows isocontours of temperature gradient during the autoignition event in the range of condition of the autoignition experiment. The region of maximum gradient identifies a minimum autoignition time (τ_{REF}) for a well defined mixture fraction named by Mastorakos et al. (1997a) as the 'most reactive' mixture fraction (ξ_{MR}). It can be noticed, furthermore, that ξ_{MR} is characterized by the maximum gradient of temperature, which suggests that an autoignition definition based on a temperature threshold can also be appropriate and will be used in the following sections. ξ_{MR} depends on the composition, moves towards richer values with increasing the fuel dilution and the initial temperatures, and is higher for higher T_{FU} at constant T_{AIR} (not shown).

Second, autoignition for a homogeneous mixture at a composition defined by the fuel and air flow rates assuming perfect mixing before reaction occurs. The autoignition delay at this condition (τ_{PREMIX}) is greater than τ_{REF} depending how far the homogeneous composition is from the most reactive one. In the present experiment, $\xi_{PREMIX} = 0.033$ can be estimated. The resulting autoignition delays for various conditions are reported in table 4.2. The autoignition delay predicted by the CMC is expected to be bounded within τ_{REF} and τ_{PREMIX}.

Third, autoignition of turbulent inhomogeneous mixture in which the effects of dissipation due to the scalar gradient are explicitly treated through the con-

ditional scalar dissipation rate $\langle N|\eta\rangle$. The calculations are performed using a homogeneous CMC formulation using a constant (in time) $\langle N|\eta\rangle$. As a way to explore how $\langle N|\eta\rangle$ may affect autoignition, figure 4.5 shows the evolution of the ignition delay as function of η and $\langle N|\eta\rangle$ at the conditions as figure 4.4. The Amplitude Mapping Closure (AMC) model (equation 2.69), parameterized on its maximum value at $\eta = 0.5$, has been used to model $\langle N|\eta\rangle$. It can be seen, as expected, that the shorter autoignition delay time is τ_{REF} obtained using $\langle N|\eta\rangle = 0$. If $\langle N|\eta\rangle$ increases, autoignition is retarded and the reaction zone gets broader as the isocontours of ignition delay get more horizontal. This can be explained by the effect of the high diffusion of radicals and temperature from the most reactive region. ξ_{MR} changes slightly moving towards richer mixture fractions. For high values of $\langle N|\eta\rangle$, autoignition can fail to occur. Now, the dissipation gets so important that it balances the production of radicals.

The locus of the minimum autoignition delay as a function of $\langle N|\eta = 0.5\rangle$ is represented in figure 4.6. A critical value for the conditional scalar dissipation rate ($\langle N|\eta\rangle_{CR}$) can be identified as the asymptotic value of $\langle N|\eta\rangle$ at which autoignition can not occur (Mastorakos et al. (1997b), Mastorakos and Bilger (1998)). In the full calculation, the history of $\langle N|\eta\rangle$ plays a role and alters the ignition location, as we shall see in section 4.4.3.

4.4.2 Mixing field

Measurement of velocity and mixing field were available for similar configurations (similarity was based on the estimated turbulent Reynolds number, Markides (2005)) to the high temperature autoignition experiment. Initially the flow field has been validated against hot-wire measurement data for flow conditions of air injected into air at ambient temperature for the equal velocity case $\nu = 1.05$. Figure 4.7 shows the axial normalized mean ($\widehat{U}$) and root-mean square (r.m.s.) ($\widehat{u}$) of velocity, calculated using a Reynolds stress turbulence model. The normalized values are defined respectively as $\widehat{U} = U/U_{BULK}$ and $\widehat{u} = u'/U$ where U is the mean axial velocity, u' its r.m.s. and $U_{BULK} \approx U_{AIR}$ is the bulk velocity. Good agreement can be found in the inner region of the flow for both mean velocity and r.m.s.. A parabolic Poiseuille laminar profile has been imposed in the injector

exit. The turbulence intensity increases in the region of high shear at the injector exit and the turbulence decays further downstream. An almost uniform profile for both velocity and turbulent intensity is recovered after $20d_{IN}$ in the inner region of the domain. The slight discrepancy of the predictions in the near wall region is not expected to significantly influence the mixing fuel-air because the fuel plume is thin and autoignition happens close to the injector.

The mixing field has been validated against experimental measurements of acetone (C_3H_6O) Planar Laser Induced Fluorescence (PLIF) in a equal velocity coflow ($\nu = 1.17$) at ambient conditions. Measurements are available for mean mixture fraction ($\widetilde{\xi}$), variance ($\widetilde{\xi''^2}$) and three-dimensional dissipation rate inferred from the two-dimensional one ($\widetilde{\chi_{2D}}$), as well as conditional statistic for mixture fraction $PDFs$ ($P(\eta)$) and conditional scalar dissipation rate defined as $\langle N|\eta\rangle = \frac{1}{2}\langle\chi|\eta\rangle$. Results are reported for the three numerical methodologies mentioned in section 4.3. The reader is reminded that option (i) represents the standard methodology which closes the turbulent flux appearing in the transport equation of $\widetilde{\xi}$ and $\widetilde{\xi''^2}$ using a gradient diffusion model and the algebraic closure for χ. Option (ii) stands for the additional solution of transport equations for the turbulent flux and the mixture fraction dissipation rate. Option (iii) is as in (ii) using the additional closure developed by Thielen et al. (2005) and Suga (1995) (details is Kim and Mastorakos (2006)). Figures 4.8(a) and 4.9(a) show $\widetilde{\xi}$ and $\widetilde{\xi''^2}$ axial profiles. The different methods are compared, (iii) appear to be superior in particular to capture the rapid decay of $\widetilde{\xi}$ at the injector exit. $\widetilde{\xi''^2}$ is also predicted satisfactorily using (iii), although underprediction in its initial rise at the injector exit and a decay slightly lower than the measured is noticed. This is also visible in figures 4.8(b) and 4.9(b) where the radial profiles for method (iii) are presented. Overall good agreement between prediction and experiment is reported in figure 4.10 for $\widetilde{\chi}$ using method (iii). The predictions along the centerline tend to underestimate the experimental value close to the injector exit while over predicting the maximum peak in a location slightly shifted downstream.

$P(\eta)$ and $\langle N|\eta\rangle$ have also been validated against experimental measurement. Figure 4.11 shows the profile of the presumed $P(\eta)$ for three points along the centerline. Poor prediction has to be reported close to the injector for both β-function and clipped gaussian, the reason being the low predicted $\widetilde{\xi''^2}$ at this

location as well as the inadequacy of these presumed shape to model the bimodal PDF caused by the air entrainment. Far from the injector the $P(\eta)$ resemble a J-function so that the β-function appears to be superior to the clipped gaussian in this region. Far downstream, experimental data are not available due to the low signal intensity. $P(\eta)$ eventually approaches a gaussian-like shape to become a δ-function in the perfectly mixed region and the two models becomes very similar (not shown).

The measurement and prediction of $\langle N|\eta\rangle$ are compared in figure 4.12 for the same location as in figure 4.11. It is worthwhile to notice that the large scatter in the measurements is due to the small number of samples available in the region of low $P(\eta)$. Two-dimensional conditional scalar dissipation rate ($\langle N_{2D}|\eta\rangle$) measurements were available from the experiment. An estimation of the three-dimensional one ($\langle N_{3D}|\eta\rangle$) was done along the centerline under the assumption of axi-symmetric flow. Calculating separately the radial and axial component, respectively $\langle N|\eta\rangle_r$ and $\langle N|\eta\rangle_z$, along the centerline the full $\langle N|\eta\rangle$ was estimated $\langle N_{3D}|\eta\rangle = 2\times\langle N|\eta\rangle_r + \langle N|\eta\rangle_z$. Comparison between the Girimaji (equation 2.70) and the AMC model (equation 2.69) using the β-function for $P(\eta)$ and the AMC model joint with the clipped gaussian PDF against the experiments is reported. In the region close to the injector, despite the accurate prediction of the mean χ, the error committed in the prediction of $P(\eta)$ yields an underprediction of $\langle N|\eta\rangle$. At locations downstream of the injector, the predictions get closer to the experiments. In general the AMC model coupled with the β-function PDF gives a better prediction. The different plots reveal the inadequacy of all models tested to reproduce fully $\langle N|\eta\rangle$ and more sophisticated models (Devaud et al. (2004), Mortensen (2005)) are needed. In the following the β-function PDF and the AMC model have been retained as they best reproduce the experimental measurement in the region of interest and will hence be used throughout the present section.

Having selected the best modelling strategy for this flow, two different conditions at high temperature have been considered respectively at $U_{AIR} = 13.8$ m/s and $U_{AIR} = 17.64$ m/s. Details on the boundary conditions can be found in table 4.1. Figure 4.13 shows the comparison between the two computed cases in terms of $\tilde{\xi}$ and $\tilde{\chi}$. Experiments showed that increasing the coflow velocity maintaining constant the velocity ratio υ, did not modify the shape of the plume defined as the

contour field of the marker $\widetilde{\xi}$. Figures 4.13(a) and 4.13(b) on the left hand side show $\tilde{\xi}$ iso-contours. The two modeled cases have a similar behaviour. Despite of the 27% rise in bulk velocity the iso-contours of $\tilde{\xi}$ do not get strongly modified. The differences that can be noticed are mainly attributed to the difference in υ and the fine color scale used. However, the use of a more advanced turbulence models like LES might improve predictions. Figure 4.13(a) and 4.13(b) on the right hand side show $\tilde{\chi}$ iso-contours. The higher velocity results to a higher initial value but also to a more rapid decay. The consequences of this will be analyzed in more detail in section 4.4.3.

4.4.3 Parabolic CMC first-order closure

Results obtained using a parabolic first-order closure formulation are reported in the present section. As described in section 4.3, the assumption of a parabolic flow is unable to describe phenomena like the 'flash-back', but it is still considered appropriate until autoignition since no strong gradients of species and temperature are present. It represents moreover a way to isolate and better understand the effect of chemistry and turbulent mixing on autoignition.

General description of the phenomena

Before entering into a detailed analysis of autoignition, a global description of the phenomenon is useful. Convoluting the CMC solution with the PDF of mixture fraction calculated at the fine CFD grid resolution, according to equation 3.6, contour of average quantities can be calculated.

Figure 4.14 shows profiles of average temperatures ($\widetilde{T}$), at the top, and temperature reaction rates ($\widetilde{W_T}$), at the bottom, along the centerline, calculated for the high-velocity case at different initial conditions, here defined with T_{AIR}. It can be seen that the autoignition location, which can be identified as a sudden increase in the average temperature, is dependent on T_{AIR} as expected. After a small decrease of temperature at the injector exit due to endothermic reactions predicted by the mechanism at these conditions, the temperature starts rising monotonically with the distance from the injector until autoignition. A qualitatively different behaviour is observed at high and at low T_{AIR}, which is more

evident from the plot of the temperature reaction rate. At high T_{AIR}, W_T is a monotonic function of the axial direction. Decreasing T_{AIR}, not only W_T gets reduced (the curves are less steep) but below a certain value is stabilizing, or even reducing, before autoignition occurs.

A similar conclusion can be drawn from figure 4.15, where isocontours of $\tilde{Y}_{CH_2O}$ and $\tilde{Y}_{OH}$ are reported for two of the conditions earlier presented, respectively the higher and the lower T_{AIR} in the curve envelope in figure 4.14. Since the autoignition length in both cases is very different, the y-axis in the plots is not in scale. These two species have been selected since the first gives an indication of the advancement of the pre-ignition reactions, while the second is created in the high reactive region and can be considered as a marker of the reaction zone. Figure 4.15(a), high temperature case, shows that the CH_2O concentration rises monotonically until ignition and is depleted in the reaction zone when OH is formed. Figure 4.15(b), low temperature case, shows a non monotonic increase of CH_2O with the axial distance, which is evident from its high-concentration region before the OH rise. This indicates that the reactivity of the mixture is reduced before autoignition occurs. The reason of the large spreading of the high reactive region in the direction perpendicular to the flow, is determined by the CMC cross stream averaging formulation used.

Theses trend in temperature or species concentration, could not be justified by direct measurement, however, plot similar to figure 4.14 were sketched in Markides (2005) as possible explanation to the different autoignition behaviours encountered. The reason will be better explained later in the section where the effect of the mixture fraction statistics is analyzed.

Autoignition location

Figure 4.16(a) contains the main results concerning the location of autoignition in the tube as a function of the inlet air temperature (T_{AIR}). The sensitivity of the model predictions has been explored for a broad range of T_{AIR}. A linear fit has been used to estimate the initial conditions in terms of T_{AIR} and T_{FU} when outside the experimental range of investigation. In the experiments, the two curves of L_{MIN} and L_{MODE} bracket the true mean autoignition spot location,

while in the predictions, autoignition is the location where the conditional temperature first rises above 1600K at some value in η-space. This definition does not compare directly with the one given in the experiment that refers, essentially to unconditional values of OH chemiluminescence. However, since the equations are evaluated in the region of finite $\tilde{P}(\eta)$, this definition gives a good indicator where autoignition occurs first. Using this definition, the predictions are expected to follow the lower experimental curve (L_{MIN}). Data groups belonging to the same conditions are connected by lines, with each line representing a different set of constant U_{AIR} and υ.

Figure 4.16(b) presents the same data, but in terms of the natural logarithm of the mean residence time until autoignition ($ln(\tau_{IGN})$). Furthermore, the independent axis is now $1000/T_{AIR}$, such that this figure can be considered an Arrhenius plot and its gradient an activation temperature, T_{ACT}. For a situation in which the mixing is not playing an active role in determining the delay time until autoignition, one would expect straight lines in this plot (as previous stated, the range of temperature analyzed is outside the range of NTC for n-heptane).

The effect of air temperature is directly evident from these plots. The experimental results show a decreasing trend for both L_{MIN} and L_{MODE} with increasing T_{AIR}. Because U_{AIR} (and hence υ) is constant for all points on each line, as the temperature is increased (and $1000/T_{AIR}$ is decreased), τ_{MIN} and τ_{MODE} decrease monotonically, following the decrease in length. From the delay time plots, figure 4.16(b), where it is apparent that the gradient is not constant, it is possible to conclude that turbulent mixing is actively affecting the pre-ignition chemistry. At higher temperatures, autoignition occurs closer to the injector, where the local scalar dissipation rate is higher. At these locations, the effective activation temperature increases, reflecting a decelerating effect on the chemistry.

In section 4.4.1 the concept of τ_{REF} was defined as the autoignition delay time for a homogeneous stagnant adiabatic mixture with initial composition and temperature corresponding to the frozen values of a mixture with ξ_{MR} and representing the minimum possible ignition delay. Values for τ_{REF} at different conditions can be found in table 4.2 where the data of figure 4.16(a) for the experimental conditions are compared with additional calculations for the homogeneous autoignition delay time τ_{PREMIX} of the fully premixed mixture asymptotically

reached far from injection with the flow rates used in the experiments, which corresponds to a mixture fraction ξ_{PREMIX} about 0.033. The autoignition time from experiment and CMC is longer than τ_{REF} consistent with Mastorakos et al. (1997a) which shows that mixing delays autoignition. τ_{PREMIX} is longer, which shows that in autoignition of a bounded non-premixed flow the well-mixed equivalence ratio is an upper limit to autoignition delay.

Predictions reproduce the salient behaviour of autoignition with respect to the air temperature and are correctly located within the experimental L_{MIN} and L_{MODE} in terms of length and τ_{MIN} and τ_{MODE} in terms of delay time. Nevertheless, discrepancies can still be noticed at the low and at the high temperature regions. At high T_{AIR} 'flash-back' occurs in the experiments. The assumption of parabolic nature of the CMC equations is not valid and an elliptic formulation is needed. At low T_{AIR} the underprediction in autoignition length (and delay time) is attributed to various causes for example the assumption of adiabatic wall and the disregard of the radiation effects. The modelling choices for $\tilde{P}(\eta)$ and the region $[\eta_{MIN}, \eta_{MAX}]$ have a non-negligible effect in these regions, as will be discussed later in this section.

Effect of scalar dissipation rate

A closer look at T_{AIR}=1113 K reveals that for the same T_{AIR} and an increase in U_{AIR} from 13.8 to 17.8 m/s, autoignition is shifted non-linearly downstream, such that the autoignition delay time is increased. This is captured by both experiment and simulation and can be explained by the increase in the scalar dissipation caused by the increase in u' (that increases with U_{AIR}) (see figure 4.13). This retardation of autoignition with increasing air velocity has been previously found for hydrogen (Markides and Mastorakos (2005)) and acetylene (Markides (2005)) and can be explained as an effect of the conditional scalar dissipation rate. As discussed in section 4.4.1, autoignition occurs at ξ_{MR} and at $\chi < \chi_{CR}$. ξ_{MR} can be evaluated from figure 4.16(c) being $\xi_{MR} = 0.135$ and $\xi_{MR} = 0.145$ respectively for the low for the high velocity case. All other conditions being the same, as the conditional scalar dissipation rate at ξ_{MR} increases, the autoignition delay increases. Figure 4.17(a) shows the evolution, along the axial direction, of the conditional scalar dissipation rate evaluated at ξ_{MR} and ξ_{ST} for the same

initial temperatures ($\langle N|\eta = \xi_{MR}\rangle^*$ and $\langle N|\eta = \xi_{ST}\rangle^*$), for different velocities. It is evident that the high velocity flow experiences a higher conditional scalar dissipation rate, which is higher than the critical value for a longer distance, than the low velocity flow. The same conclusions can be drawn normalizing the graphs by the conditional velocity and argue in terms of autoignition delay time instead of ignition length (not shown). This explains fully why the high velocity plume autoignites later than the low velocity plume. The relative difference between ξ_{MR} and ξ_{ST} scalar dissipation histories is also interesting, which underline the importance of employing accurate sub-models for the conditional scalar dissipation. The effects of the conditional scalar dissipation rate fluctuations in second-order closure are discussed in section 4.4.4.

Effect of mixture fraction statistics

Proceeding downstream from the injector, $\tilde{P}(\eta)$ changes from a bimodal to unimodal shape and then it becomes a δ-function where the flow mixes perfectly. The region of finite $\tilde{P}(\eta)$ changes, according to the threshold defined in section 4.3 on its lower limit, with the downstream distance. Solving the CMC equations in the interval defined by $\tilde{P}(\eta)$, two conditions can be encountered depending on whether ξ_{MR} has a finite probability or not in the domain of interest. In the first case, the autoignition is located at ξ_{MR} and the scalar dissipation rate will determine the delay from τ_{REF}. In the second case, the farther the η interval is from the nominal ξ_{MR}, the slower the reaction rate is and ignition will be further delayed. This argument supports the experimental observation that autoignition time may increase very quickly at operating conditions that shift autoignition downstream, to the point that suddenly no ignition spots are observed in the tube (Markides (2005); Markides and Mastorakos (2005)). A further explanation is provided in figure 4.16(c), where at the same conditions as in figure 4.16(a) the location of the first igniting mixture fraction η_{MR} is plotted for different values of the threshold for $\tilde{P}(\eta)$. As expected η_{MR} is sensitive to the threshold used. At the lower T_{AIR} (long L_{IGN}) $\tilde{P}(\eta)$ approaches a δ-function and the range of available η reduces with the effect of spreading L_{IGN} predictions. As a consequence, in an unsteady calculation using an LES turbulence model, the predicted $\tilde{P}(\eta)$ can be fluctuating with the effect of significantly altering the autoignition location. It is

worth to notice that for the definition given above, $\eta_{MR} = \xi_{MR}$ if ξ_{MR} belongs to the interval of realizability for $\tilde{P}(\eta)$.

Figure 4.17(b) presents the statistic of ξ_{MR} and ξ_{ST} along the axial direction. After a first rise, the probability to find ξ_{MR} decays, more rapidly for the higher velocity case, indicating that for long L_{IGN} a more homogeneous ignition is achieved and τ_{IGN} is delayed. The effect of the reduced statistics of ξ_{MR} has therefore a direct consequence on the mean reaction rate and temperature rise as was presented earlier in figures 4.14 and 4.15.

A summary of the joint effects of $\tilde{P}(\eta)$ and $\langle N|\eta\rangle$ can be seen in figure 4.18 where iso-levels of $\tilde{P}(\eta)$ are super imposed on contours of $\langle N|\eta\rangle$ for the two velocity cases. $\langle N|\eta\rangle$ decays rapidly from the initial high values, higher than its unconditional mean, and $\tilde{P}(\eta)$ evolves from a double peak to a J-shape to a uni-modal PDF approaching the homogeneous condition. The high velocity case, because of the higher turbulent diffusivity, reaches the homogeneous condition before the lower velocity case, which explains its higher sensitivity to the PDF threshold.

The transition from a non-premixed to a more homogeneous autoignition requires accurate modelling of $\tilde{P}(\eta)$ and of the boundary conditions in η-space. It is a subject of interest for all combustion devices based on quasi-homogeneous reactant conditions as for HCCI (Homogeneous Charge Compression Ignition) engine or LPP (Lean Premixed Pre-vaporized) gas turbine. In those conditions furthermore the extension of the present formulation towards an elliptic formulation and eventually a double-conditioning might be needed to resolve the propagation front in a more homogeneous environment.

4.4.4 Parabolic CMC second-order closure

The predictions of section 4.4.3 based on a conditional first-order closure for the reaction rate, have been revisited at the light of higher-order closures in the present section. The aim is to assess the effects of conditional fluctuations and understand the limit of first-order closure in predicting autoignition. Nonetheless, the strengths and the limits of the present implementation will be shown in order to validate the numerical method used, which represent an additional novelty of

the present work. To allow the comparison between the first and second-order closure, the same parabolic formulation and a threshold $\tilde{P}(\eta) < 1 \times 10^{-50}$ has been considered.

Three different second-order implementations have been applied (refer to section 4.3.2), (i) a second-order closure based on a Taylor expansion of the conditional reaction rate applied to all the reactive species in the mechanism, (ii) the same methodology as (i) but solving only for the temperature variance, (iii) a PDF method restricted only to the conditional PDF of temperature, $P(T|\eta)$.

Taylor expansion method - full second-order closure

Simulations using second-order closure does not present major differences compared to the first-order ones and the description provided in section 4.4.3 still holds.

Figure 4.19 presents the differences between the ignition length predicted by the first- and second-order methods in terms of an error parameter defined as $\varepsilon = (L_{CMCI} - L_{CMCII})/L_{CMCI}$. Results are reported for method (i) with respect to T_{AIR} for the high velocity case and are extended for an arbitrary chosen $T_{AIR} = 1135K$ with predictions for methods (ii) and (iii). Sensitivity of the predictions to the term $T4$, therefore to the scalar dissipation rate conditional fluctuations, and to the term $T6$, that represent the source term due to the gradient of conditional scalars, in equation 4.2 is presented. ε spans a small interval from very small negative values to less then 2%. Even though the overall predictions do not change substantially, for a reason that will be better explained later, the use of second order closure gives better insight into the mechanism leading to autoignition.

The positive value of ε reported in figure 4.19 demonstrate that $L_{CMCII} < L_{CMCI}$ that is consistent with the findings of Mastorakos and Bilger (1998). ε tends to increase moving towards higher T_{AIR} to then stabilize or even decay slightly at high temperature. Increasing T_{AIR} has the effect of moving the autoignition location upstream the flow, hence in region of higher mean scalar dissipation rate and, from equation 2.117, higher fluctuations. At the same time an increase in T_{AIR} corresponds to an increase to the conditional scalar dissipation rate critical value and, according to figure 4.17(a), to a reduced time (or length) that a fluid particle spend in this region. Figure 4.19 can, thus, be explained as

the competition between those two effects. The importance of the conditional scalar dissipation rate fluctuations have been assessed in the sensitivity analysis on the constant $F = [1, 1.3]$ appearing in the model for the term $T4$ (equation 2.117. Autoignition is enhanced showing that the term $T4$ is the driving term in autoignition calculation, consistently with the findings of Mastorakos and Bilger (1998). This conclusion urges better insight in the understanding of this term in particular to find more universal closures applicable for both autoignition and flames. The effect of term $T6$ has also been shown in figure 4.19. In the autoignition situation, the temperature rises monotonically with distance, therefore, $T6$ is a source term with the overall effect of enhancing autoignition. The reader is reminded that this term scales as the diffusion term in equation 4.2 and in a elliptic formulation its effect would partly be balanced.

Figure 4.20 shows the evolution of the conditional temperature and its root mean squared (r.m.s) at condition $T_{AIR} = 1135K$ and $T_{AIR} = 1035K$ for three locations close to autoignition. The conditional temperature and its fluctuations peak at ξ_{MR} as expected. Autoignition is characterized by a sudden rise in conditional temperature as well an increase in its fluctuation that reaches a segregation coefficient of about $\widehat{S}_T = \frac{\widehat{G}}{\widehat{Q}_T(1-\widehat{Q}_T)} \approx 0.85$, indicating a bimodal behaviour of the conditional temperature. Figure 4.21 shows at the same locations the evolution of the conditional temperature reaction rate calculated as a first-order term $\langle W_T^I|\eta\rangle$ and a second-order correction $\langle W_T^{II}|\eta\rangle$. Far from the initial conditions, where the reaction rate is characterized by endothermic reactions, hence negative in sign (not shown), $\langle W_T^I|\eta\rangle$ is positive and monotonically increases. $\langle W_T^{II}|\eta\rangle$ behaves differently. It enhances autoignition during the pre-ignition phase but at autoignition changes its sign at ξ_{MR} reducing its reactivity while showing a double front in the vicinity of ξ_{MR}. This apparent contradiction can be explained as a perturbation in the mean conditional reaction rate caused by the conditional fluctuations. At autoignition $\langle W_T^I|\eta\rangle$ is at its maximum, hence, any perturbation yields a negative correction.

An analysis of the species conditional variances and covariances shows that before autoignition the most important contributions to the second-order correction comes from temperature followed by n-heptane (C_7H_{16}), ethylene (C_2H_4), oxygen (O_2), carbon monoxide (CO), propene (C_3H_6), water vapor (H_2O), formaldehyde

(CH_2O) and later by the hydroxyl radical (OH). The results for the species covariances are reported in figure 4.22 using the correlation coefficient defined as $R_{ij} = G_{ij}/(\sqrt{G_{ii}}\sqrt{G_{jj}})$. Beside the major species, C_2H_4, C_3H_6 and CH_2O are recognized as intermediate species ignition precursors. The mechanism of autoignition can be further investigated using the species correlation, it is worth to underline the negative correlation between CH_2O and OH at autoignition that show the consumption of formaldehyde in the reaction zone where the hydroxyl radical is formed as reported in figure 4.15.

Autoignition calculations using the Taylor expansion method couldn't proceed further than the first temperature rise. Limitations in the numerical evaluation of the reaction rate Hessian matrix, based on scalar perturbations (first-order accurate), becomes inappropriate, in particular during the autoignition thermal 'run-away'. The results reported in this section can still be considered relevant, an important test for their validity is given by the hypothesis used in the Taylor expansion method, in which it is assumed small second-order contribution to the mean reaction rate (figure 4.21), low conditional fluctuations above its conditional mean (4.20) and a correlation coefficient of the reactive scalar R_{ij} bounded between [-1,1] (figure 4.22).

Figure 4.23 shows the balance of terms in the variance equation for temperature at the same location as figure 4.20. In the pre-ignition phase, figure 4.23(a), $T4$ involving the conditional scalar dissipation rate fluctuations is the driving term, and is mainly balanced by the reaction rate term $T2$. Approaching autoignition, figure 4.23(b) the gradient term $T6$ becomes important together with $T4$ still balanced by $T2$. At autoignition, figure 4.23(c), the reaction rate term $T2$ has the most important positive contribution.

Taylor expansion method - conditional temperature variance

In the aim of simplifying the system of equations to solve, a closure based on the temperature variance only has been attempted. Under this assumption the reaction rate Hessian reduces to the second derivative with respect to temperature only.

Autoignition lengths for conditions $T_{AIR} = 1135K$ and $T_{FU} = 1035K$ are shown in figure 4.19 with and without the gradient term $T6$ for $F = 1$. The

error parameter ε for both cases becomes negative, indicating an increase in the autoignition length with respect to a first-order closure. This apparent inconsistency with the results found using the full Taylor expansion will be better explained later in this section.

The evolution of the conditional temperature and its fluctuations is shown in figure 4.24 for different locations before, during and after the autoignition event. The selected locations are, when possible, as in figure 4.20 so as to compare results directly with different methodologies. The evaluation of only the temperature variance allowed the progression of the calculation without instabilities after ignition allowing the modelling of the autoignition kernel propagation. The conditional temperature fluctuations evolve in similar manner as in figure 4.20 but slightly underpredicted. It is noticeable how after the first peak at autoignition, a double front corresponding to two flame fronts arises.

Figure 4.25 reproduces at the same locations the evolution of $\langle W_T^I|\eta\rangle$ and $\langle W_T^{II}|\eta\rangle$ as previously defined. The first-order term in the reaction rate shows how ignition, after the first kernel, develops into a double flame (not shown) and consequently to a triple-flame. The flame fronts visible in $\langle W_T^I|\eta\rangle$ are much narrower than the ones inferred from the fluctuating temperature that involved broader regions. The evolution of $\langle W_T^{II}|\eta\rangle$ gives an explanation for the increase in autoignition length using a second-order formulation. During the pre-ignition reaction leading to autoignition, the chemistry does not behave as an exponential function with temperature. Mathematically, temperature is still a monotonic function with positive first derivative since a positive perturbation produces a positive variation of the reaction rate, but its second derivative, represented by the Hessian of the temperature reaction rate with respect to temperature is negative. This explains the initial negative contribution of the second-order correction that yields to a retardation of autoignition. After ignition $\langle W_T^{II}|\eta\rangle$ acts in two opposite ways. It reduces the high reaction rate at the flame fronts in the inner region and at the flame front while enhances the propagation of the flame in the flame adjacent regions.

Figure 4.26 shows the contributing terms in the variance equation for temperature at the same location as figure 4.24. The evolution is similar to figure 4.23 for the full second-order closure. Its is significant to notice that without the

other species contributions, the reaction rate term $T2$ always acts as to balance the scalar dissipation rate term $T4$ and the gradient term $T6$.

Despite the effect of reducing the temperature conditional reaction rate during the pre-ignition phase as en effect of the complex chemistry, a Taylor expansion method with second order correction based on only the temperature variance offers a stable and computationally efficient methodology to introduce the effects of conditional fluctuations in CMC to evaluate autoignition and flame propagation.

PDF Method - Conditional Temperature variance

Alternative to the Taylor expansion, the joint-PDF method offers the possibility to close the reaction rate without any assumption on the magnitude of the conditional scalar fluctuations. Because no clear indication exists in the literature on the shape of the conditional joint-PDF of the reactive species during autoignition and with the intent to validate the numerical methodology, the conditional joint-PDF of species has been simplified to a single scalar PDF ($\tilde{P}(T|\eta)$ that can be closed with a presumed β-function. Results using this methodology can de directly compared with the Taylor expansion method applied only to the temperature variance.

Autoignition lengths for conditions $T_{AIR} = 1135K$ and $T_{FU} = 1035K$ are shown in figure 4.19 with and without the gradient term $T6$ for the constant $F = 1$. The error parameter ε is higher in the case without $T6$ showing an opposite behaviour with respect to the Taylor expansion with full closure.

Results of conditional temperature and its fluctuation are presented in figure 4.27 for the same locations considered in the Taylor expansion method using only the temperature variance. Autoignition occurs at earlier times compared to figure 4.24 so the plots are more slightly more advanced in the reaction, however, the characteristics of the autoignition kernel development is analogous to what previously reported. Figure 4.28 show the evolution of the conditional temperature reaction rate as calculate by equation (2.58). The different phases of ignition, double flame propagating into a triple flame are shown. The balance of terms in the variance equation at the same locations is plotted for completeness in figure 4.29 and is similar to the evolution of the Taylor expansion method.

Figure 4.30 shows, at the same location as in figure 4.27, the evolution of $\tilde{P}(T|\eta)$. The temperature is bounded between frozen and equilibrium temperature. Starting from a narrow $\tilde{P}(T|\eta)$ due to the low variance, as the reactions proceed, in the region of ξ_{MR} the $\tilde{P}(T|\eta)$ becomes broader leading to autoignition, represented by a J-shape. The subsequent flame propagation is clearly visible from the bimodal shape of the PDF at the η corresponding to the flame fronts. The shapes of $\tilde{P}(T|\eta)$ are consistent with the one reported by Mastorakos et al. (1997a).

The Joint-PDF method to close the reaction rate terms, has as main limitation the definition of consistent bounds, necessary to apply a presumed shape. At autoignition, from laminar autoignition theory (Liñan and Crespo (1976)), the lower branch of the S-shape does not correspond to the frozen mixing of the reactants but to somehow higher temperature. This implies that at autoignition in turbulent cases the lower boundary should evolve during the calculation. A possible lower limit being the conditional temperature calculated at the same time but with very high conditional scalar dissipation rate. Convoluting the reaction rate calculated with a broad or even bi-modal $\tilde{P}(T|\eta)$ at autoignition, between frozen and equilibrium limit, would result to a lower unphysical reaction rate. This is the explanation for the inconsistency in the autoignition length predictions previously mentioned in figure 4.19. Without the gradient term the $\tilde{P}(T|\eta)$ behaves has a gaussian-like PDF so that the influence of low temperature region becomes less important and the reaction rate is enhanced.

4.5 Conclusion

The conditional moment closure model has been applied to model autoignition of an n-heptane plume in a turbulent heated coflow. A homogeneous parabolic CMC formulation has been implemented. The conditional reaction rate has been closed using first and second-order closure. Two methodologies have been implemented for the second-order closure, a Taylor expansion method solving for the full matrix of variances and covariances of the species in the chemical mechanism and a conditional joint-PDF method in which only the temperature statistic has

been used to evaluate the conditional reaction rate, presuming the conditional temperature PDF to be a β-function.

Results show that the increased scalar dissipation rate created by faster background turbulence delays autoignition, as revealed by a disproportionate increase of ignition length with air velocity. At low air temperature (long ignition delay) autoignition is shifted downstream towards more homogeneous mixtures and the location of the most reactive mixture fraction within the mixture fraction PDF becomes important.

Second order-closure, using a Taylor expansion method applied to all species, predicts shorter autoignition lengths than first-order closure consistent with DNS results. The conditional scalar fluctuations enhance autoignition. The driving term in the conditional covariance equation, during an autoignition calculation, is the one dependent on the conditional scalar dissipation rate fluctuations.

In the present case first and second-order closure had small differences in the predictions. The reason is attributed to the rapid decay of the conditional scalar dissipation rate below its critical value. First-order closure appears, therefore, to be adequate at these conditions.

The Taylor expansion method can predict autoignition, however, it is inappropriate to predict the initial phase of kernel development. The assumption of small conditional fluctuations necessary for the expansion is not valid after ignition. However, the method can be effective to predict pollutant formation in flames with low but still non-negligible conditional fluctuations.

The conditional joint-PDF method limited to the temperature only, can be an efficient alternative to introduce the effects of conditional fluctuations without solving the full set of covariances. Without assumption on the magnitude of the conditional fluctuation, it can be applied to predict autoignition as well as flame development with careful definition of the PDF bounds.

4.6 Tables and Figures

Type	U_{AIR} $[m/s]$	$\upsilon = U_{FU}/U_{AIR}$ $[-]$	T_{AIR} $[K]$	T_{FU} $[K]$	ρ_{AIR} $[kg/m^3]$	ρ_{FU} $[kg/m^3]$
Velocity	2.66	1.08	297	297	1.180	1.180
Mixing	3.09	1.17	473	438	0.747	0.919
Autoignition	13.80	1.05	1109	1029	0.318	1.037
	17.64	1.20	1126	1032	0.313	1.030

Table 4.1: initial condition CFD modelling.

U_{AIR} $[m/s]$	T_{AIR} $[K]$	T_{FU} $[K]$	$\tau_{IGN,CMC}$ $[ms]$	τ_{PREMIX} $[ms]$	τ_{REF} $[ms]$	ξ_{MR} $[-]$
13.8	1104	1027	5.35	7.83	4.13	0.157
	1109	1029	5.02	6.72	3.85	0.147
	1113	1030	4.77	6.14	3.65	0.143
17.6	1113	1028	5.01	6.17	3.69	0.132
	1124	1032	4.31	4.80	3.13	0.122
	1132	1036	3.81	3.98	2.74	0.109
	1135	1035	3.67	3.73	2.63	0.106
	1138	1043	3.38	3.44	2.42	0.109

Table 4.2: Autoignition delay time predicted by CMC, corresponding estimated autoignition delay time of a homogeneous premixed mixture at $\xi_{PREMIX} = 0.033$ and autoignition delay time of a homogeneous mixture at ξ_{MR}.

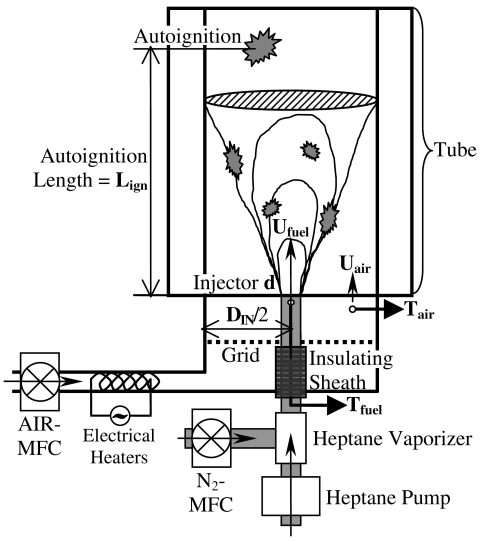

Figure 4.1: Experimental apparatus (reproduced from Markides et al. (2007)).

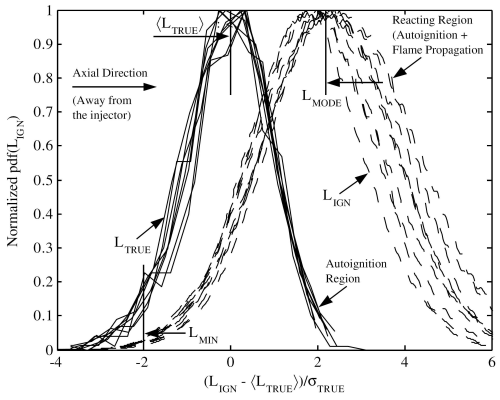

Figure 4.2: Normalized probability density function of the true autoignition location and of the location of light-emitting regions after the first propagation has occurred (reproduced from Markides et al. (2007)).

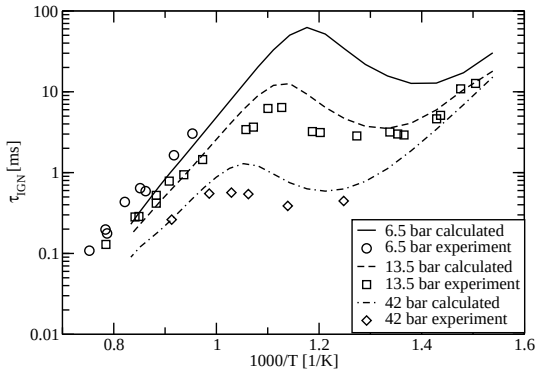

Figure 4.3: Auto-ignition delay time for a constant-volume perfectly homogeneous reactor at stoichiometry. Computation performed using the chemical mechanism from Bikas (2001). Experimental data from Ciezky and Adomeit (1993).

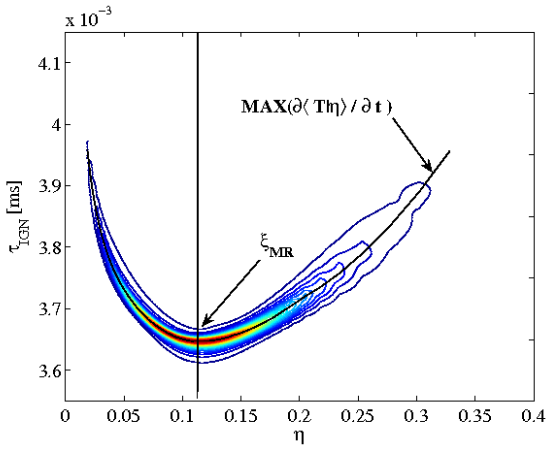

Figure 4.4: Autoignition-delay time [ms] for a homogeneous reactor as a function of composition η. Contour plot of $\frac{\partial \langle T|\eta \rangle}{\partial t}$ identifies the location of auto-ignition. The solid line $(-)$ defines the locus of maximum gradient, hence auto-ignition. The most reactive mixture fraction (ξ_{MR}) is defined at the minimum ignition delay time (τ_{REF}). Initial conditions: $Y_{N_2,OX} = 0.767$, $Y_{O_2,OX} = 0.233$, $T_{OX} = 1113\ K$, $Y_{C_7H_{16},FU} = 0.95$, $Y_{N_2,FU} = 0.05$, $T_{FU} = 1030\ K$.

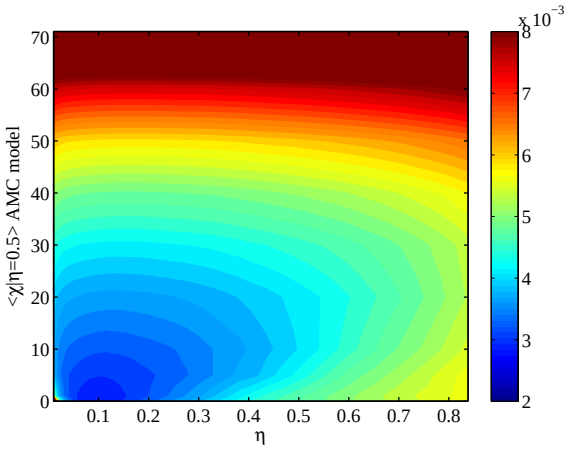

Figure 4.5: Autoignition-delay time [ms] for homogeneous CMC as a function of composition η, and conditional scalar dissipation rate [1/s] (AMC model) parameterized on $\langle N|\eta = 0.5\rangle$. Initial condition as in figure 4.4.

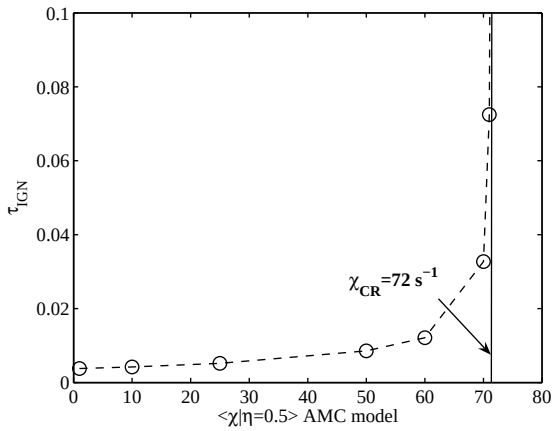

Figure 4.6: Locus of minimum auto-ignition delay time [ms] as a function of $\langle N|\eta = 0.5\rangle$ [1/s] from figure 4.5.

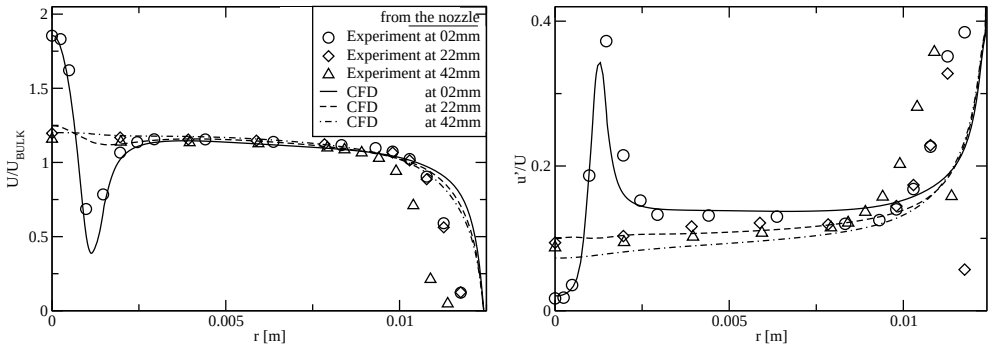

(a) (b)

Figure 4.7: (a) Normalized axial velocity along the radial direction. (b) Normalized r.m.s. of axial velocity along the radial direction at different axial locations (2 mm, 22 mm, 42 mm). Experimental conditions as in table 4.1.

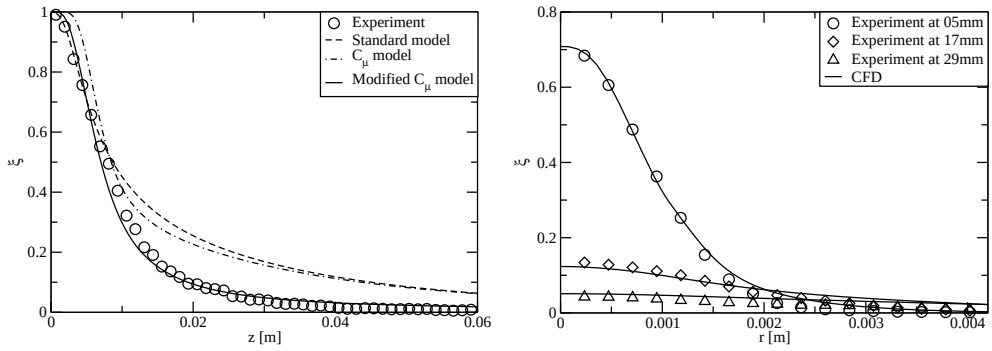

(a) (b)

Figure 4.8: Favre-mean mixture fraction ($\widetilde{\xi}$), comparison (a) along the axis among (i) standard closure, (ii) turbulent flux, (iii) turbulent flux with modified C_μ, (b) along the radial direction for closure (iii) at different axial locations (5mm, 17mm, 29mm). Experimental conditions as in table 4.1.

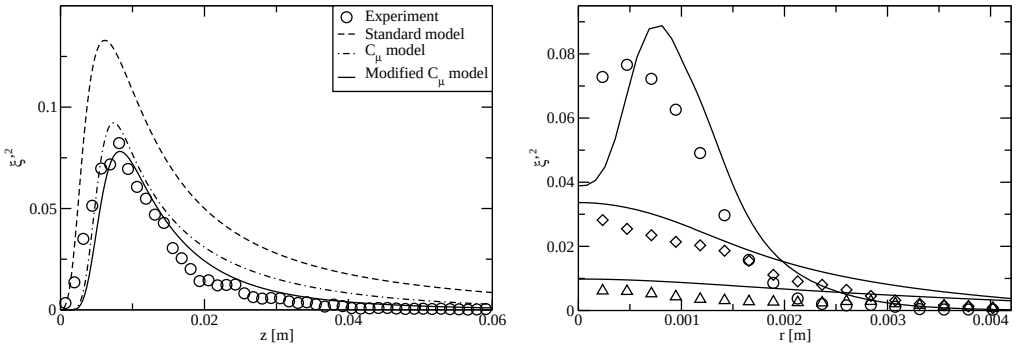

(a) (b)

Figure 4.9: Favre-mean variance of mixture fraction ($\widetilde{\xi''^2}$), legend as in figure 4.8.

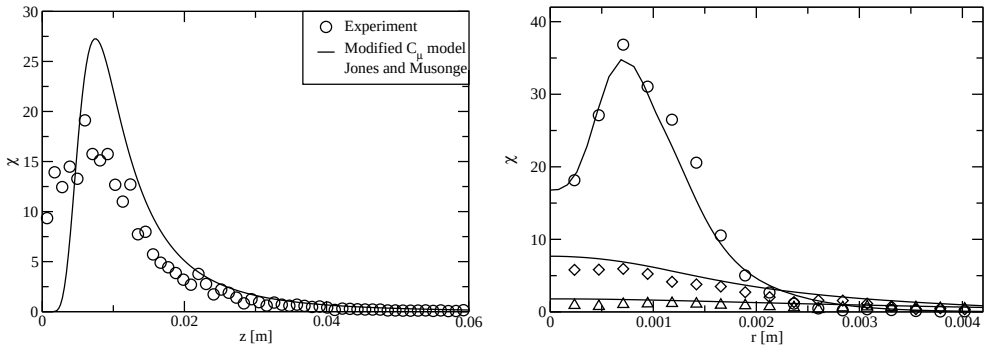

(a) (b)

Figure 4.10: Favre-mean scalar dissipation rate ($\widetilde{\chi}$) [1/s], (a) along the axial direction, (b) along the radial direction at locations as in figure 4.8.

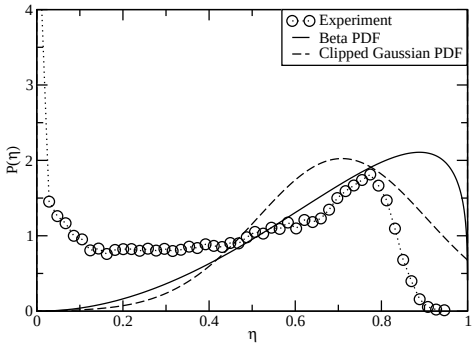

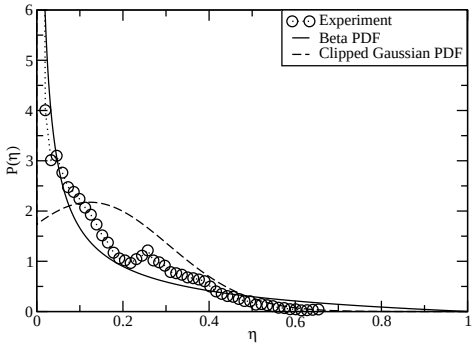

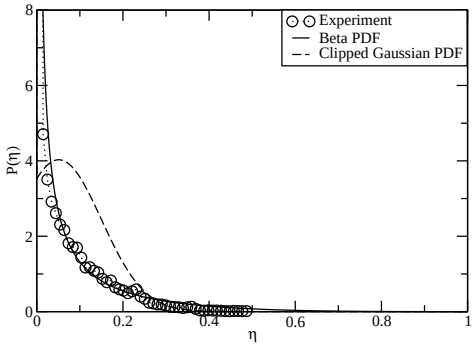

(c)

Figure 4.11: Probability density function of mixture fraction $P(\eta)$. Comparison between experiments and prediction using the β-function and clipped-gaussian along the centerline. (a) 5mm, (b) 17mm, (c) 29mm.

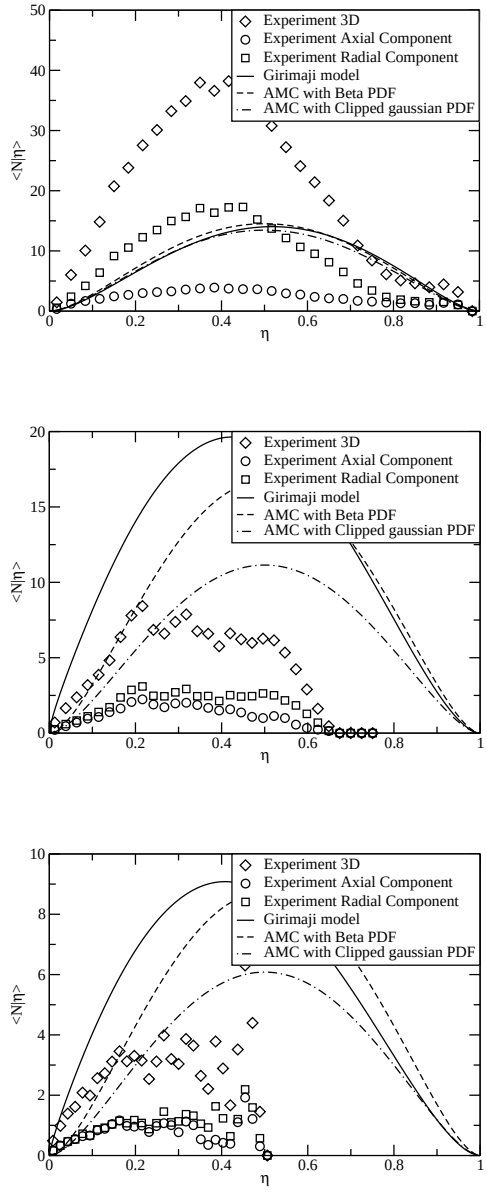

(c)

Figure 4.12: Conditional scalar dissipation rate $\langle N|\eta\rangle$, comparison among experiment, AMC - β-function, AMC - clipped gaussian and Girimaji - β-function. The experimental measurements report separately the radial $\langle N|\eta\rangle_r$ and the axial component $\langle N|\eta\rangle_z$. At the centerline the estimated $\langle N|\eta\rangle$ is $2 \times \langle N|\eta\rangle_r + \langle N|\eta\rangle_z$. Locations as in figure 4.11.

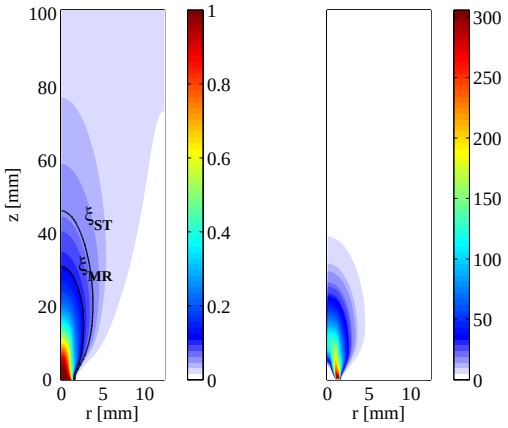

(a)

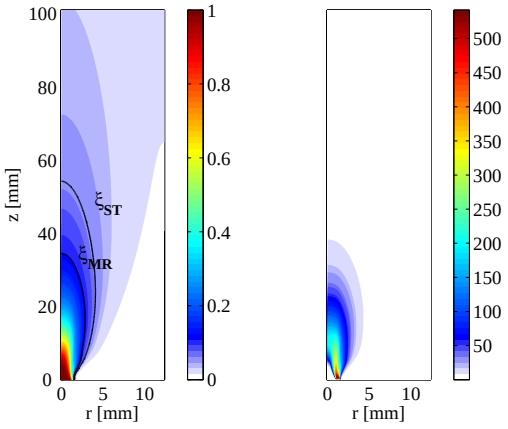

(b)

Figure 4.13: $\widetilde{\xi}$ and $\widetilde{\chi}$ [1/s] at hot conditions as for auto-ignition experiments at (a) $U_{AIR} = 13.8$ m/s, (b) $U_{AIR} = 17.64$ m/s. Experimental conditions in table 4.1. $\xi_{ST} = 0.065$, $\xi_{MR} = 0.12$.

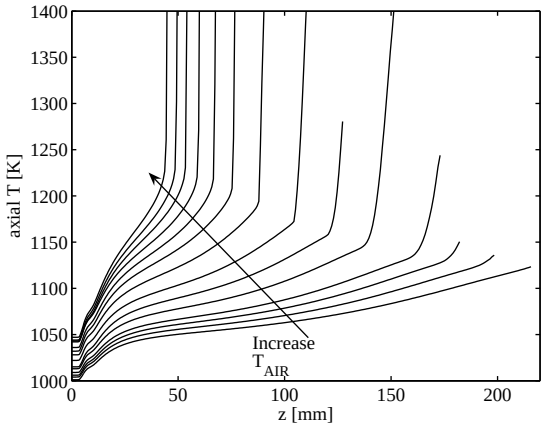

(a)

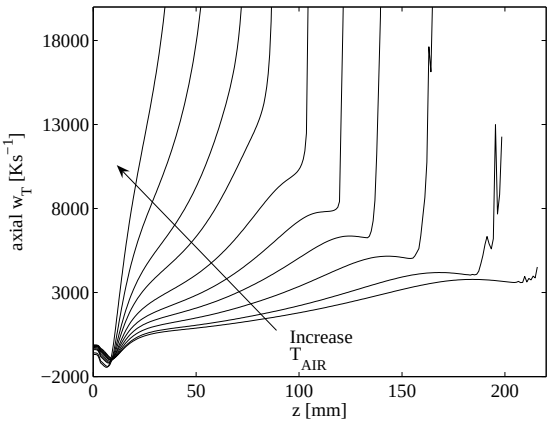

(b)

Figure 4.14: (a) Favre-mean temperature ($\widetilde{T}$), (b) Temperature reaction rate ($\widetilde{W_T}$) profile along the centerline. Case $U_{AIR} = 17.64$ m/s. Sensitivity to T_{AIR}.

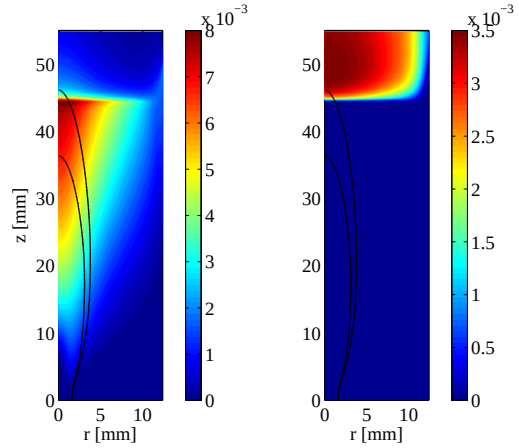

(a)

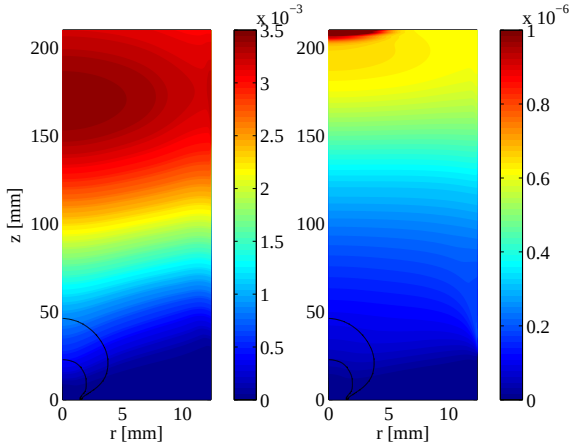

(b)

Figure 4.15: Typical results for autoignition obtained using the CMC parabolic formulation. (a) $T_{AIR} = 1155$ K $T_{FU} = 1047$ K (b) $T_{AIR} = 1055$ K $T_{FU} = 1001$ K. (left) $\widetilde{Y}_{CH_2O}$, (right) $\widetilde{Y}_{OH}$. Case $U_{AIR} = 17.64$ m/s.

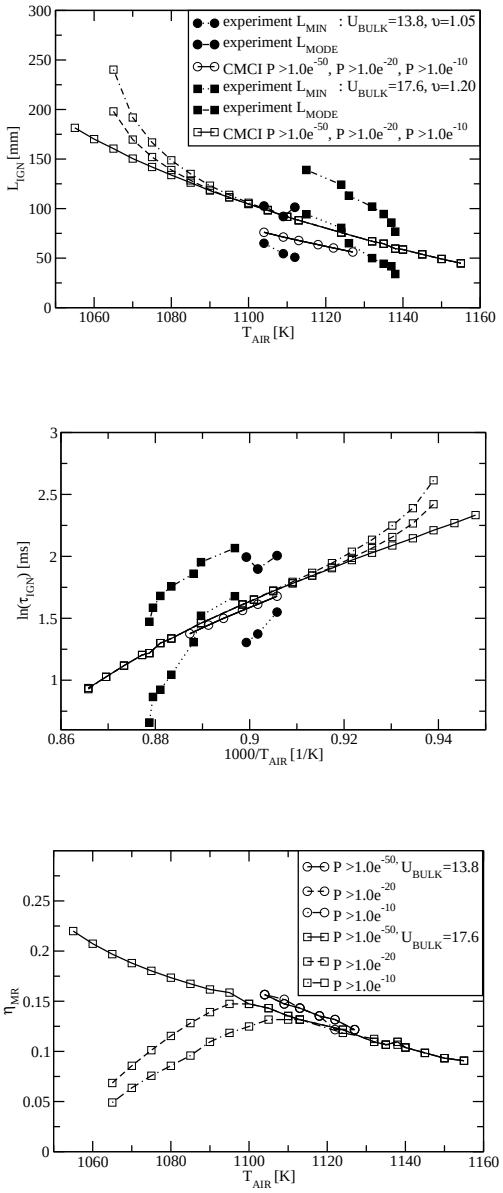

(c)

Figure 4.16: (a) Minimum L_{MIN} and L_{MODE} as a function of T_{AIR}. (b) Natural logarithm of autoignition delay times, τ_{MIN} and τ_{MODE} based on L_{MIN} and L_{MODE} function of the inverse of T_{AIR}. (c) Location of η_{MR} defined as the location of maximum conditional temperature in η-space at auto-ignition function of T_{AIR}. Sensitivity of prediction on the threshold of finite $P(\eta)$.

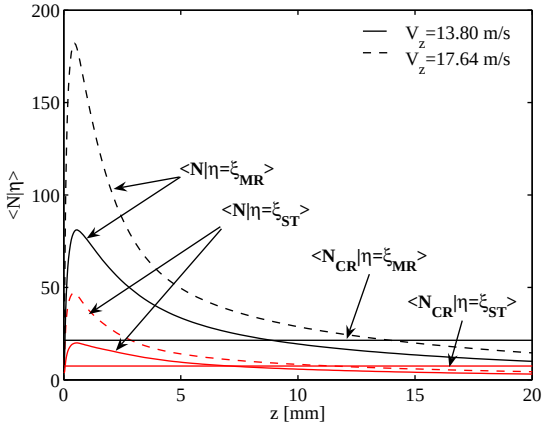

(a)

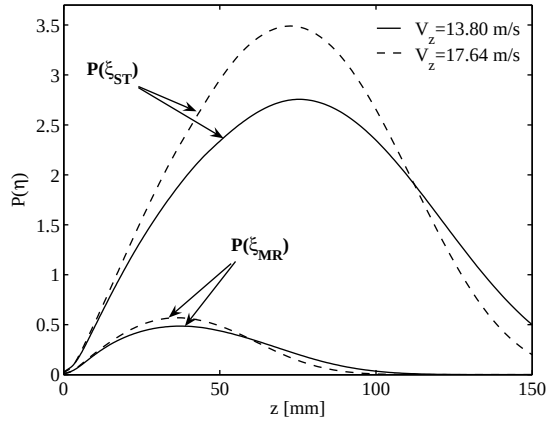

(b)

Figure 4.17: Axial evolution for $\langle N|\eta = \xi_{MR}\rangle$ and $\langle N|\eta = \xi_{ST}\rangle$ for both low and high velocity cases. (a) Comparison with $\langle N|\eta\rangle_{CR}$ calculated in figure 4.6.(b) Axial evolution for $P(\xi_{MR})$ and $P(\xi_{ST})$ for both low and high velocity cases. $\xi_{ST} = 0.065$, $\xi_{MR} = 0.12$.

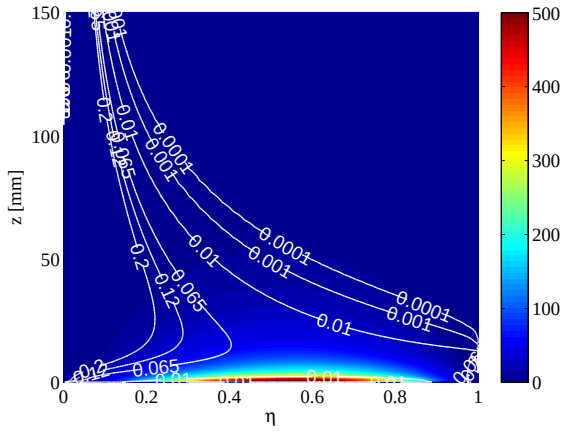

(a)

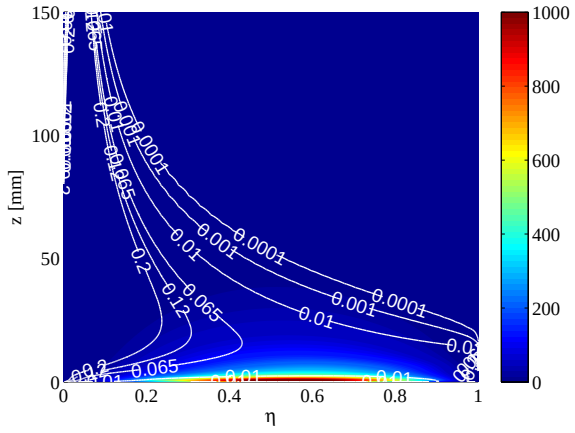

(b)

Figure 4.18: Iso-lines of $P(\eta)$ (in white) super imposed to iso-contours of $\langle N|\eta\rangle$ [1/s] along the axial direction. Case at (a) $U_{AIR} = 13.8$ m/s, (b) $U_{AIR} = 17.64$ m/s.

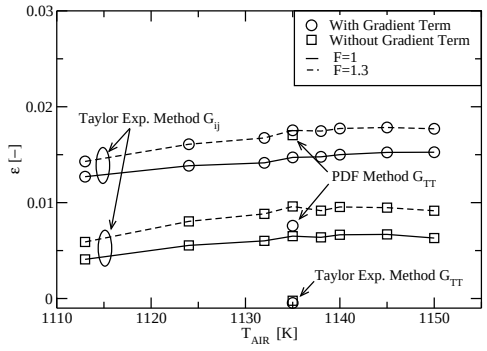

Figure 4.19: Relative difference in the auto-ignition predictions between first- and second-order parabolic CMC. Second-order CMC closed using a Taylor expansion method, applied to all reactive species in the chemical mechanism. $\epsilon = \frac{CMCI-CMCII}{CMCI}$. Sensitivity on the value $F = \frac{\langle N''^2|\eta\rangle^{1/2}}{\langle N|\eta\rangle}$, (a) including and (b) not including the gradient terms into the parabolic formulation.

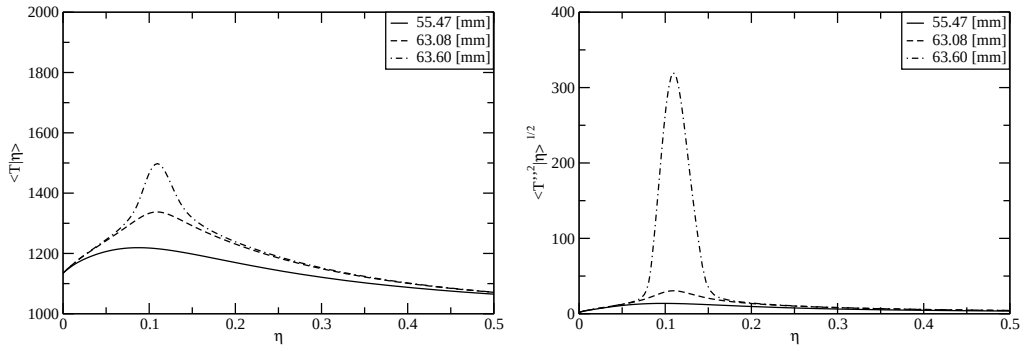

(a) (b)

Figure 4.20: (a) Evolution of $\langle T|\eta\rangle$ and (b) $\langle T''^2|\eta\rangle^{1/2}$ at 55.47 mm, 63.08 mm, 63.60 mm from the injector. Simulation conditions: $U_{AIR} = 17.64$ m/s, $T_{AIR} = 1113$ K, $T_{FU} = 1030$ K, $F = 1$.

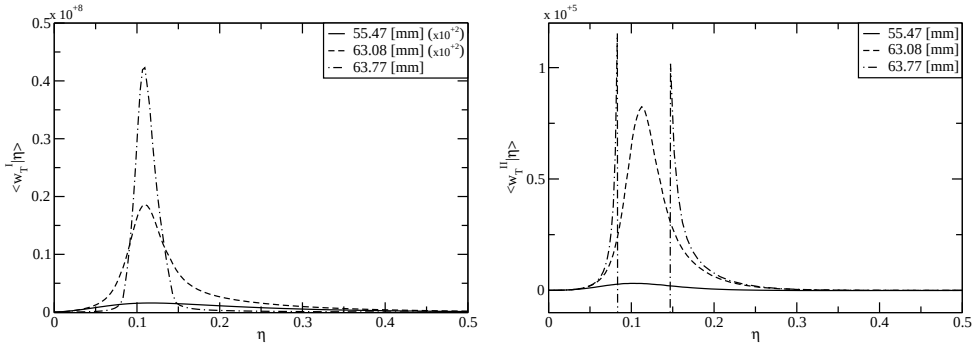

(a) (b)

Figure 4.21: Evolution of the reaction rate (a) first-order term, (b) second-order term. Simulation conditions as in figure 4.20.

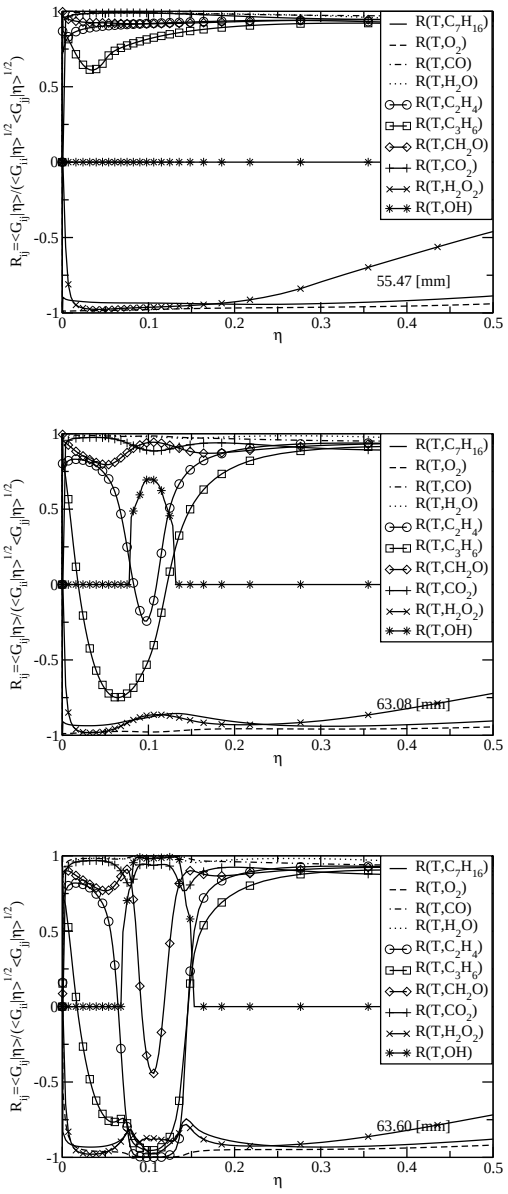

(c)

Figure 4.22: Evolution of the correlation coefficient R_{ij} between temperature and some of the most significant species during auto-ignition at (a) 55.47 mm, (b) 63.08 mm, (c) 63.60 mm from the injector. Simulation conditions as in figure 4.20.

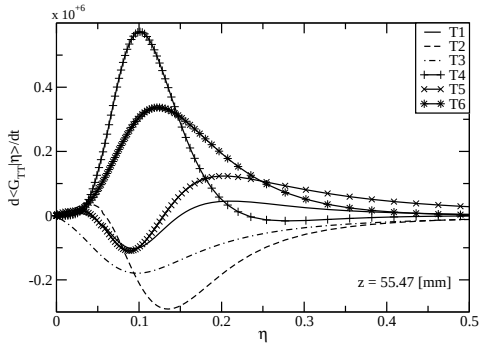

(a)

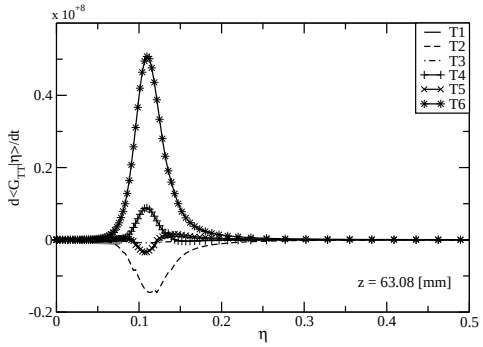

(b)

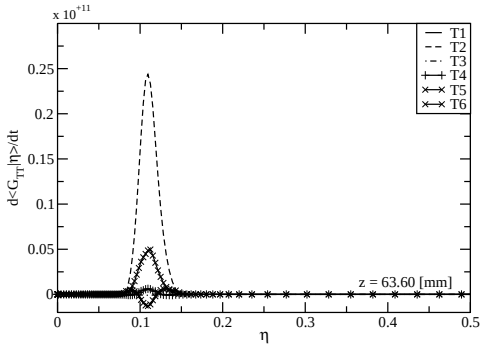

(c)

Figure 4.23: Balance of terms in G_{TT} transport equation at (a) 55.47 mm, (b) 63.08 mm, (c) 63.60 mm from the injector. Simulation conditions as in figure 4.20.

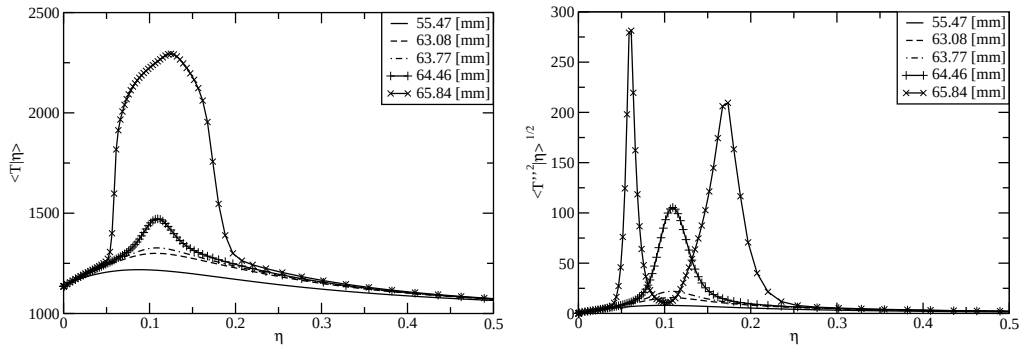

(a) (b)

Figure 4.24: (a) Evolution of $\langle T|\eta\rangle$ and (b) $\langle T''^2|\eta\rangle^{1/2}$ at 55.47 mm, 63.08 mm, 63.77 mm, 64.45 mm and 65.84 mm from the injector. second-order parabolic CMC closed using a Taylor expansion method using only the G_{TT} transport equation. Simulation conditions: $U_{AIR} = 17.64$ m/s, $T_{AIR} = 1113$ K, $T_{FU} = 1030$ K, $F = 1$.

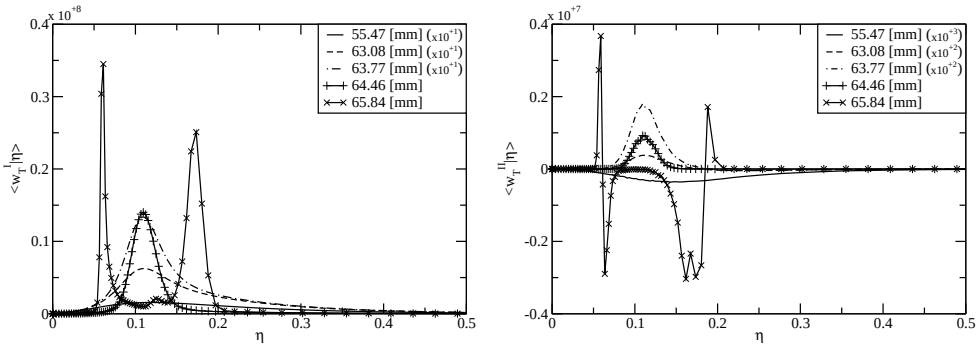

(a) (b)

Figure 4.25: Evolution of the reaction rate (a) first-order term (W_T^I), (b) second-order term (W_T^{II}). Simulation conditions as in figure 4.24.

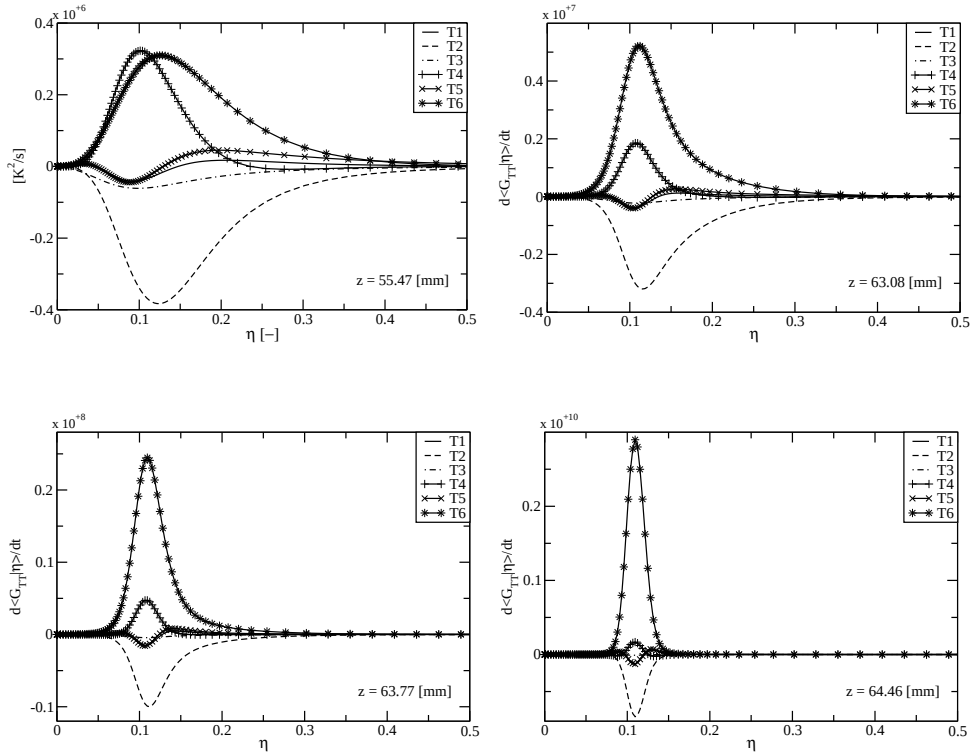

(c

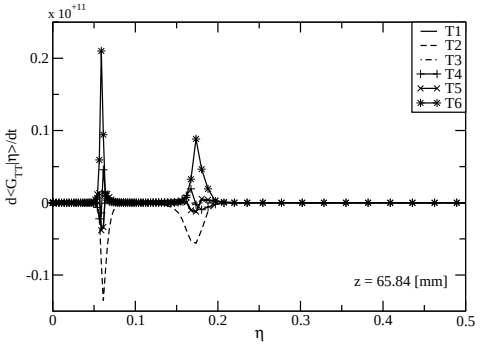

(e)

Figure 4.26: Balance of terms in G_{TT} transport equation at (a) 55.47 mm , (b) 63.08 mm, (c) 63.77 mm, (d) 64,46 mm, (e) 65.84 mm from the injector. Simulation conditions as in figure 4.24.

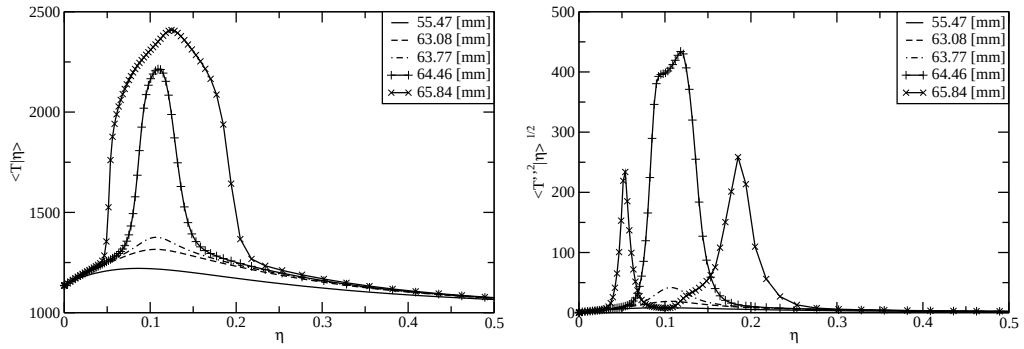

(a) (b)

Figure 4.27: (a) Evolution of $\langle T|\eta\rangle$ and (b) $\langle T''^2|\eta\rangle^{1/2}$ at 55.47mm, 63.08mm, 63.77mm, 64.45mm and 65.84mm from the injector. second-order parabolic CMC closed using a joint-PDF method using only the G_{TT} transport equation. Simulation conditions: $U_{AIR} = 17.64$ m/s, $T_{AIR} = 1113$ K, $T_{FU} = 1030$ K, $F = 1$.

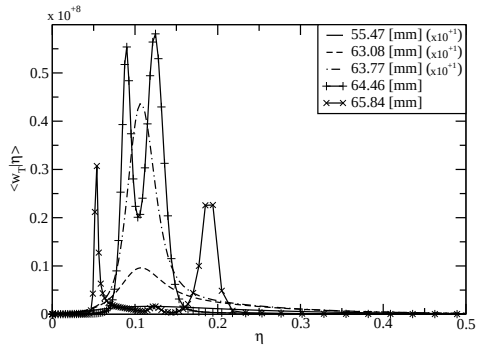

Figure 4.28: Evolution of the reaction for conditions as in figure 4.27.

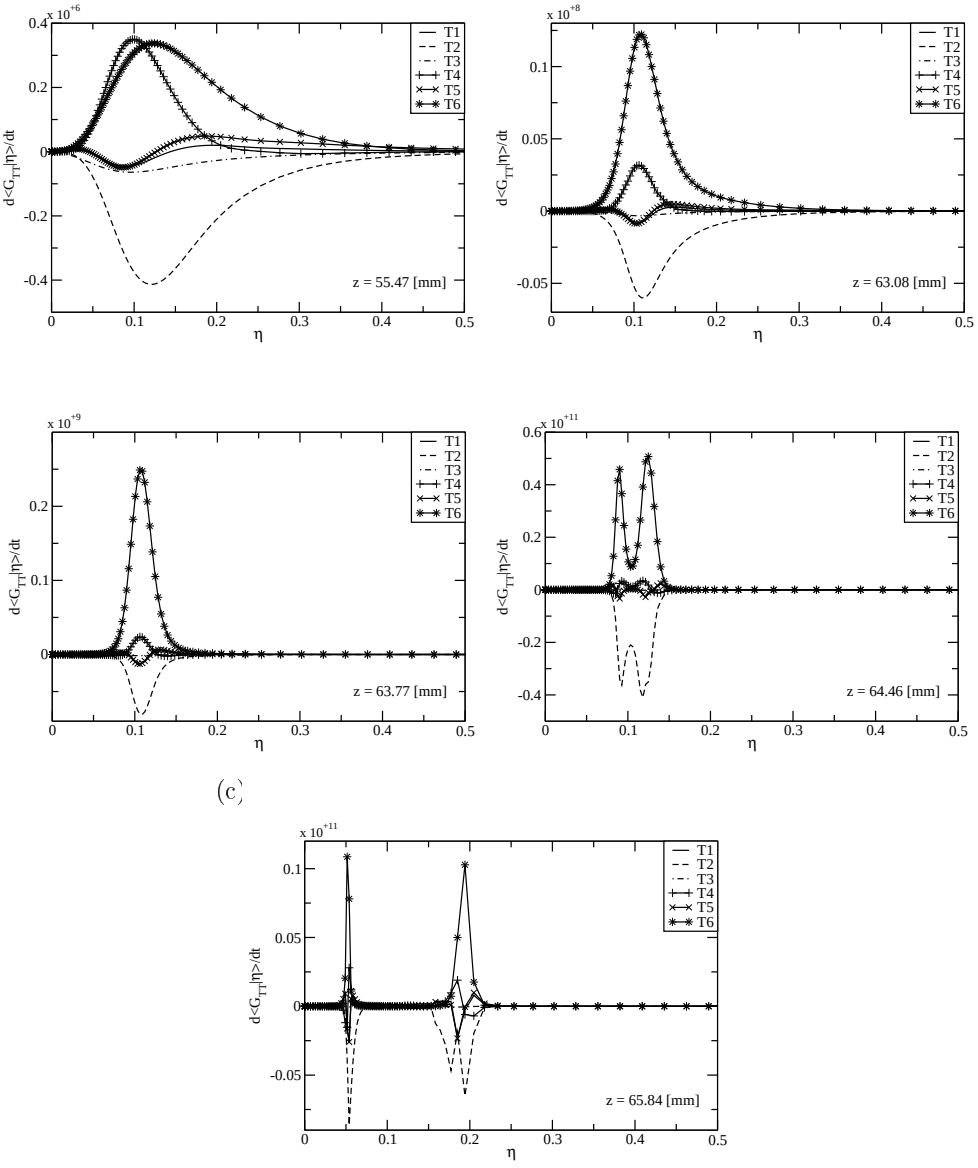

(c)

(e)

Figure 4.29: Balance of terms in G_{TT} transport equation at (a) 55.47 mm, (b) 63.08 mm, (c) 63.77 mm, (d) 64,46 mm, (e) 65.84 mm from the injector. Simulation conditions as in figure 4.27.

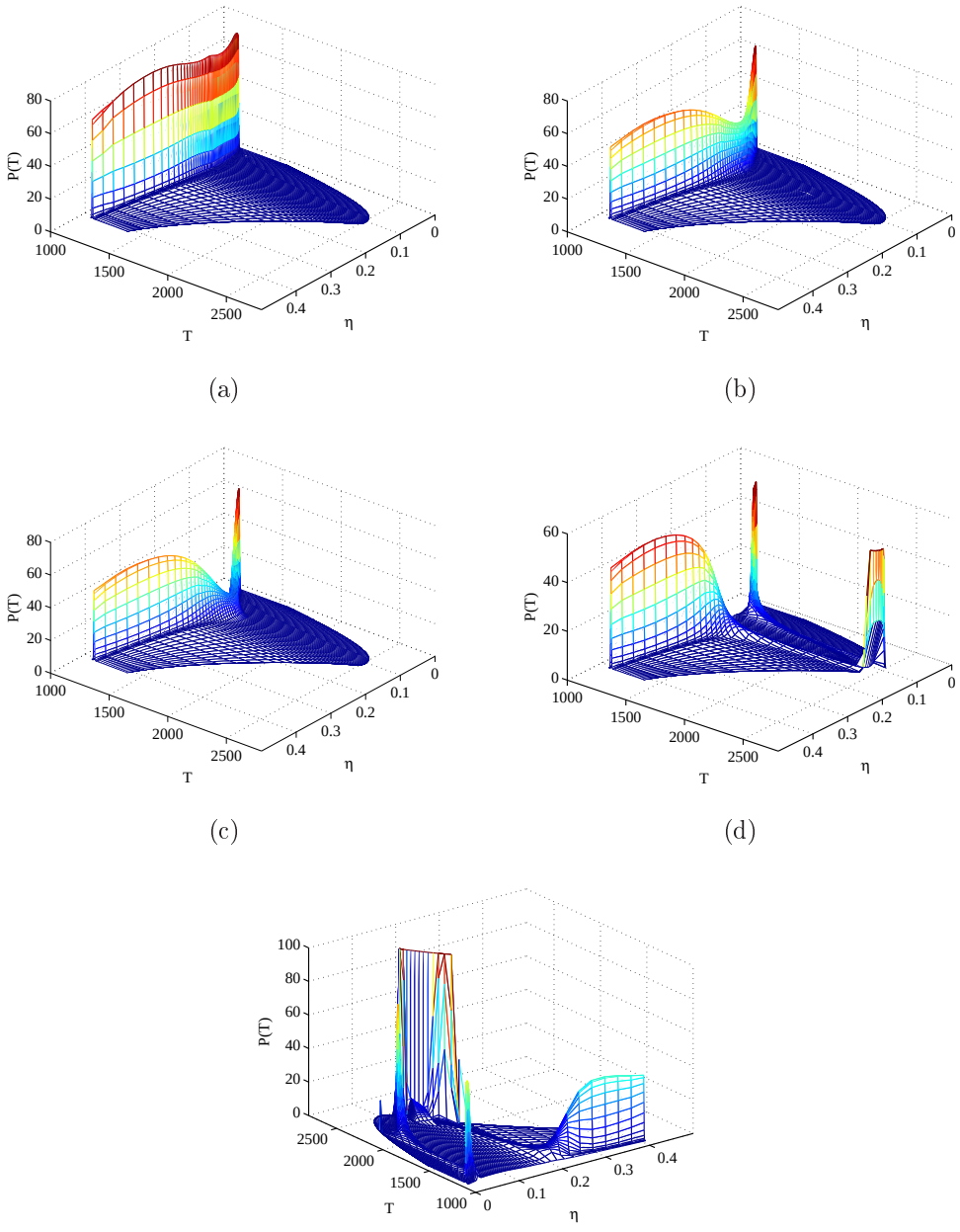

Figure 4.30: Evolution of the conditional pdf of temperature $P(T|\eta)$ assumed to be a β-function, at (a) 55.47 mm, (b) 63.08 mm, (c) 63.77 mm, (d) 64,46 mm, (e) 65.84 mm from the injector. Conditions as in figure 4.27.

Chapter 5

Results - II Autoignition in a high pressure spray bomb

Unsteady n-heptane spray autoignition in a diesel engine-like environment has been investigated using a multidimensional CMC model with first-order closure for the conditional chemical source term. The objectives of the present chapter are to investigate the mechanism of autoignition and flame development in dense sprays under different turbulent conditions. Considering the elliptic axisymmetric CMC predictions as a reference, different modelling approximations have been considered to reduce the computational domain of solution, hence improve the numerical efficiency of the code. The present test case has been, furthermore, considered to validate the code implementation and the integration procedure described in chapter 3 in terms of accuracy and numerical efficiency. The chapter closes with various conclusions and additional note on droplet evaporation modelling in CMC.

5.1 Background and objectives

Autoignition and combustion in spray-driven fuel jets in high-pressure, high-temperature combustion chambers, have been extensively studied as representative of diesel engine combustion (Dec (1997), Verhoeven et al. (1998), Pickett and Siebers (2004)). Here, an evaluation of the CMC developments for transient au-

toignition calculation will be given. Some comments specific to spray are included at the end of this chapter.

Diesel spray combustion is indeed an unsteady problem, in which the effects of density variation, in particular during the flame propagation phase following autoignition, are not negligible and requires, therefore, a two-way coupling of the combustion model with the fluid-mechanics solver. Examples of unsteady autoignition calculations using the CMC model can be found in Kim et al. (2000a) and Kim and Huh (2002) for, respectively, a methane jet and n-heptane spray. The combustion code was solved in parallel with a CFD solver, to which only the unconditional temperature was reported, calculated as the convolution of the conditional one with the local mixture fraction PDF. A fractional step method was used to integrate the CMC equations, therefore treating transport and reaction term sequentially. The CMC grid employed was much coarser than the CFD one in the hypothesis of weak dependence of the conditional scalars from spatial coordinate and a 50-node grid clustered around the stoichiometric mixture fraction was used to discretize η-space. The results were presented in terms of autoignition delay for a case in which no initial turbulence was present prior injection with reasonable agreement against experimental measurement.

Interesting developments in the solution of the CMC equations are presented in Cleary et al. (2002) and in Rogerson et al. (2007). A finite volume formulation was implemented using the same computational mesh for both CFD and CMC solution. Furthermore, the idea of a η-domain reduction was presented based on the existence of finite-width PDF of mixture fraction and justified by numerical efficiency arguments so that only few of the defined grid-nodes were effectively solved. The calculations performed were steady.

To the author's knowledge, an unsteady calculation to investigate the flame propagation subsequent the autoignition event, using the CMC model, has not been realized yet. Such a test case can give interesting insight into autoignition and the flame structure during the first development. Furthermore, it represents a test-bench where the applicability of the developed closures and the integration procedure for a transient calculation can be verified. It is also an important first step towards the diesel engine simulations of next chapter.

One of the limiting factors for the application of the CMC model to combustion simulation in realistic geometries has always been the limited computational efficiency determined by the addition of an extra dimension (η-space) and by the stiffness of the complex chemistry used. A more efficient integration of the CMC equation would result to more affordable CMC calculations for real industrial problems.

The diesel spray combustion studied in this chapter models a dense spray configuration representative of an external sheath combustion in the combustion diagram proposed by Chiu et al. (1982). Qualitative studies performed by Verhoeven et al. (1998) show that autoignition occurs in the vapour cloud in region at the tip or at the edge of the spray depending on the spray characteristics far from the liquid core. The focus of the present chapter is on the effect that turbulence has on autoignition and on the flame development as well as a validation of the numerical method used, hence, at a first approximation, the effects of droplet vaporization will not be considered. This assumption can be restrictive in particular during the flame stabilization at the typical diesel spray lift-off height (Dec (1997)) but it might be acceptable for autoignition and the early stage of flame development. Future work is aimed to extend the present formulation to include the effect of the evaporating dispersed phase.

5.2 Experimental configuration

A very comprehensive set of data of an autoigniting n-heptane spray in a high-pressure, high temperature open reactor with laminar or turbulent background flow has been presented in Koss et al. (1992). The reactor consisted of a 90mm diameter vessel and the fuel was injected along the centerline in the direction of the co-flowing hot air. Figure 5.1 shows a representation of the burner. The air was pressurized at 50bar and at a temperature ranging between 783 and 823K. It is reminded that the n-heptane critical conditions are at 27.4 bar and 540.3 K. The spray evaporation rate is expected to be strongly dependent on the spray dispersion. Details of the conditions are listed in Table 5.1. A number of different temperatures were investigated, with and without initial turbulence prior to injection. Turbulence was generated by a rapid motion of a perforated plate

in the axial direction and was accompanied by laser optical measurements, indicating when the mean velocity had completely decayed and only the fluctuations remained. The turbulent setup was modeled using an initial turbulence intensity and length scale of respectively 2.5 m/s and 10mm, values estimated from the experimental data. The ignition delays are defined based on the detection of light emission in the UV and visible range by means of three optical fibers and photomultipliers as described in Koss et al. (1992).

5.3 Numerical method

The CMC model has been integrated within the CFD package STAR-CD (2004) to resolve unsteady turbulent combustion. Details on its implementation and coupling are reported in chapter 3. Here, the modelling options chosen respectively in the CFD and in the CMC settings are reported and discussed.

The flow has been considered axi-symmetric and a two-dimensional grid, clustered along the injector axis has been constructed. The liquid phase has been modeled by a Lagrangian-Eulerian particle tracking procedure, denoted as a standard discrete-droplet model (DDM), in which the physical spray is represented by a finite number of computational parcels. The Reitz-Diwakar model with standard model constants has been used for both the atomization process (with a prescribed cone angle of 10 degrees) and the secondary break-up. Turbulence is modeled by the κ-ε RNG model. Documentation concerning both models implementation can be found in STAR-CD (2004). The thermo-physical properties of the fuel, initialized as liquid n-heptane, were defined internally into the CFD solver. Enthalpy in STAR-CD is solved in the form of the total enthalpy and care was taken to ensure that all species thermodynamic properties were the same in the two codes. No heat transfer to solid boundaries and no radiation were considered. No transport equations for the species mass fractions were required in the flow-field solver, as the species mass fractions were computed by the CMC. The mean values returned to STAR-CD were obtained by integrating the conditional averages over the (presumed) PDF in conserved scalar space. A β-function PDF of the mixture fraction was assumed, which is controlled by its first two moments, therefore transport equations for the mean and variance of the

mixture fraction were solved by STAR-CD. Standard modelling procedures were employed for both equations (STAR-CD (2004)). It is emphasized here that full coupling between the combustion model and the aerodynamics calculation has been hence achieved, with the only caveat that the conditional averages respond to the mixing field corresponding to the beginning of the (CFD) timestep, while the aerodynamics respond to the density field corresponding to the end of the previous timestep. However, this inconsistency introduces almost negligible errors, as the CFD timestep is small enough to adequately resolve even the sharpest transients during the evolution of the spray.

Equation 3.2 was implemented, therefore adding to the convection term the contribution of the PDF derivative. Finite differences were used to discretize the CMC equations (equation 3.2). The convection term uses an upwind differencing scheme, whilst central differences are applied for the diffusion terms in both conserved scalar space and real space. Standard practice was used to model the unclosed terms in the CMC equations: the linear model for the conditional velocity (equation 2.71), the Amplitude Mapping Closure (equation 2.69) model for the conditional scalar dissipation rate and first order closure for the conditional reaction rate (equation 2.57) using the n-heptane chemical mechanism (Bikas (2001)) validated in chapter 4. In conserved scalar space, 101 nodes were used, clustered around the stoichiometric value to enhance resolution in this region. The most reactive mixture fraction ξ_{MR}, which is the mixture fraction where auto-ignition is expected (Mastorakos et al. (1997a)), is close to stoichiometry for the present chemistry and conditions (as we shall see later) and hence this resolution is retained as adequate to resolve both autoignition and flame propagation. The CMC grid in spatial coordinates, was defined to have high resolution along the axis where autoignition was expected. A structured grid of 27×40 nodes respectively in the radial and axial direction was used with a one to one correspondence between CFD and CMC grid was obtained in the region of interest to resolve ignition and the first propagation of the flame.

In order to improve the computational efficiency of the code, different integration procedures have been tested. In one approach, the CMC transport equations have been discretized by the method of lines (MOL) in a large set of ordinary differential equations (ODEs). These were subsequently integrated with the stiff

integrator VODPK (Byrne (1992), Brown et al. (1989), Brown and Hindmarsh (1989)). An alternative way to solve the CMC equations is the Operator Splitting (OS), or fractional step, approach. In the present implementation the chemical (and stiff) part of the system was separated from the non-stiff convection-diffusion part. In a first implementation the physical space transport was hence computed in a first step, followed by a second step solving together the reaction and diffusion in conserved scalar space part of the whole CMC equation (OS1, equation 3.3). Alternatively, a third step can be introduced splitting further the conserved scalar space (OS2, equation 3.4). The advantage of this method is (i) the reduced number of ODEs solved simultaneously and (ii) the possibility to use two different solvers for each sub-step depending on the characteristics of the ODE system. The errors that occur using OS methods are largely described in Schwer et al. (2003). The use of an Operator Splitting method, furthermore, allows an easy parallelization procedure in which, as explained in chapter 3, the physical transport can be calculated into the main node while homogeneous CMC calculations can be proceed in parallel on multiple processors.

Different settings were therefore considered here in order to estimate the influence of splitting error and of the solver on ignition timing. At first a validation of OS2 was performed using a homogeneous CMC formulation. This simple configuration aims to assess the influence of the splitting on autoignition and flame propagation in conserved scalar space. The results for the simultaneous integration have been compared with the sequential one using four different splitting timesteps 1×10^{-5}s, 1×10^{-6}s, 1×10^{-7}s and 1×10^{-8}s for increasing values of the conditional scalar dissipation rate. VODPK was used, maintaining the same tolerances throughout all calculations. The choice of using OS2 as method of integration not only reduces even further the size of the system the solver has to integrate, but allows to evaluate the chemical source term, and more computationally expensive part, only for the grid-nodes with finite mixture fraction PDF with consequent improvement in computational time. This is not only determined by efficiency criteria as stated in Cleary et al. (2002) and in Rogerson et al. (2007) but is fundamental as described in chapter 4 to define the limit of integration in η-space. The additional advantage to solve the chemistry in a separate step is

the possibility to use a tabulated chemistry to evaluate the chemical source term; however, this extension has not been investigated in the present work.

To separate the effects of the splitting in conserved scalar and physical space, the OS1 formulation have been applied to the elliptic spray combustion and the results compared with the ones obtained with the MOL with quite tight tolerances (absolute tolerance 1×10^{-14}, relative tolerance 1×10^{-6}), considered as the 'exact' solution. The physical space transport part of the equations was solved implicitly by VODPK using non-stiff settings, although any other conventional solution method for elliptic convection-diffusion equations would do equally well. Two different solvers were tested for the solution of the stiff part, i.e. reaction and diffusion in conserved scalar space. One of these used VODPK with the same settings as in the MOL code. Because the solution for each grid point has to be recalculated 'from scratch' at each time-step, VODPK (like other BDF methods) suffers from high restart costs due to the recalculation of the Jacobian matrix for the very small (internal) time-steps used at the beginning of the time-step. An alternative ODE solver called CHEMEQ2 has recently been presented and claimed to have very small restart costs (Mott et al. (2000)) and is also explored here. It is a single point method so the restart costs should be small compared to VODPK, but the solver may be less accurate. The accuracy of the solution with CHEMEQ2 is validated against the MOL and also against the one obtained with the OS code using VODPK in the stiff reaction-diffusion part. The second comparison assesses the magnitude of the splitting error as it avoids any influence coming from the choice of the stiff solver.

The CFD solver used a time-step of 1×10^{-6}s, which also denotes how often the aerodynamics (i.e. velocities, diffusivity, mixture fraction field, scalar dissipation rate, pressure, and pressure rate of increase) was updated. Results for two different splitting time-steps for the CMC equation are reported: (a) 1×10^{-6}s, where for each CFD time-step the CMC equations are solved in only two sub-steps and (b) 1×10^{-7}s, where for each CFD time-step ten internal CMC time-steps have been used, each of which was further divided into two sub-steps. The timestep of the MOL solver, called every outer CFD timestep, was internally determined.

5.4 Results and discussion

The results in this section validate the numerical method used to integrate the elliptic CMC equation. Results for an homogeneous CMC have been used used to validate the chemical mechanism at these particular conditions as well as the splitting procedure defined as OS2. A sensitivity analysis on the integration procedure and on the stiff solver used follows for the elliptic spray autoignition test-case. Besides the accuracy of the method, particular emphasis is given to the numerical efficiency of the method evaluated in terms of computational time (CPU time).

The results in terms of autoignition delay as function of temperature are given next for both turbulent and non-turbulent cases. The effects of turbulence on the structure of the spray and on autoignition will be described. An analysis of the different terms in the conditional temperature equation will be reported in the aim of analyze the flame propagation phase of combustion.

5.4.1 Solver comparison

The reaction rates throughout this chapter have been calculated using the 31-species reduced mechanism by Bikas (2001) based on a detailed mechanism of n-heptane from Hewson (1997). The mechanism was validated in chapter 4 for homogeneous auto-ignition against shock-tube experiment and for high-temperature inhomogeneous autoignition experiments. The condition investigated in the spray autoignition experiment falls in the region of NTC as defined from figure 4.3. At this temperature range a typical two-stage ignition process is present as discussed in Liu et al. (2004). Figure 5.2 shows the evolution of the conditional temperature and its derivative in time, predicted by a transient igniting homogeneous CMC at constant value of the scalar dissipation rate $N_0 = \langle N|\eta = 0.5\rangle = 10$ 1/s. The time derivative plot, in particular, shows explicitly the effects of the NTC evident from the initial rise of temperature prior the main autoignition event.

As additional validation of the chemical mechanism, homogeneous CMC calculations have been performed over a wide range of N_0 using VODPK solver for both detailed and reduced mechanisms. The fair agreement evident in figure 5.3 shows also that the critical scalar dissipation rate above which no ignition occurs

is close to 100 1/s for the studied pressure and fuel and oxidiser temperatures. This value will prove useful later on during the discussion of the spray autoignition results in the turbulent spray analysis. Additionally figure 5.3 shows, as a preliminary comparison, the same calculations repeated using CHEMEQ2. Results compares favourably to the results from VODPK throughout the entire range of N_0 examined. This justifies the use of CHEMEQ2 for reaction-diffusion problems, hence extending the regime of use of this solver from the one originally described by its developers (Mott et al. (2000)). CHEMEQ2 encountered some instability problems at high scalar dissipation rates, but these were controlled by tightening the internal tolerances of the solver.

The same homogeneous calculations have also been used to validate the OS2 methodology. In this case, we refer for simplicity only to the VODPK solver. The analysis of the error due to the sequential solution of the diffusion and reaction terms have been evaluated as function of the time splitting (Δt_{SPLIT}) and $\langle N|\eta\rangle$. Figure 5.4(a) shows ignition delay (τ_{IGN}) as function of η for two conditions of $\langle N|\eta\rangle$ (10 and 60 s^{-1}). The differences with respect to the MOL solution is given by Δt_{SPLIT}. The piecewise linear profile of the curves is because the results are printed every 1×10^{-5}s. At low conditional scalar dissipation rate the autoignition time does not present differences, in the interval of confidence of 1×10^{-5}s. Nevertheless splitting has an effect in the propagation velocity of the flame, represented by the inverse of the curves derivative, which for large Δt_{SPLIT} is underpredicted. Note that the propagation velocity is affected by the preignition reactions and it is not necessarily the same than an ignition front caused by en external source of energy. At high conditional scalar dissipation rate case, closer to the critical value, autoignition is underpredicted for large Δt_{SPLIT}. This is due to an underestimation of the effects of diffusion in η-space which at this conditions tends to balance the chemical reaction term. The splitting error reduces reducing Δt_{SPLIT} and in general for $\Delta t_{SPLIT} = 1 \times 10^{-6}$s, equal to the time at which the CFD solution is updated, the error is reasonable. Interesting results are shown in figure 5.4(b) concerning the CPU time. OS2 is computationally more efficient. Its benefits are noticeable in particular during the propagation phase when the MOL has a sharp increase in CPU time.

The results reported next aim to assess the influence of the splitting between physical and η-space and the effect of the solver choice, so only OS1 will be considered. All computations in this section refer to the n-heptane spray setup at 823 K with initial turbulence. Four different methods (denoted M1 to M4 in the following) are presented here: MOL solved with VODPK (M1), OS1 with $\Delta t_{SPLIT} = 1 \times 10^{-7}$s solving the reaction-diffusion sub-step with VODPK (M2), OS1 with $\Delta t_{SPLIT} = 1 \times 10^{-6}$s solving the reaction-diffusion sub-step with VODPK (M3), and OS1 with $\Delta t_{SPLIT} = 1 \times 10^{-7}$s solving the reaction-diffusion sub-step with CHEMEQ2 (M4). Hence, a comparison between M2 and M4 checks CHEMEQ2 against VODPK for the reaction-diffusion stiff part of the system, while a comparison between M2 and M3 checks the effect of Δt_{SPLIT}. A comparison with the exact solver M1 shows the accuracy of the method. A comparison of the conditional temperature and of the OH mass fraction is shown in figure 5.5 for a node on the axis and at the tip of the spray 1.0 ms after start of injection. It is evident that the differences are very small. The Favre-averaged temperatures are compared in figure 5.6 for the same time for solvers M1 and M4 and very good agreement is evident. Since both the conditional averages and, in consequence, the spatial distributions of the unconditional averages are very similar, we conclude that the operator splitting method is accurate, as long as the fractional timestep is not too large.

Finally, we compare the computational cost of the different approaches. For the current conditions, ignition occurs around 1.35 ms. Figure 5.7(a) shows that a rapid increase in CPU time occurs when auto-ignition occurs, an observation typical of all solvers and conditions. Operator splitting results in a significant reduction of CPU time: considering the more accurate solution M1, the gain is one order of magnitude. M4 has a computational cost similar to M3 in the phase up to ignition. Before ignition, and despite the restart cost of VODPK relative to CHEMEQ2 that would show in the use of the BDF method in the Operator Splitting code, solving the chemistry and mixture-fraction diffusion with VODPK is faster. However, after ignition, the benefits of CHEMEQ2 are very significant, as the MOL fails to advance in reasonable CPU times. The Operator Splitting code with CHEMEQ2 was the only solver that could advance the calculation until a full diffusion flame establishment, when OS1 was used.

Further test cases with CHEMEQ2 solver have shown that for high temperature condition close to equilibrium or for condition in which the diffusion is the most important term in the equation, CHEMEQ2 becomes unstable and an oscillatory solution is obtained. To avoid this problem OS2 (equation 3.4) has been implemented, since chemistry is solved separately CHEMEQ2 can be used without any stability problem. Furthermore, reducing the size of the working array, VODPK becomes more computationally efficient so that no significant difference in computational time was noticed between the two solvers in the present test case. Figure 5.7(b) shows a comparison in CPU time for OS1 and OS2 both using VODPK with the same tolerances and $\Delta t_{SPLIT} = 1 \times 10^{-6}$s. The solution in physical and conditional space are hardly distinguishable (not shown) and the CPU time, confirming what was demonstrated from the homogenous test case, is indeed favorable. The Operator Splitting method is clearly a way to to improve the computational efficiency of the CMC solver given a careful sensitivity analysis to the Δt_{SPLIT}. The solver VODPK has demonstrated better accuracy and stability properties so it has been considered as the solver of choice, nevertheless for very large systems a less accurate solver can be more efficient.

The Operator Splitting method apart from the improved efficiency, allows a natural parallelization of the code. As explained in chapter 3, a simple and efficient way to parallelize the code is to solve the physical transport part (non-stiff) onto the main node while the solution in η-space (stiff) can be performed in parallel on a multiprocessor machine. The result in CPU time is shown in figure 5.8 for OS1 using the auto-balancing algorithm proposed in chapter 3. The CPU time reported is the time spent from the cluster main node on the process without considering the data transfer among the different machines, therefore it would correspond to the effective CPU time for an infinite-band parallel machine. The scalability in this test case is almost linear.

5.4.2 Mixing field

For the test case modeled, calculated spray tip penetrations were compared with experimental data. To investigate the grid dependence expected from the Langrangian-Eulerian spray modelling used here, three different mesh resolutions

were compared and a suitable refinement selected. As can be observed in figure 5.9, the calculated spray tip penetration for this reference grid shows good agreement with the reported data. At the early stages, a slight over prediction is noticeable, which could be due to the simplified square injection profile. According to the experimental data, the presence of turbulence did not affect the macroscopic spray propagation. In the simulation, penetration for the set-up without initial turbulence was slightly higher at the later stages. These inaccuracies are typical in Diesel engine calculations and are due to the spray models used. The good agreement shown in figure 5.9 shows that the present CFD code is adequate for the problem considered and this suggests that the mixing field (mean and variance mixture fraction), for which no experimental data are available, should also be reasonably predicted.

5.4.3 Ignition delays: influence of turbulence

Figure 5.10 shows the comparison of the computed ignition delays with the experimental data. In both cases (with and without initial turbulence) the expected trend that a decreasing temperature increases the ignition delay time is captured well, which also gives further credence to the chemical mechanism used. The two solvers using respectively the MOL and the OS1 method of solution, predict somewhat different ignition times. This difference is attributed to CHEMEQ2 inaccuracy and to the splitting errors. If turbulence is present initially in the air, a reduction of the ignition delay can be observed in the experiment and this trend is captured successfully by the simulation. Various conclusions can be drawn from the data shown in figure 5.10. First, the fair agreement of the ignition delays predicted by the OS solution procedure with the ones obtained by the MOL for all six validation points confirms the validity of this approach, although the splitting errors are not negligible. Second, the predictions over-predict ignition delay by about 10%, which can be due to deficiencies in the spray modelling but also to the neglect of second-order terms in the chemistry term of the CMC equation, as we saw in chapter 4. However, we may conclude that the close agreement with experimental data suggests that the first-order CMC method is adequate for this problem, at least in the context of a practical calculation.

Next, we attempt to investigate the mechanisms by which the turbulence affects the ignition delay. Stand-alone CMC computations for a homogeneous CMC at a constant pressure of 50 bar and 823 K have been carried out to investigate the influence of the scalar dissipation rate on the ignition delay and the evolution of the conditional quantities and these were presented previously in figure 5.3. It is evident that, initially, the ignition delay decreases very slightly as the scalar dissipation rate increases until it reaches a minimum at a N_0 of around 10 1/s. For values larger than 25 1/s, a strong increase can be observed until we approach a scalar dissipation rate, for which ignition no longer occurs.

When examining the evolutions of the conditional temperature in figure 5.2(a), we observe the following. Starting from the frozen solution, the initial increase in temperature and the radical build-up takes place very close to the oxidizer. This observation is largely independent of the scalar dissipation rate. As time evolves, these radicals diffuse towards higher mixture fractions and ignition eventually takes place at a richer mixture fraction ξ_{MR}, which could be richer even than the stoichiometric value (ξ_{ST} =0.062), depending on the fuel and air stream temperatures and the scalar dissipation rate. For low values of $\langle N|\eta\rangle$, little diffusion in conserved scalar space takes place, and hence temperature and radicals are not transported to the mixture fractions favorable for ignition, hence providing an explanation for why the ignition time slightly decreases as N_0 increases from zero. For higher values of $\langle N|\eta\rangle$ that significantly retard the ignition delay, ξ_{MR} is approximately 0.085 at the prescribed conditions, found from examining the peak of the curve just before ignition in figure 5.2(a). The retardation in ignition time for high scalar dissipation rates is explained by the fact that heat diffuses from ξ_{MR} to other mixture fractions (see chapter 4). Hence we conclude that, depending on what scalar dissipation rates the spray experiences relative to the critical value (which depends on the chemistry, the fuel and oxidiser temperatures, and the pressure), its auto-ignition time may be made slightly faster, be uninfluenced, or retarded significantly by the turbulence.

In order to explore in more detail how the presence of turbulence alters the auto-ignition of the particular spray studied here, the evolution of the scalar dissipation rates at the most reactive mixture fraction for the nodes located on

the spray axis up to ignition are shown in figure 5.11 and figure 5.12. In the non-turbulent case (figure 5.11), non-zero values of the scalar dissipation rates start to appear earlier than in the turbulent case. This is true in particular for nodes between 24 mm and 60 mm from the nozzle and is supported by the slower spray propagation in the presence of initial turbulence as mentioned previously. In the turbulent set-up (figure 5.12), considerably lower values of the scalar dissipation rate are reached at the end of the rapid build-up phase for most nodes. In the non-turbulent case, the ignition delay of approximately 1.49 ms is longer than the injection duration, which ends at 1.4 ms. A rapid decay of the scalar dissipation rate can be seen for the two nodes closest to the injector exit following the end of injection. Evaporation at the early stages is very similar for both cases. However, differences of an order of magnitude were observed in the variance of the mixture fraction. This large difference leads, on the one hand, to much higher values for the unconditional scalar dissipation rate in the case of turbulence. On the other hand, a larger value of the variance strongly affects the shape of the presumed PDFs and hence explains the large differences in the conditional scalar dissipation rates. Turbulence creates initially high scalar dissipation rates that decay quicker with than without background turbulence. The nodes at which ignition occurs – at 54 mm and 60 mm axial position for the non-turbulent case, at 42 mm and 48 mm for the turbulent case – have a history of low values of the scalar dissipation rate prior to ignition, which is in agreement with the explanations in the previous section. The values for both nodes in the turbulent set-up are significantly lower than the ones in the non-turbulent case. We hence conclude that the influence of turbulence on ignition delay is two-fold. Firstly, presence of initial turbulence leads to increased mixing which manifests itself in shorter, broader distributions of the flow-field quantities and strongly different shapes of the mixture fraction PDF. Secondly, turbulence causes the creation of initially higher, but then lower scalar dissipation rate at the most reactive mixture fraction for the nodes where ignition finally takes place. This results in earlier ignition.

It is important to note that the scalar dissipation rates that the most-reactive fluid experiences before ignition are low compared to the critical value of about 10 1/s (from figure 5.3, the critical N_0 is about 100 1/s and, from equation 2.69, $G(\eta) \equiv 0.1$ for $\eta = \eta_{MR} = 0.085$), which suggests that the retardation of ignition

due to straining in this spray is not very large. Whether this observation applies to diesel engines as well is not clear and no generalizations can be made. However, the type of comparison presented here (i.e. to compare the conditional scalar dissipation that the most reactive mixture fraction actually experiences with the critical value needed to preclude autoignition) may offer an explanation as to why many different models, even quite simplistic, perform well for some Diesel or HCCI engines: in those engines, the scalar dissipation rates are probably not high enough to cause ignition retardation. It is conjectured that for highly-strained sprays, such as those in complex and very turbulent flows or those from small injectors, the CMC model presented here will capture better the expected stronger turbulence-chemistry interactions.

5.4.4 Influence of CMC transport terms and flame propagation

Figure 5.13 displays the distributions of mean temperature, axial and radial mean velocities, pressure and the conditional scalar dissipation rate at stoichiometry (i.e. $\langle N|\eta = \xi_{ST}\rangle$) for various times. Unfortunately, no quantitative experimental results are available to compare with in the flame propagation phase (In an engine, the rate of rise of the pressure trace could provide such a comparison and it will be reported in chapter 6.) Following ignition at the spray tip, we see a rapid propagation of the flame upstream along the stoichiometric mixture fraction until the entire spray is alight. The duration of this premixed combustion phase is of the order of 0.20 ms. The distribution of the mean axial velocity shows that, the sudden heat release locally affects the velocity. This leads to a high radial velocity. Downstream of the ignition location the axial velocity is accelerated, whereas upstream it can even become negative, hence assisting the flame spreading towards the nozzle.

The flame propagation phase in the present spray corresponds to one part of the premixed mode of Diesel combustion. The relative importance of the various CMC terms during this phase is presented in figure 5.14. Each of the terms in the transport equation for the conditional temperature is calculated for every grid point and for all mixture fractions and its absolute value at stoichiometry,

normalized by the sum of these absolute values, is shown. Hence, for example, if the chemistry dominates (i.e. drives the unsteady term of the CMC equation), the normalized term will be close to unity, while if a term is negligible, the corresponding normalized value will be zero. Contours of these terms for the same times as those of figure 5.13 show the following: (i) prior to ignition the chemical source term dominates, with diffusion in mixture fraction space being the second largest term and the pressure work being negligible. The physical space transport terms are small, but not negligible, as they are high enough to affect the ignition delay and location as discussed previously. (ii) At the time of ignition, chemistry and diffusion in conserved scalar space are both large, and the convection term is significant. Despite the fact that the conditional averages are strong functions of space, the spatial diffusion term is not very large. (iii) The flame propagates upstream by the combined action of pre-ignition reaction (i.e. the mixture there is already close to the thermal run-away) and the convection caused by the dilatation following the initial explosion. The pressure work is still negligible in this flow since the domain is open. Again, the spatial diffusion term is small, with the exception of a small region at the edges of the spray. (iv) Long after ignition, physical space transport becomes very small due to the relatively steady nature of the fully developed spray flow field. In addition, chemistry balances molecular diffusion, as expected from the structure of a non-premixed flame.

The spatial diffusion effects during this flame propagation phase are not very large, which suggests that the flame spreading is not described by a conventional turbulent flame propagation mechanism, which would be driven by turbulent diffusion. Examination of the conditional temperature equation in the limit of a uniform stoichiometric mixture (i.e. a delta function of the presumed mixture fraction PDF at stoichiometry) shows that it becomes similar to the equation describing a laminar flame, but with an eddy diffusivity instead of a laminar one. Hence, one could conjecture that, given that the chemistry is right, a solution of that equation would give a flame propagation speed of the order of $S_L(D_t/\alpha)^{1/2}$, where S_L is the laminar burning velocity at the pressure and temperature conditions used here, D_t the turbulent diffusivity, and α the thermal diffusivity. Such an estimate gives a turbulent flame speed of about 10-20 m/s, which is about

an order of magnitude lower than the rate of spreading of the burning region in our spray. Hence we conclude that eddy diffusion is probably not the major factor in flame spreading, although it plays a role. The flame propagation phase of the premixed mode of the present spray involves flame spreading along the stoichiometric mixture fraction contour due to short-lived but fast velocity waves that transport heat and radicals to regions that were not far from auto-ignition anyway.

These observations are further substantiated by examination of the magnitude of the terms in the CMC temperature equation in conserved scalar space (figure 5.15, figure 5.16 and figure 5.17). These will also serve to identify the second part of the premixed mode. Before ignition (figure 5.15), the chemistry term is the largest and peaks at the most reactive mixture fraction. The scalar dissipation rate is low enough so that diffusion in η-space is not very large. (In a situation that shows significant retardation of autoignition due to straining, the term corresponding to diffusion in η-space is expected to be much higher). Depending on the flow location, the spatial transport terms can also be important. During flame propagation (figure 5.16), we observe that the chemistry is active in a range of mixture fractions, which indicate reaction zones propagating across all mixture fractions to consume the premixed fluid. We also observe that the conditional convection term is important, while the axial diffusion term is smaller, but of comparable magnitude to the molecular mixing. The radial convection and diffusion terms are small, but not negligible. Long after ignition (figure 5.17), we observe that chemistry is almost perfectly balanced by molecular mixing everywhere. The structure is still not that of a normal non-premixed flame, with a very lean and a very rich reaction zone still evident long after auto-ignition. This is consistent with DNS (Mastorakos et al. (1997a)) and corresponds to a triple-flame structure (Yu et al. (2001)), with ever decreasing importance of the lean and rich flame branches as time evolves. This phase is the second part of the premixed mode of diesel combustion and, as we can see, lasts long after the full spray is alight. The duration of this part decreases with increasing scalar dissipation rate. We have seen similar structures in chapter 4 (figures 4.20 and 4.21).

We conclude that the premixed mode of Diesel combustion involves flame propagation across mixture fraction space by action of molecular mixing, flame propagation along the stoichiometric contour by action of the conditional convection term, chemistry proceeding independently at different parts in the flow, and, in enclosed environments, pressure work. It is evident that the elliptic CMC equation can capture many of the expected phenomena present in Diesel combustion. The fact that a single model can be used for the auto-ignition mode, premixed mode, and diffusion mode of Diesel combustion is an important practical advantage over the current industrial practice of switching between various models. The magnitude of molecular mixing affects the auto-ignition delay time and also the duration of the premixed phase. Hence modelling of the conditional scalar dissipation rate is a crucial aspect for CMC. In addition, the importance of the physical transport terms suggests that attention should be given in validating the models that are used at present (Richardson et al. (2007), Richardson and Mastorakos (2007)), a conclusion also reached by examination of the structure of a lifted flame in Kim and Mastorakos (2005). Further advances would be feasible by implementing full second-order closure following the methodology discussed in chapter 4 or double conditioning (Kronenburg (2004)). The former may be necessary for accurate predictions of ignition time in the presence of high scalar dissipation rates (relative to the critical value), while the latter may be necessary for a more accurate treatment of the flame propagation phase along the mixture fraction contours.

5.4.5 Note on CMC with droplet evaporation

Droplet evaporation is still an active field of research, and it has several implications for mixing and combustion. From the point of view of cold flow mixing, additional terms appear in the transport equations for mean mixture fraction and its variance. While the mixture fraction generation due to evaporation can be closed by the Lagrangian-Eulerian formulation used to represent the dispersed phase, the variance equation needs additional modelling to close the extra terms due to evaporation and to define a corrector factor in the expression for the

scalar dissipation rate (Vervisch (2006)). Closure for the mixture fraction variance transport equation can be found in Demoulin and Borghi (2000), Reveillon and Vervisch (2000) and Hollmann and Gutheil (1996).

Development of CMC for turbulent spray combustion has been initially approached in Klimenko and Bilger (1999), where the use of two mixture fractions and one related to the macro-transport and defined as gaseous mixture fraction, the second involving the inter-droplet transport and associated with the droplet evaporating mass fraction, was proposed.

Additional work has been carried by Smith et al. (2000), where CMC modelling of a dispersed evaporating phase combustion has been attempted and the results compared with DNS predictions. No distinction was done between the gaseous mixture fraction and its evaporating contribution. An additional term in the transport equation for the mixture fraction PDF was derived, dependent on the conditional droplet evaporation rate, which yields an extra term in the CMC equations representing a convective flux in η-space proportional to the conditional evaporation rate ($\dot{s}_\xi(\eta)$). It is worth underlining that no additional term in the conditional enthalpy equation were introduced due to the heat latent of vaporization. Mixture fraction was treated as a scalar bounded between 0 and its value of saturation at the droplet surface ξ_{SAT}. New transport equations were derived for the normalized variable $\zeta = \eta/\xi_{SAT}$, in which the conditions at the right, 'floating', boundary could be extracted from DNS.

An alternative treatment has been recently proposed by Rogerson et al. (2007). In their work new transport equations for the mixture fraction PDF and the conditional species mass fractions were derived from the unconditional scalar transport equations written in the presence of the evaporating phase. A more complete treatment of the dispersed phase was presented: the source term due to evaporation into the conditional fuel transport equation, missing in previous formulation, was explicitly derived. However, no hypothesis was made on the upper boundary of mixture fraction space. The conditional temperature, rescaled from the adiabatic conditional temperature profile based on its calculated unconditional value, was not very rigorously treated.

All the models proposed need additional information concerning $\dot{s}_\xi(\eta)$, which is assumed to be a presumed function of η. Smith et al. (2000), analysing DNS of

burning droplet in stagnant flow, employed a presumed function $\dot{s}_\xi \sim \eta^n$, which was found to vary almost linearly in η with $n \simeq 1.1$ in the interval $[0,\xi_{SAT}]$. Reveillon and Vervisch (2000), and later Vervisch (2006) introduced the effect of the droplet relative velocity, and $\dot{s}_\xi(\eta) \sim (\eta/\xi_{SAT})^n(1-\eta/\xi_{SAT})$ was suggested, where n takes values between 1 and 8 respectively for weak and high droplet slip velocities. Sreedhara and Huh (2007) have recently presented results on a similar configuration where the conditional evaporation rate was modeled as to differ from 0 only in the interval between $[\tilde{\xi},\xi_{SAT}]$ where a linear model was employed $\dot{s}_\xi \sim \eta$.

Some comments on the above models are due. (i) In all cases presented, the DNS considered droplets much smaller than the Kolmogorov length scale, representative of external group combustion around clusters of droplets in the combustion diagram of Chiu et al. (1982). In diesel engine spray this assumption can be restrictive since in the core of the spray this hypothesis might drop in favor of an external sheath combustion as defined in the same diagram. (ii) All models are defined based on a given value of ξ_{SAT} in the computational cell. Generally ξ_{SAT} is calculated based on the droplet surface temperature and the mean temperature of the cell. In diesel spray combustion the droplet temperature depends on the droplet size and the droplet history in the flow (viewed in a lagrangian manner), for many droplet belonging to the same cell ξ_{SAT} is not univocally defined. The mean cell temperature on the other hand is not necessarily the temperature that the droplet experience because of the effect of turbulence so an averaged definition of ξ_{SAT} must be given. (iii) The normalizing argument proposed in Smith et al. (2000) regarding the CMC solution domain, or the possibility to re-scale the submodels for the PDF of mixture fraction and conditional scalar dissipation rate based on ξ_{SAT}, as advanced by Vervisch (2006), becomes impractical in the regions of the domain where only evaporated fuel is present, therefore, an estimation of its value based on the cell thermodynamic conditions or through the resolution of a transport equation might be considered Demoulin and Borghi (2000). (iv) Consistency is required between the mixture fraction PDF and the conditional evaporation rate. In case of dense sprays cells in the injector vicinity exist, in which high evaporation rate coexist with narrow mixture fraction PDF modeled having a J-shape. This might result in non realistic

value for the conditional evaporation rate. (v) The CMC derivation in case of evaporating dispersed phase need to consider an extra flux in both conditional fuel mass fraction and conditional enthalpy due to the release of fuel from the droplet source and its latent heat of vaporization. The first, in particular, might be relevant in pollutant prediction, since the addition of fuel at rich mixture fractions might determine the level of pollutants in the reaction zone (i.e. soot prediction). The second might affect the autoignition prediction because of the sensitivity of the prediction to the initial temperature.

A sensitivity analysis on the various models has been performed in Kim and Huh (2002) in case of n-heptane spray autoignition. The CMC formulation following Smith et al. (2000) was implemented in a transient calculation in which the variance of mixture fraction was modeled using three different methods respectively: the standard transport equation for gaseous fuel, the model from Reveillon and Vervisch (2000) and the model of Hollmann and Gutheil (1996). It was reported that the discrepancies among the predicted variances were less then 5%. Furthermore, the effect of the additional term in the CMC equation was negligible with respect to the calculated autoignition delay. A possible explanation to these results can be found in point (v) above since the CMC implementation disregarded the sink term due to the latent heat of evaporation in the temperature equation.

A more complete formulation of the CMC for an evaporating dispersed phase was presented in Rogerson et al. (2007) applied to a bagasse-fired boiler with overall good agreement with the experimental measurements. Nevertheless, its application to a diesel spray simulation presents some limitations: the calculation was steady and the mixture fraction PDF gaussian-like so the problem risen in point (iv) based on the consistency between mixture fraction PDF was not evident. It is worthwhile to mention that the conditional evaporation rate was treated according to Smith et al. (2000) using $n = 2$ in their model, without limitations based on ξ_{SAT}. Furthermore, the conditional temperature equation was not directly integrated, but its profile re-scaled based on budget considerations from the unconditional temperature equation, which limit considerably the application of the method to an autoignition problem.

No consensus is yet reached on the way to treat droplet evaporation into the CMC. Work is still needed to understand and model the evaporation and combustion in the inter-droplet space to be able to include evaporation consistently into the CMC formulation. A very recent paper was presented by Klimenko and Abdel-Jawad (2007), in which the combustion in porous media using a CMC-like formulation was discussed. The porous space could be regarded as an inter-particle space and similar treatment can be extended to combustion in a evaporating dispersed phase.

5.5 Conclusion

Two-dimensional Conditional Moment Closure has been applied to study n-heptane spray auto-ignition at Diesel engine conditions. Fully implicit and operator splitting solution procedures and two stiff solvers have been compared and the results analyzed with respect to both accuracy and computational cost. Using appropriate splitting, both conditional quantities and spatial distributions agree very well and significant reductions in computational time can be achieved. Splitting physical transport, molecular mixing and chemistry in three sequential steps (OS2) is the most stable and efficient procedure and is the integration procedure selected in this thesis. The analysis of the error introduced by the method suggests that reducing the splitting timestep the accurate solution obtained by the Method of Lines can be recovered. Integrating simultaneously molecular mixing and reaction (OS1), motivated by the strong coupling between the two in a diffusion flame, results in a much larger computational time due to the much larger system to solve. Only the use of a solver like CHEMEQ2, with small restart costs, for the integration of the second and stiff part can predict the full evolution of the flame from auto-ignition to diffusion flame in a reasonable computational time.

The calculated ignition delays show very good agreement with the experimental data for various temperatures and the effects of initial turbulence of the background air are also correctly captured. The premixed mode of diesel combustion has been shown to comprise a flame propagation phase along the stoichiometric mixture fraction contour, driven mostly by the volumetric expansion following

auto-ignition, and a longer flame propagation phase across mixture fraction contours to consume the premixed fluid driven by molecular mixing.

The results show that two-dimensional CMC can be used very effectively to accurately predict the ignition phase, flame propagation and the subsequent diffusion flame phase for auto-igniting sprays. The present work is a step towards using fully elliptic first-order CMC in practical engine calculations. Further improvements can be derived by better validated models for the physical transport terms present in the CMC equation, by second-order closure, which can make ignition time predictions more accurate, and by double conditioning, which may be necessary for an accurate treatment of the flame propagation phase.

5.6 Tables and Figures

Fuel type	*n*-heptane
Fuel temperature	300 K
Total fuel injected mass	6 mg
Injection duration	1.4 ms
nozzle diameter	0.2 mm
Nozzle L/D	4
Air pressure	50 bar
Air temperature	823 K, 813 K, 803 K 823 K, 813 K, 803 K 763 K

Table 5.1: Aachen bomb operating conditions

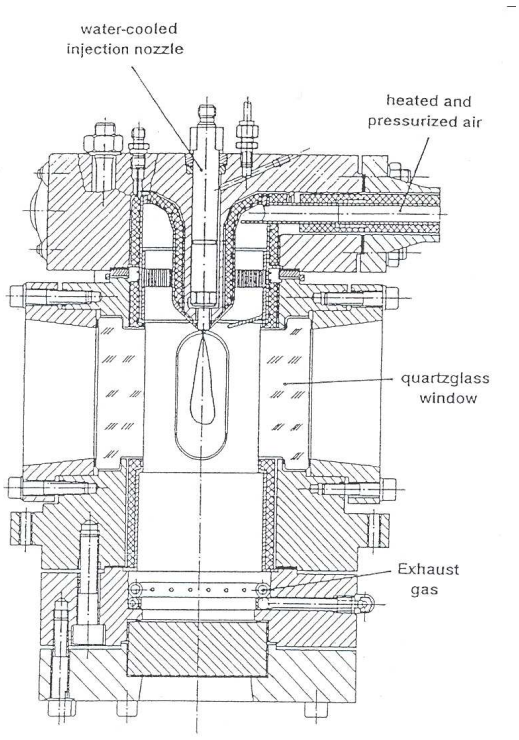

Figure 5.1: Schematic of the experimental setup (reproduced from Koss et al. (1992)).

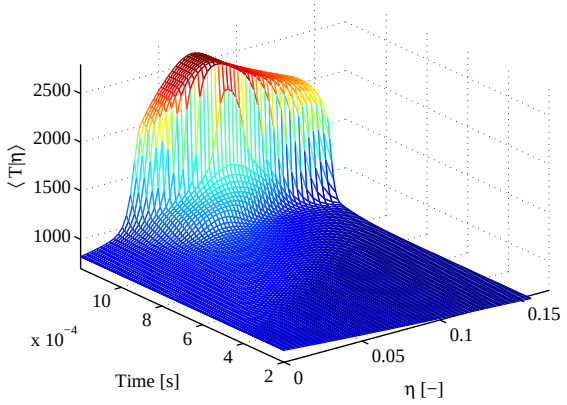

(a)

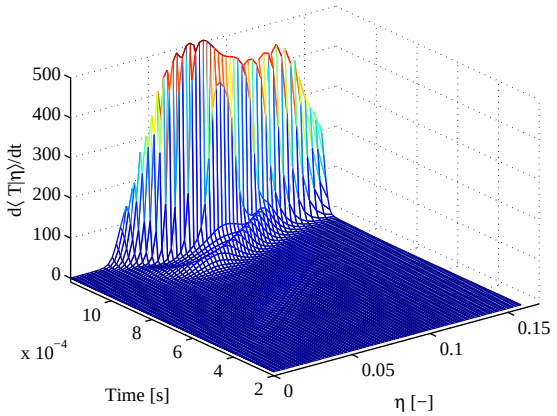

(b)

Figure 5.2: Autoigniting homogeneous CMC: (a) $\langle T|\eta\rangle$ [K]. (b) $\partial\langle T|\eta\rangle/\partial t$ [K/s]. $\langle N|\eta = 0.5\rangle = 10$ [1/s] Initial conditions $Y_{C_7H_{16}}$=1, Y_{O_2}=0.233, Y_{N_2}=0.767; T_{FU}=300[K], T_{OX}=823[K].

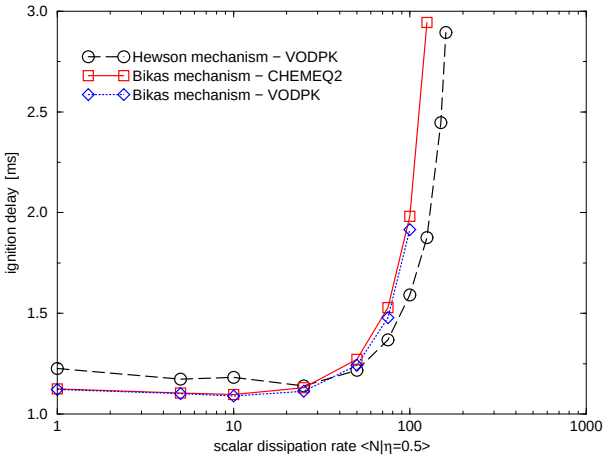

Figure 5.3: Ignition delay [ms] for a homogeneous CMC function of $\langle N|\eta = 0.5\rangle$ [1/s]. Initial conditions as in figure 5.2.

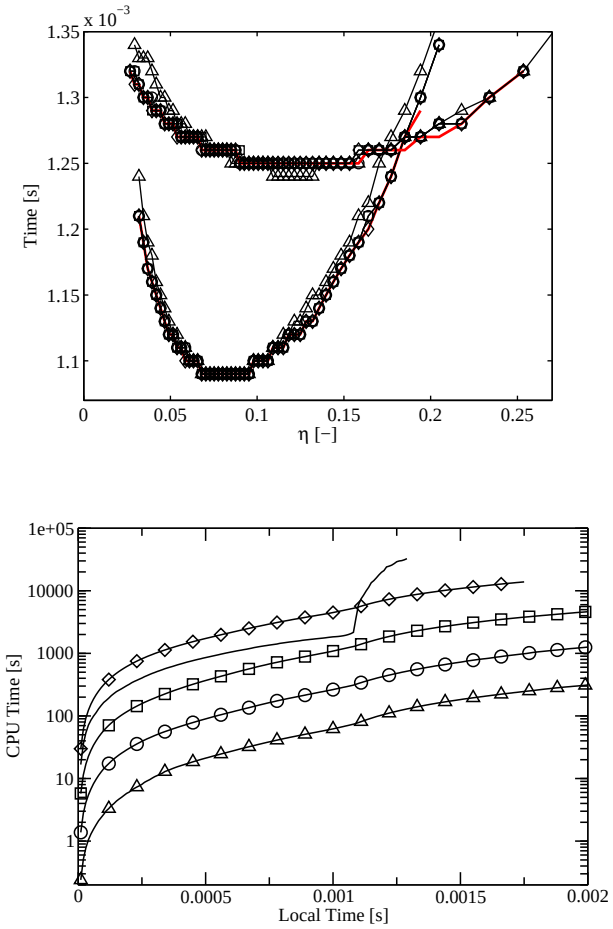

(b)

Figure 5.4: Comparison between MOL and OS2 for homogeneous CMC. Autoignition delay and flame development identified as the locus of maximum conditional temperature gradient in time as function of η for $\langle N|\eta = 0.5\rangle = 10$ 1/s and $\langle N|\eta = 0.5\rangle = 60$ 1/s (a). MOL (solid line), OS2 with splitting time 1×10^{-5}s (triangle), 1×10^{-6}s (circle), 1×10^{-7}s (square), 1×10^{-8}s (diamond) (b). Initial conditions as in figure 5.2.

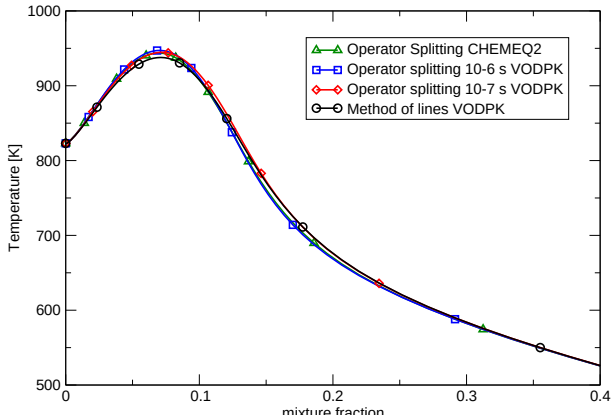

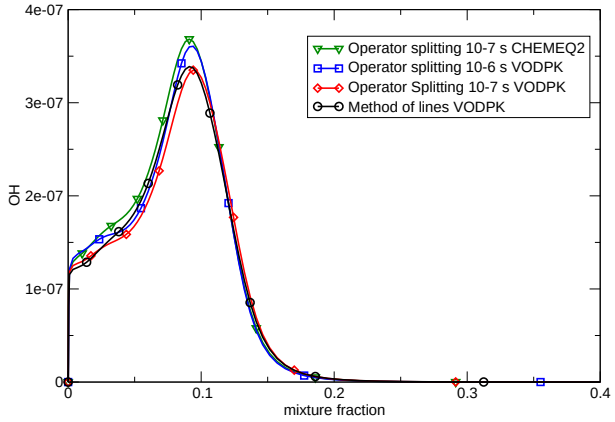

(b)

Figure 5.5: Conditional temperature [K] (a) and OH mass fraction [-] (b) at t=1.0ms at 0.0mm radial and 42mm axial position from the injector.

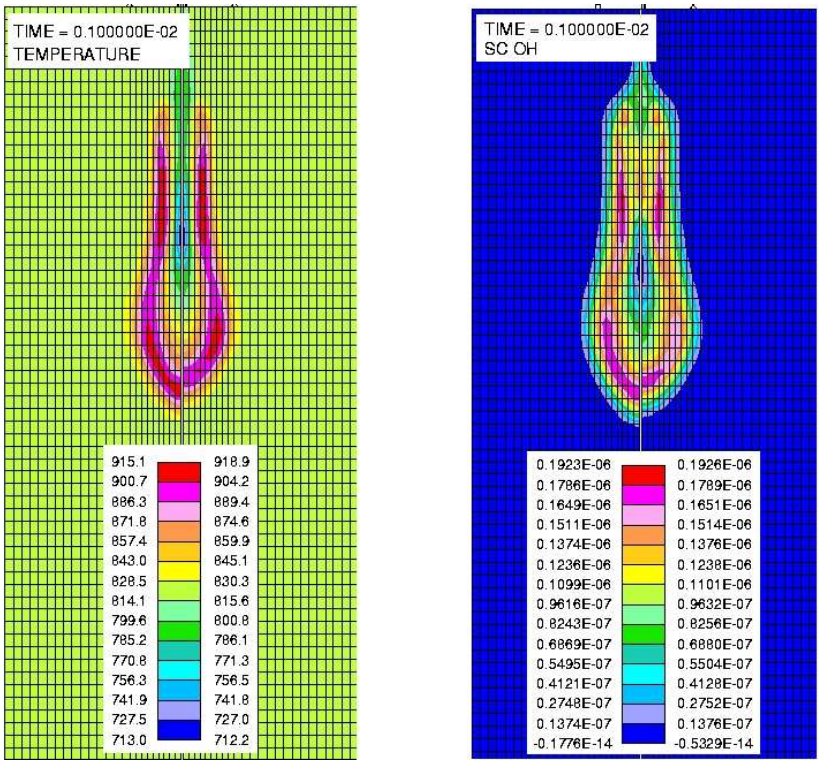

(a) (b)

Figure 5.6: Favre-average temperature [K] (a) and OH mass fraction [-] (b), 1.0ms after SOI. In each of the plots, the left side is from the OS1 solver using CHEMEQ2 with a fractional time step of 10^{-7}s, while the right side is from the MOL solver.

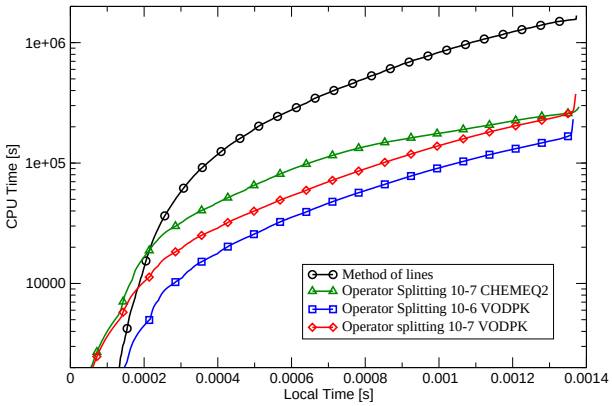

(a)

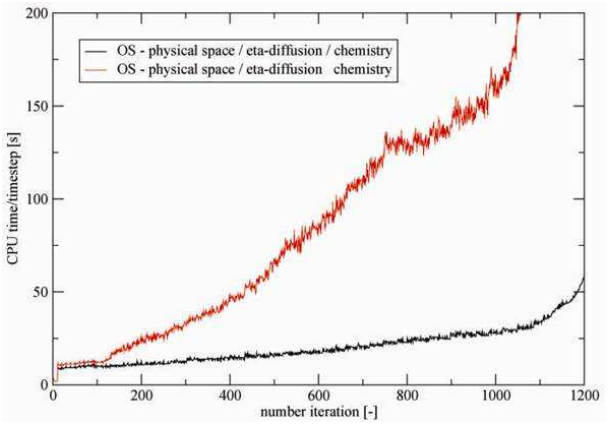

(b)

Figure 5.7: (a) Comparison of the real CPU time taken from various solvers to advance the calculation to the 'local' time through the injection for the spray combustion test case. (b) Comparison of CPU time between splitting the η-diffusion and chemistry (OS2) and treating them together (OS1).

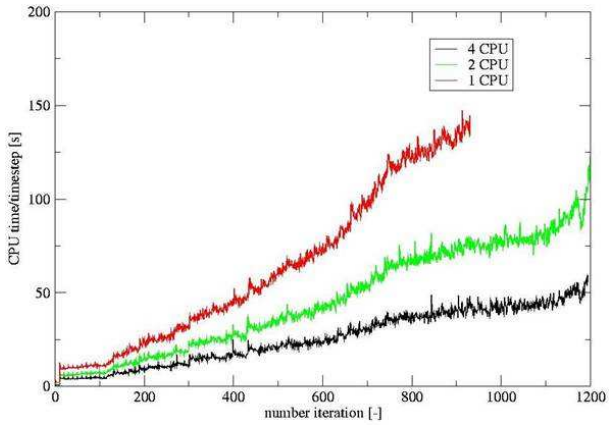

Figure 5.8: Parallel efficiency using OS1.

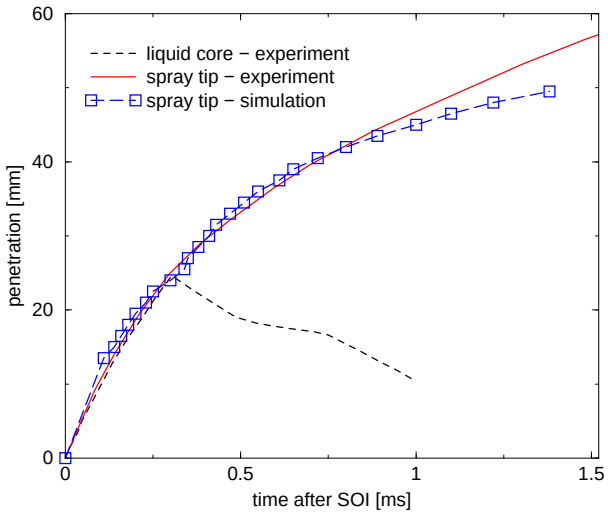

Figure 5.9: Comparison of predicted and measured spray penetration length [mm] vs. time after start of injection (SOI). Experimental data from Koss et al. (1992).

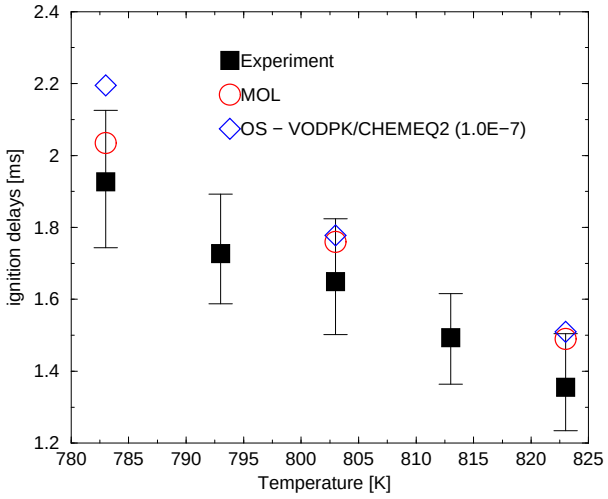

(a)

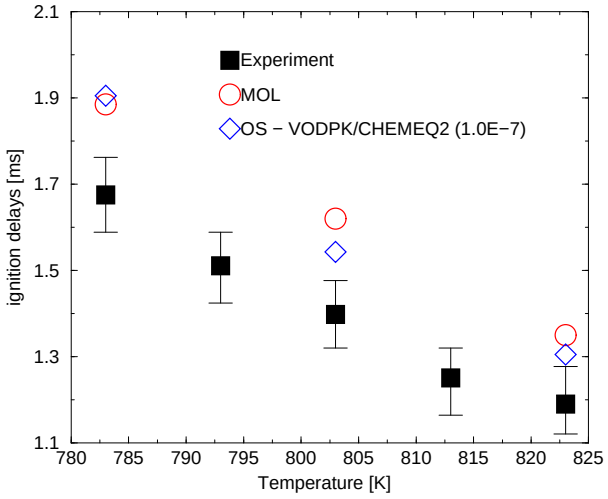

(b)

Figure 5.10: Prediction and measured ignition delay [ms] without (a) and with (b) initial turbulence. Experimental data from Koss et al. (1992).

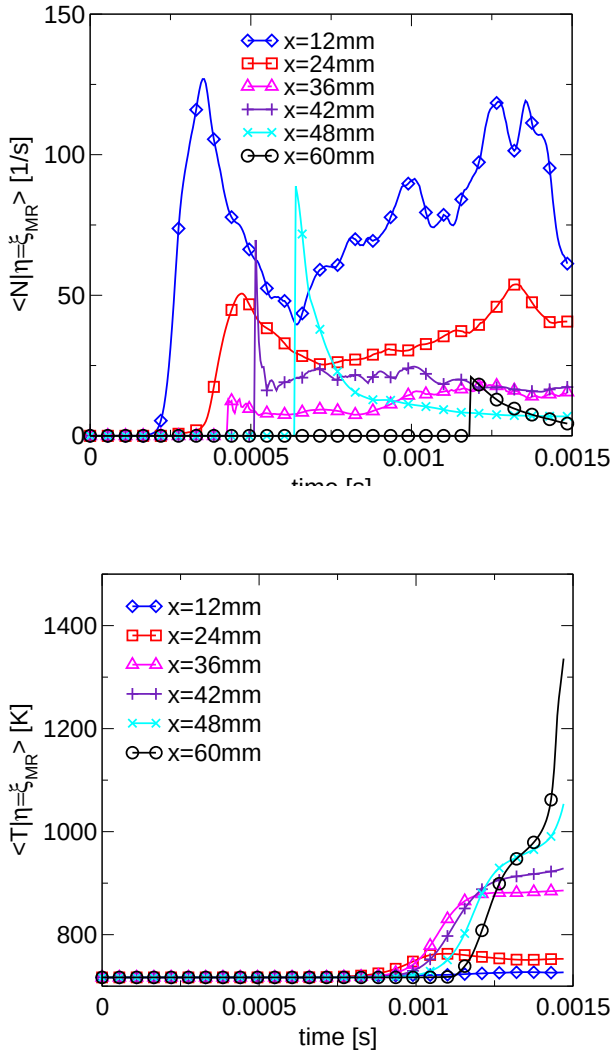

(b)

Figure 5.11: Evolution of $\langle N|\eta = \xi_{MR}\rangle$ [1/s] (upper) and $\langle T|\eta = \xi_{MR}\rangle$ [K](lower) for the CMC nodes on the spray axis, no initial turbulence.

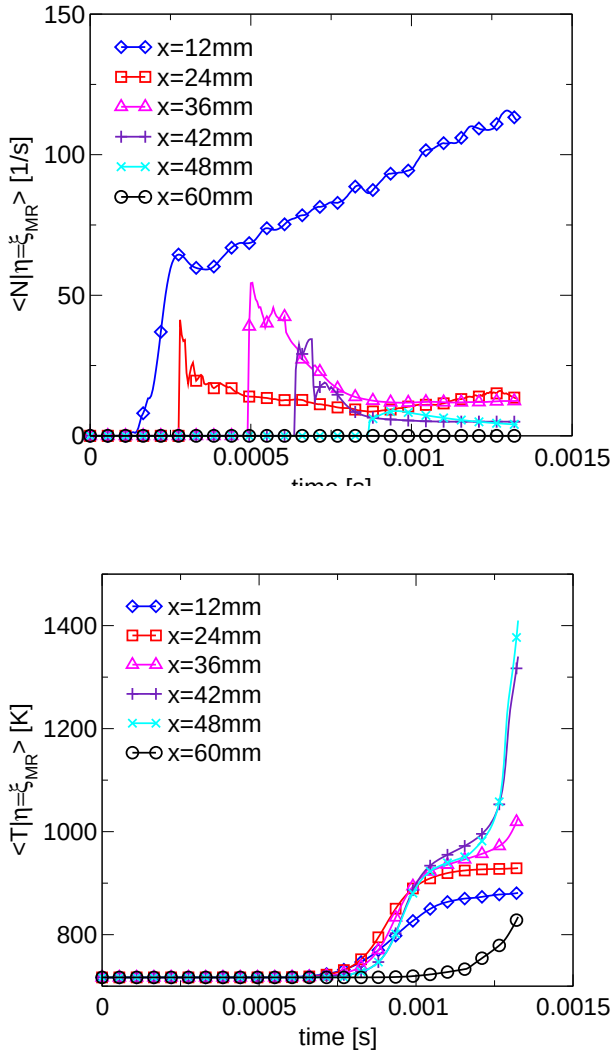

(b)

Figure 5.12: Evolution of $\langle N|\eta = \xi_{MR}\rangle$ [1/s](upper) and $\langle T|\eta = \xi_{MR}\rangle$ [K] (lower) for the CMC nodes on the spray axis, with initial turbulence.

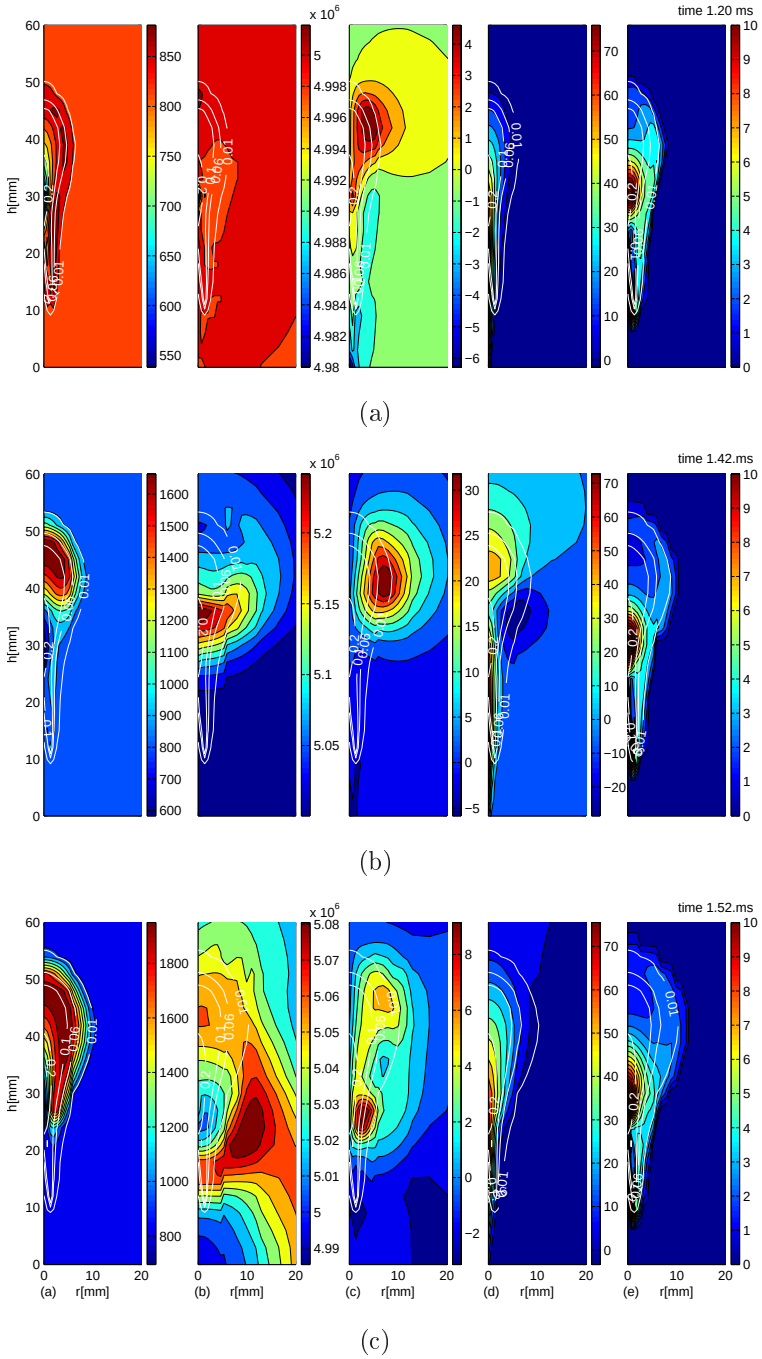

Figure 5.13: Spatial distribution at 1.2ms (a), 1.42ms (b), 1.52ms (c). From left to right: mean temperature [K], pressure [Pa], mean radial velocity [m/s], mean axial velocity [m/s], conditional scalar dissipation rate [1/s] evaluated at stoichiometry. Superimposed in white are the mean mixture fraction isolines.

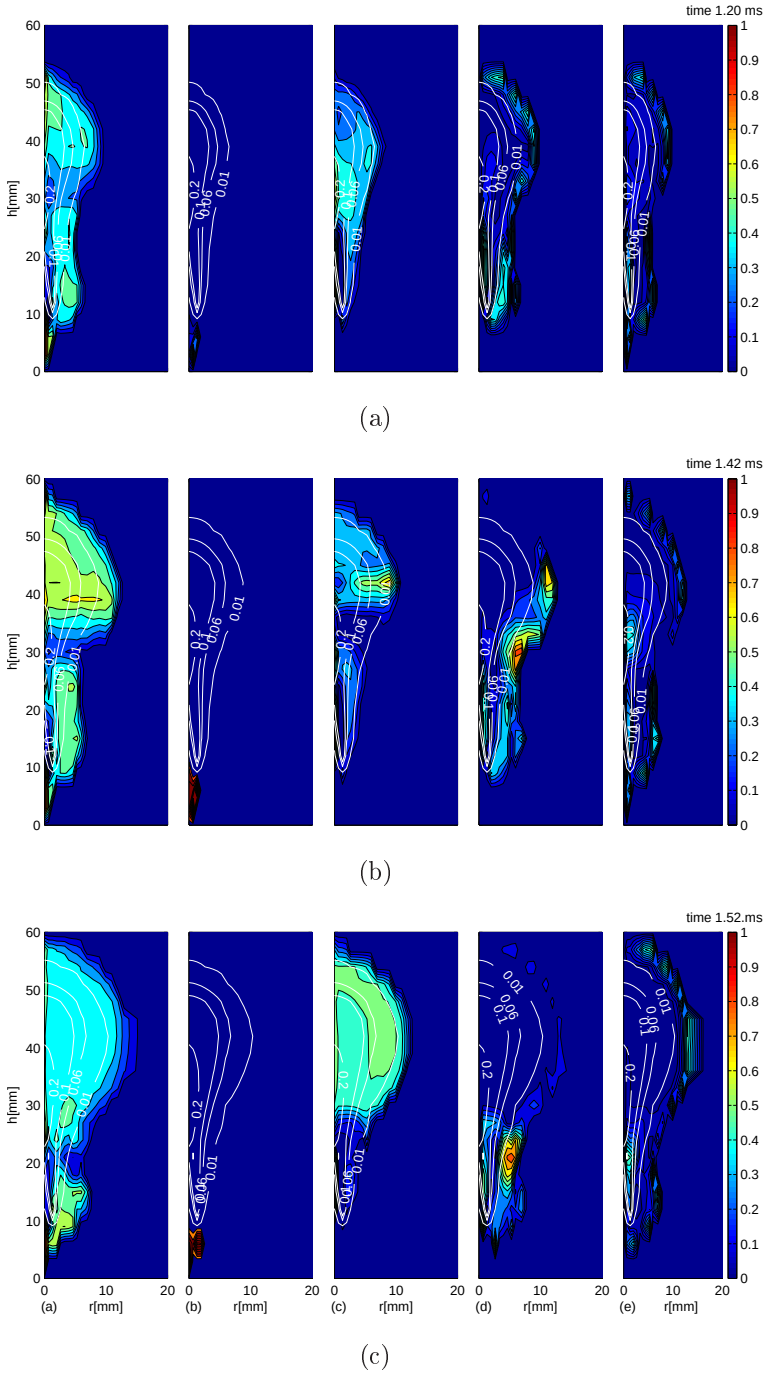

Figure 5.14: Normalized source terms of the CMC temperature equation evaluated at the stoichiometric mixture fraction at 1.2ms (a), 1.42ms (b), 1.52ms (c). From left to right: chemical source term, pressure work, diffusion in conserved scalar space, physical space convection, physical space diffusion. Superimposed in white are the mean mixture fraction isolines.

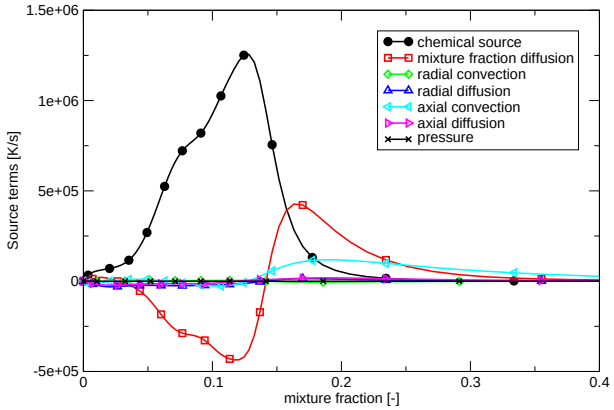

Figure 5.15: Source terms [K/s] in the CMC temperature equation during the ignition phase: 1.2ms after SOI at 0.6 mm radial and 48mm axial position, $T_{AIR} = 823K$ with initial turbulence.

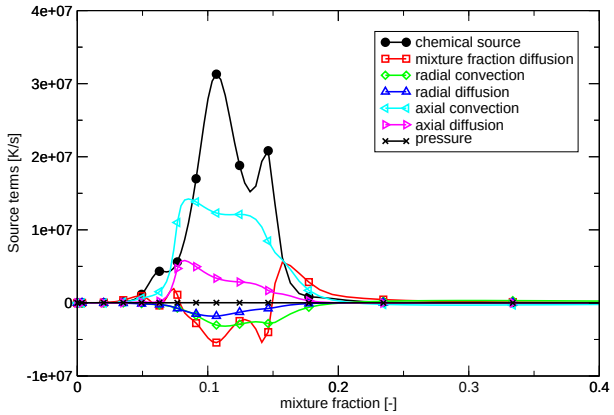

Figure 5.16: Source terms [K/s] in the CMC temperature equation during flame the propagation phase: 1.42ms after SOI at 6mm radial and 36mm axial position, $T_{AIR} = 823K$ with initial turbulence.

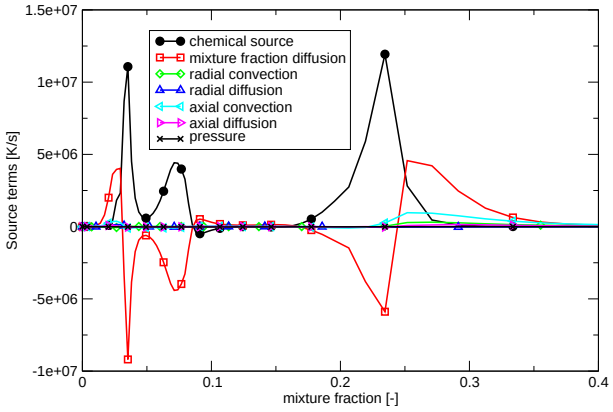

Figure 5.17: Source terms [K/s] in the CMC temperature equation during the diffusion flame phase: 1.52ms after SOI at 2.6mm radial and 42mm axial position, $T_{AIR} = 823K$ with initial turbulence

Chapter 6

Results - III Diesel Engine modelling

First-order elliptic CMC, coupled with a commercial CFD solver, has been applied to diesel engine combustion modelling. The CMC has been interfaced to an unstructured CFD mesh typical of diesel engine modelling. The implementation of a moving CMC grid to reflect the changes in the domain due to the compression and expansion phases has been achieved using an algorithm for the cell addition/removal and modelling of the relative velocity due to the CMC cell movement. Special care has been considered for the boundary conditions and the wall heat transfer. An efficient OS formulation has been used to integrate the CMC equations. A CMC domain reduction of the 3D problem to axi-symmetrical two-dimensional and zero-dimensional, has been explored in terms of accuracy and computational time. Additional considerations are reported concerning the initialization of the CMC domain in conserved scalar space during transient calculations.

The present chapter represents, to the author's knowledge, the first application of CMC to diesel engine. It sets the framework for further improvement in diesel engine modelling using the same combustion code for all diesel engine combustion modes (i.e. multiple injections and Homogeneous Charge Compression Ignition (HCCI) combustion). The present chapter, after a background on diesel engine modelling, introduces the new developments to extend the CMC equations and solver to a moving grid formulation and to a complex geometry. Results are

presented for a Direct Injection (DI) heavy-duty engine under two different loads at intermediate engine speeds.

The chapter is organized as follows: after a background on diesel engine modelling some details on the engine and the experimental configuration is given. A description of the numerical method and the models follows. The main results together with their discussion are presented. The chapter closes with various conclusions.

6.1 Background and objectives

The drive towards the stringent legislation in emission and consumption motivates developments of new combustion modes taking advantages of slow chemistry effects (i.e. high Exhausted Gas Recirculation (EGR) rate) and very lean inhomogeneous mixture (i.e. multiple injections, Homogeneous Charge Compression Ignition (HCCI)). Numerical tools are therefore required to accurate predict combustion, which implies the use of complex chemistry and a rigorous treatment of the turbulence/chemistry interaction. There are several modelling challenges involved in engine calculation: an accurate prediction of the flow field which includes the effects of spray injection and vaporization, the combustion and its interaction with turbulence, a complex chemical mechanism and the effect of the solid walls.

A variety of modelling approaches has been used to model diesel engine combustion. In the aim of obtaining simple engineering quantities like pressure traces or heat release rates, models based on the characteristic timescales (Kong et al. (1995)) developed from the Eddy Break-up model of Magnussen (1981), can give reasonable agreement with the experimental data, but additional modelling is required to treat ignition (Halstead et al. (1977)).

The lack of universal validity, particularly given by the arbitrary transition criteria between the two models, and the use of various constants, gave rise to more advanced models offering a more promising way to treat the turbulence-chemistry interaction and allow the inclusion of complex chemistry. Flamelet-based models (Peters (1984), Peters (1986)), originally based on precalculated lookup tables, have been successfully applied in the context of representative interactive flamelet

(RIF) model to unsteady spray calculation (Wan et al. (1997)) and diesel engine combustion (Pitsch et al. (1996)). However, the use of a single flamelet to represent the entire domain was found insufficient to accurate model the premixed stage of the combustion. Better predictions were obtained with the Eulerian particle flamelet model (EPFM), therefore employing multiple RIFs and additionally solve an Eulerian transport equation to obtain the probability of finding the corresponding flamelet in each cell. An extension to the EPFM model to treat the heat transfer to the wall is presented by Hergart and Peters (2001). By introducing a second mixture fraction coordinate, the RIF model was extended to more complex problems involving multiple injections (Hasse and Peters (2005)). The number of RIFs to use during a diesel engine cycle calculation is not universally defined and can be problem dependent, furthermore the lack of physical interaction among the flamelets might cause issues in the accurate prediction of the lift-off height in spray diesel combustion. An interesting development of RIFs has been proposed by Lehtiniemi et al. (2006), who starting from the work of Zhang et al. (1994), defined a progress variable to mark the flamelet evolution during the autoignition process. Solving a transport equation for this progress variable into the CFD grid allows for the effects of spatial transport to be added. The progress variable, chosen to be sensible enthalpy, was solved with the use of precomputed table, as function of the local thermodynamic conditions, mixture fraction, scalar dissipation rate and progress variable itself.

An alternative approach is represented by the extension of the coherent flame model (CFM). The so-called ECFM3Z uses a three-zone reactor concept based on a pre-assumed PDF of mixture fraction to define the state of mixing and a progress variable approach to characterize the advancement of reaction. ECFM3Z represents a computationally non-expensive method able to predict the different modes of non-premixed turbulent combustion as for diesel engines (Colin et al. (2003), Colin and Benkenida (2004)). However, it has not been validated for generic flames yet.

Recently, due to the advancement in the chemical tabulation to speed-up the evaluation of the species reaction rate, the transported PDF method, being by reputation computationally expensive, has shown successful application to HCCI engine combustion (Zhang et al. (2005)).

In the context of this work, CMC has proved to be able to treat all phases of diesel engine combustion (i.e. autoignition, premixed mode, diffusion mode) offering a solid theory to treat turbulence/chemistry interaction using a complex chemistry avoiding any assumption on the topology of the reaction zone (chapter 5). The elliptic formulation of its equation overcomes the problem revealed by the flamelet based methods making the CMC one of the most promising model to treat all modes of diesel engine combustion.

In chapter 4 it was shown that the influence of conditional fluctuations does not have a significant effect if the conditional scalar dissipation rate falls rapidly below its critical value. The analysis performed in chapter 5 revealed that for spray-driven diesel combustion the conditional scalar dissipation rate has a rapid decay. Second-order closure appears, at first approximation, unnecessary. Nevertheless, in case of the spray impinging against the wall, as is the case inside the piston bowl of a DI-diesel engine, the igniting zone become closer to the droplet cloud and the assumption of low conditional scalar dissipation rate might not be valid. In the present simulations a first order-closure will be considered. However, further studies are needed to evaluate the sensitivity to conditional fluctuations.

The simulations reported have still to be considered as exploratory, since many the parameters influencing combustion in an engine cycle modelling could not be explored in the present work. Among all, an accurate definition of the initial conditions in terms of initial temperature, pressure, species concentration and turbulence characteristic (i.e. influence of valve motion) is essential and should come from the convergence of different cycles. Not less important is a validation of the spray prediction (i.e. in-cylinder optical measurement) that would determine the main flow as well as the state of mixing inside the cylinder.

6.2 Experimental configuration

The engine modeled has been extensively investigated experimentally and numerically in ETH-Zurich in Prof. K. Boulouchos's group. The work done by Wright (2005), which provided the test case and the initial conditions for the present calculations, is gratefully acknowledged.

The engine is four-stroke, turbo-charged, built with inter-cooled charge air, displacement with roughly 1.6 liter per cylinder derived from the heavy-duty Liebherr D924. The in-line four-cylinder variant, for which the data has been reported, produces a peak power output of 183kW at 2100 RPM. The cylinder head configuration has two valves per cylinder type with push-rod actuation. The common-rail fuel injection system consists of a suction-throttled pump and an eight-nozzle injector (nozzle diameter 200 μm). Further details concerning both the engine and the fuel injection system are listed respectively in table 6.1 and table 6.2.

The operating conditions simulated are part of the set of the European Stationary Cycle (ESC) test that the heavy-duty engines have to fulfil for on-road applications. Details on the measurement can be found in Boulouchos et al. (2003). Selection of two of these points at respectively 50% and 100% load have been investigated by means of simulation. The engine conditions are summarized in table 6.3.

All points measured are with zero exhaust gas recirculation, nonetheless small quantities of residual gases are trapped in the chamber. These have not been medelled in the simulation. The flow is initialized as technical air with a prescribed swirl profile and turbulence parameter at the time of intake valve closure, i.e. no valve motion and intake flow have been included.

6.3 Numerical method

The CMC model integrated within the CFD package STAR-CD (2004) has been used. Due to the eight-hole injector, only 45 deg of the whole combustion chamber have been modeled exploiting symmetry. A multi-block unstructured hexahedral grid, which makes use of the O-grid capabilities and local refinement of STAR-CD, has been employed. Figure 6.1 shows a schematic of the CFD mesh close to TDC. STAR-CD uses a formulation of cells addition/removal that adds or deletes layers of cells during the expansion or the compression stroke respectively. The mesh is updated on the basis of discrete events. According to the piston movement, the cells belonging to the stroke block get compressed or expanded and, based on a user-defined cell aspect ratio, the number of layers is modified. The piston

bowl mesh is instead simply translating without getting distorted. The geometry, therefore, consisted of 26945 cells at BDC and of about 3680 at TDC. At TDC the average cell volume was approximately 4.6 mm^3. Higher cell density and better boundary resolution might be considered for future work.

The modelling settings used into the CFD solver follow the one reported in chapter 5 if not explicitly stated. No information concerning the spray penetration nor angle were available. The spray has been modeled by the Huh model for the atomization and the Reitz-Diwakar for the secondary break-up (STAR-CD (2004)). Droplet impingement on the solid wall has been modeled following Bai and Gosman (1996), available into STAR-CD. The κ-ε RNG model has been selected to treat turbulence. The solid boundaries have been assumed at constant temperature (i.e. infinite heat capacity) at 500K. The thermo-physical properties of the fuel, initialized as liquid dodecane, were defined internally into the CFD solver. Since the combustion is modeled by an n-heptane chemical mechanism, the injected quantity has been calculated to obtain equal energy content. The timestep used in the calculation was about $\Delta t_{CFD} \simeq 1 \times 10^{-6}$s.

Following the implementation described in chapter 3, a three-dimensional first-order CMC has been applied to this diesel engine test case. The CMC grid built as a structured cylindrical grid around the CFD unstructured mesh, uses of a cylindrical formulation to allow the definition of cyclic boundary conditions in the azimuthal direction. An automatic mesh-recognition algorithm defines the matching between the CMC and the CFD cells. The CMC cells that does not correspond to any CFD cells are deleted whilst the one corresponding to the CFD boundary cells are identified for an adequate boundary treatment. The resulting CMC grid becomes a piece-wise linear structured grid surrounding the unstructured CFD mesh and updated at every timestep. The resolution of the CMC is limited by the size of the CMC cells as to have minimum one CFD cell per CMC cell. Because the CMC cell density close to the axis was higher than the CFD one, due to the cylindrical formulation, a linear interpolation along the azimuthal direction of the CFD solution is used to restore the CMC grid connectivity. Consistent with the CFD, the piston bowl is defined as a sliding grid whereas the stroke part gets modified using an analogous formulation of cell addition/removal as implemented in the CFD part. It results in a grid of

$30 \times 10 \times 12 - 40$ respectively in the radial, azimuthal and axial direction at TDC and BDC. The implication of a sliding grid into the CMC equation formulation consists in an additional convection term due to the grid relative velocity that can be included in the conditional velocity term following equation 3.9.

In conserved scalar space, 101 nodes were used, clustered around the stoichiometric value to enhance resolution in this region. A PDF of mixture fraction threshold of 1×10^{-20} has been considered. Linear interpolation, between the calculated values at η_{MIN} and η_{MAX} and respectively 0 and 1 have been considered to initialize the region of negligible PDF. Standard modelling approaches have been used to close the CMC transport equation: linear model for the conditional velocity (equation (2.71)), Amplitude Mapping Closure (equation (2.69)) for the conditional scalar dissipation rate, first order closure for the conditional reaction rate (equation 2.57) using the n-heptane chemical mechanism (Bikas (2001)) and gradient diffusion for the conditional scalar flux following the implementation described by equation 3.2.

Boundary conditions of symmetry were imposed at the axis and cyclic in azimuthal direction. At the nozzle Dirichlet boundary conditions of inert mixing of the reactants have been enforced during the injection phase. The implementation of the CMC at the physical boundaries is reported in section 2.4.6 and here briefly summarized. Following Bilger (2001), no material flux through the wall was considered. The coarse representation of the non-linear boundaries did not allow the use of the proposed radical recombination. This hypothesis, however, need to be revisited in case an accurate treatment of the wall layer is needed, in internal combustion engine combustion. In fact, processes of hydrocarbon adsorption and desorption due to the thin liquid film of lubricant at the wall and species recombination are typical phenomena. In the present formulation the heat flux to the wall directly appears in the conditional temperature transport equation using the model presented in equation 2.76, consistent with the unconditional value predicted by the CFD solver. The T_{wall} appearing in equation 2.76 refers to fictitious points outside the calculated CMC domain considered at constant temperature equal to the CFD wall temperature. This allows to calculate the conditional temperature equation in the wall region not necessarily resolved by the CMC mesh. The conditional reaction rate is still calculated at the CMC

boundary cells, but only the diffusive flux is then considered under the condition of no-slip velocity. The boundary treatment here implemented allows the inclusion of wall effects into the CMC, but issues of accuracy are still present for very coarse CMC grids that do not appropriately resolve the boundary and hence further studies are needed.

An Operator Splitting method (OS2 as defined in chapter 3) has been applied to integrate the CMC equations. The three internal steps had different splitting timestep, the physical space transport $\Delta t_{SPLIT,xyz} = 1 \times 10^{-6}$s coincident with the CFD external timestep, whereas $\Delta t_{SPLIT,\eta} = 1 \times 10^{-7}$s was defined between micromixing and reaction in η-space. This option has been selected after some sensitivity analysis on zero-dimensional CMC case. VODPK has been selected as the solver for both stiff and non-stiff parts.

Additional methodologies have been tested to improve the numerical efficiency of the simulations. The integral method described in Klimenko (1995) has been applied, even thought the hypothesis of turbulent shear layer are not fully respected. According to theory the conditional averages are weak function of the flow cross stream direction so that the dimension of the CMC domain can be reduced. Its application to the present test case is represented by a two-dimensional axi-symmetric CMC grid, in which the azimuthal direction collapses. Predictions with the so defined two-dimensional CMC and a zero-dimensional one, more corresponding to a RIF-like calculation, have been compared in the results chapter with the full three-dimensional model.

To resume, the final equations integrated in this chapter can be rewritten for species and temperature as

$$\begin{aligned} \frac{\partial Q_i}{\partial t} &+ \left[\langle \mathbf{v}|\eta\rangle^* - \mathbf{v}_{REL} - \langle D_t|\eta\rangle^* \nabla \left(\ln(\bar{\rho}\tilde{P}(\eta)^*)\right)\right] \cdot \nabla Q_i \\ &= \nabla \cdot (\langle D_t|\eta\rangle^* \nabla Q_i) + \langle N|\eta\rangle^* \frac{\partial^2 Q_i}{\partial \eta^2} + \langle W_i|\eta\rangle \end{aligned} \tag{6.1}$$

$$\begin{aligned} \frac{\partial Q_T}{\partial t} &+ \left[\langle \mathbf{v}|\eta\rangle^* - \mathbf{v}_{REL} - \langle D_t|\eta\rangle^* \nabla \left(\ln(\bar{\rho}\tilde{P}(\eta)^*)\right)\right] \cdot \nabla Q_T \\ &= \nabla \cdot (\langle D_t|\eta\rangle^* \nabla Q_T) + \langle N|\eta\rangle^* \frac{\partial^2 Q_T}{\partial \eta^2} \end{aligned}$$

$$+ \quad \langle N|\eta\rangle^* \left[\frac{1}{c_{p_\eta}}\left(\frac{\partial c_{p_\eta}}{\partial \eta} + \sum_{i=1}^{n} c_{p,i_\eta}\frac{\partial Q_T}{\partial \eta}\right)\frac{\partial Q_T}{\partial \eta}\right]$$

$$+ \quad \frac{1}{c_{p_\eta}\rho_\eta}\left\langle \frac{\partial p}{\partial t}\middle| \eta\right\rangle - \frac{1}{c_{p_\eta}}\left\langle \sum_{i=1}^{n} h_i W_i \middle| \eta\right\rangle - \frac{\langle w_{wall}|\eta\rangle}{c_{p_\eta}\rho_\eta} \tag{6.2}$$

where the same nomenclature as in chapter 2 has been used. Explicit reference has been made in equations 6.1 and 6.2 to the relative velocity of the grid, appearing as an extra convection term non dependent on η. The wall heat flux is also present acting as a sink in the temperature equation. Note that in the present formulation no radiation has been considered and will be included in the future. The star superscript used refers to the process of averaging between the CFD and the CMC grid. In particular, the extension of equations 6.1 and 6.2 to the two-dimensional case yield to an integration of the stared quantities over the azimuthal direction, whereas for the zero-dimensional case are integrated over the whole domain and terms depending on the spatial gradients have been set to zero.

6.4 Results and discussion

Experimental pressure traces are available for the two cases modeled. It is underlined that in the heptane spray combustion simulated in chapter 5 no validation was available for the phase of flame development. An accurate pressure prediction, even if pressure represent an 'integrated' quantity would give substantial credence to the prediction of this phase of combustion.

Initially the 100% load test case has been investigated. Results for the three-dimensional, two-dimensional and zero-dimensional CMC are plotted in figure 6.2 together with the experimental measurements. The agreement is satisfactory in all cases. Autoignition is accurately predicted, the rise in pressure is slightly underestimate for both elliptic formulations. The over prediction observed in the homogeneous CMC with respect to the elliptic ones was expected. Without any spatial dependence, autoignition occurs simultaneously at all most reactive mixture fractions with higher peak in the heat release rate (proportional to the slope of the pressure trace). The reasons for the slight under predictions, as the

turbulent flame speed propagation or the wall effects, will be better explained later. Further work on grid sensitivity might clarify this issue. The agreement between three-dimensional and two-dimensional CMC cross stream integrated is remarkable and because of the limited computer power available the latter one will be considered for further studies.

Figure 6.3 shows a comparison of in-cylinder pressure traces between experiment and prediction for the 50% load higher-velocity. Two-dimensional and one-dimensional CMC compare very well with the experimental measurements. The two-dimensional formulation has somehow smoother pressure rise as already explained for the high load case. The results are very promising for a full integration of the CMC in the engine development process. It is worth to mention that the full cycle with the axi-symmetric CMC formulation from the Intake Valve Opening (IVO) took less then 10 days on a 2.4Ghz Linux Machine. Better performances can be achieved on a parallel machine.

Further insight into the combustion can be achieved looking on plot of the conditional and unconditional scalars. Figure 6.4, 6.5 and 6.6, show the evolution of respectively mixture fraction, temperature and OH mass fraction in different phase of combustion along the spray axis for the 100% load case. Autoignition occurs shortly after SOI (figure 6.4) on the edge of the spray, characterized by high level of OH mass fraction and an initial rise in temperature. The flame spreads and alight all the spray (figure 6.5). It may not be very clear in the figure because of the smoothing in the plotting, but the high temperature region interests the edge of the spray at its tip. The high temperature region propagates from one side close to the cold wall where high enthalpy flux was found. The location of the high temperature region is probably one of the reasons for the under-prediction mentioned in the pressure trace. Figure 6.6 shows how the flame surrounding the spray impinges against the wall.

From the solution at 3 deg three locations in space have been analyzed, marked as A, B, C in figure 6.4. As shown by the conditional temperature plot (figure 6.7) the selected points are across the spray flame. It can be observed that point A is still at low temperature although an initial rise is evident at mixture fraction $\xi = 0.1$, point B is right on the edge of the flame, since the high conditional temperature region has not propagated yet in η-space, point C a fully burning

solution, as shown by the conditional temperature profile close to the equilibrium temperature.

The mechanism for the flame propagation can be investigated looking at the balance of terms into the conditional temperature equation (figures 6.8 - 6.10). Figure 6.8 at the point A shows that the rise in temperature, is mainly due to the contribution of physical transport. The main flow is spray-driven, therefore the convection along the spray axis is the most relevant during propagation. Diffusion from the hot temperature region is also important and is of the same magnitude as the reaction rate. Figure 6.9 (point B) at the flame front, shows a different phase of propagation. A double flame is evident from the two high reaction rate peaks in η-space, and η-diffusion balances the chemical source term. From the inset in figure 6.9, which magnifies the zone around stoichiometry, it can be seen that all terms are active. Convection and diffusion act as sink terms since they transport the heat away form the reaction zone allowing propagation. The pressure term is also not negligible: its contribution is positive and tends to rise temperature. It is reminded that even if figure 6.9 is taken after TDC, the pressure is still rising in the combustion chamber because of the high temperature. Point C, illustrated in figure 6.10, is located into the flame high temperature region. The two flame fronts shown in point B have expanded reducing also their absolute magnitude and an additional peak appears at stoichiometry. The triple flame already highlighted in chapter 5 typical of a diffusive combustion is recovered here. Pressure work is also active at all mixture fractions. The magnitude of the other terms are much smaller and present only at the flame front due to the reduced gradients in physical space at this stage of flame development.

From the contour plot of unconditional temperature a very small lift-off height mainly determined by the boundary conditions at the injector has to been noticed. No results in terms of in-cylinder optical measurements are available for this engine for an accurate comparison. Nevertheless, results from the literature (Dec (1997)) has shown lift-off as a typical feature of diesel engine combustion. The reason for this underprediction is attributed to the coarse grid employed in both CFD and CMC meshes. For simpler geometry as in a constant-volume high-temperature vessel, with a better mesh resolution, as in Kim et al. (2007), CMC was able to correctly predict diesel spray lift-off height under quasi-steady

conditions. The aim of an accurate spray lift-off height prediction is determined by the consequence that this has on the pollutant emission, in particular soot. According to Dec (1997) high lift-off heights are associated with low emission of soot since the amount of air entrained in the core of the spray is responsible for their oxidation.

The snapshots presented are typical images of diesel engine combustion. They show the level of complexity reached in a diesel engine combustion calculation. In the same simulation are present turbulent spray ignition and flame development, droplet dispersion, spray flame impinging against a colder wall. Each one on their own represent important fields of research.

6.5 Conclusion

Three-dimensional Conditional Moment Closure has been applied to study diesel engine combustion. The grid movement has been considered in the CMC formulation with the inclusion of an extra convection term due to the relative velocity of the grid. An algorithm of cell addition/removal has been implemented to allow an optimal cell aspect ratio during the compression and expansion stroke. The heat transfer to the wall has also been included into the CMC equation.

Two test cases have been modeled at different loads and operating speeds, the predicted pressure traces show good agreement with the experimental ones in both cases. The agreement of the pressure traces is a validation of the flame propagation phase that was not possible to obtain from the spray bomb in chapter 5, which was at constant pressure. Further comparisons on heat release and pollutant emissions are planned for an accurate validation.

The results showed similar physics to what was presented in chapter 5. However the spray lift-off height typical of diesel combustion (Dec (1997)) was not adequately predicted. The reason for this is attributed to the coarse grid in both the CFD and CMC codes. Additional work is needed to evaluate the grid dependency of the results. A finer CMC grid is aimed in order to accurate resolve the diesel lift-off height and the solid boundaries.

The three-dimensional test case has been simplified using an appropriate integration across the azimuthal direction (two-dimensional CMC) and over the whole

domain (zero-dimensional CMC). The results compare well with the experiments showing that, in some cases where heat losses to walls are not important, an integral method can be effective in first approximation to predict combustion in diesel engine at a reduced computational cost.

6.6 Tables and Figures

Type	4-stroke, direct injection Turbocharged, intercooled
Cylinders	4
Bore	122 mm
Stroke	142 mm
Displacement	6.64 liters
Compression ratio	17.2
Crank radius / connecting rod length ratio	0.3114
Maximum boost pressure ratio	2.6
Maximum power output	183 kW
Maximum engine speed	2100 RPM
Maximum BMEP	20 bar
Maximum peak cylinder pressure	160 bar
Swirl	0.65

Table 6.1: Liebherr D924 main engine data.

Injector	Common rail technologies AG P2/ETH-LMB prototype
Maximum injection pressure	1600 bar
Nozzle diameter	8×200 μm
Nozzle length diameter ratio	5.16
High pressure fuel pump	ETH development. Maximum pressure 2000bar, suction throttled

Table 6.2: Liebherr D924 fuel injection system.

case	load	engine RPM	SOI [CA aTDC]	injection pressure [bar]
1	50%	1830	-4	1400
2	100%	1250	-4	1400

Table 6.3: Engine operating conditions for the simulations.

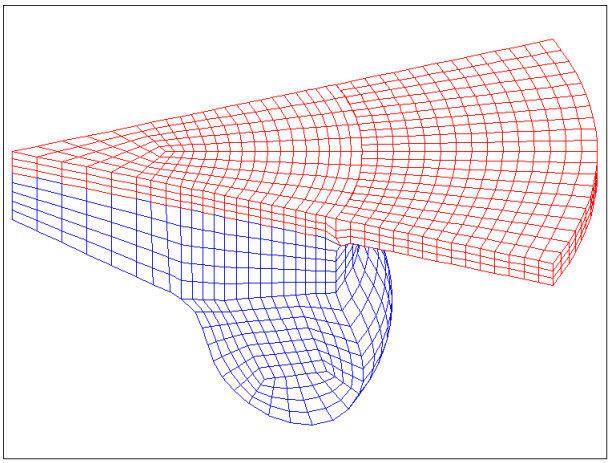

Figure 6.1: Schematic of the CFD grid close to TDC.

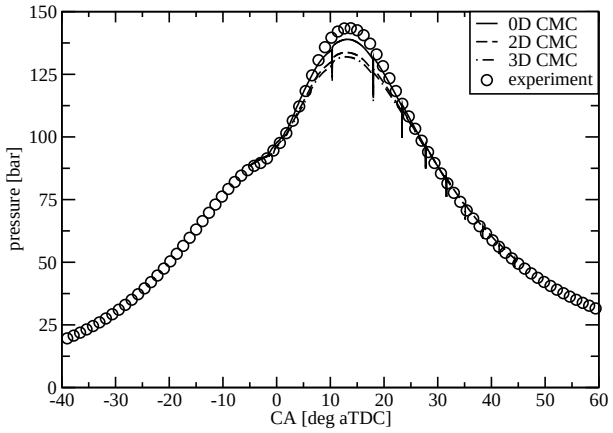

Figure 6.2: Pressure trace [bar] for 100% load (case 1).

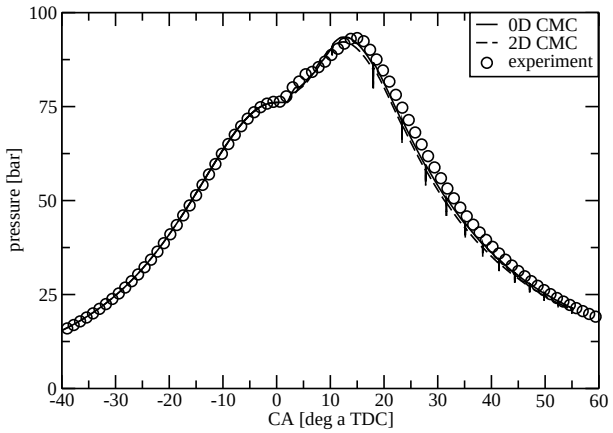

Figure 6.3: Pressure trace [bar] for 50% load (case 2).

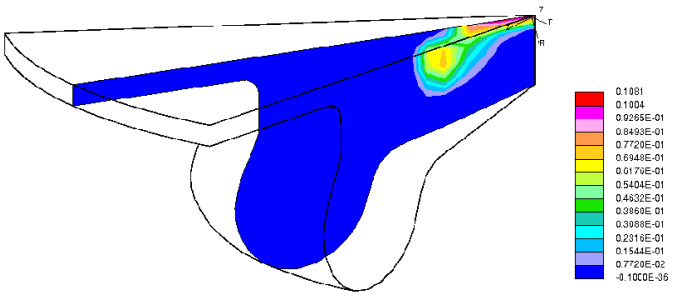

(a)

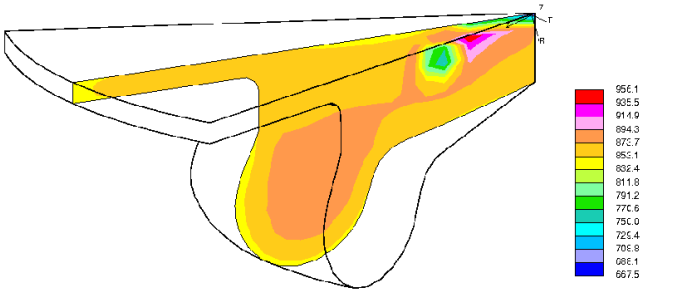

(b)

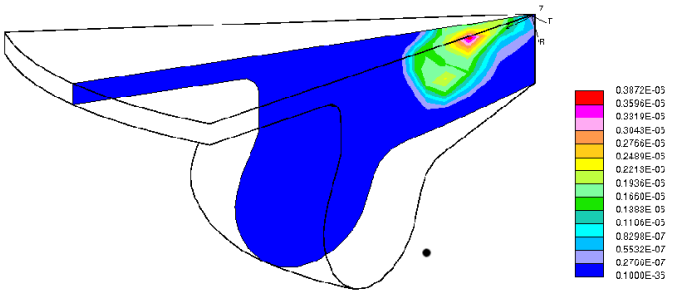

(c)

Figure 6.4: Isocontour of $\tilde{\xi}$ [-] (a), $\tilde{T}$ [K] (b), $\tilde{Y}_{OH}$ [-] (c) along the spray axis for the 100% load case - 1.5 deg aTDC.

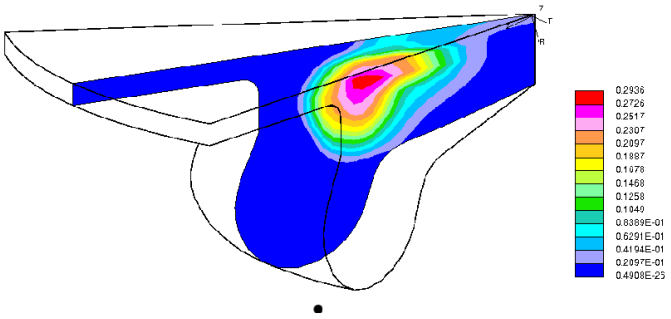

(a)

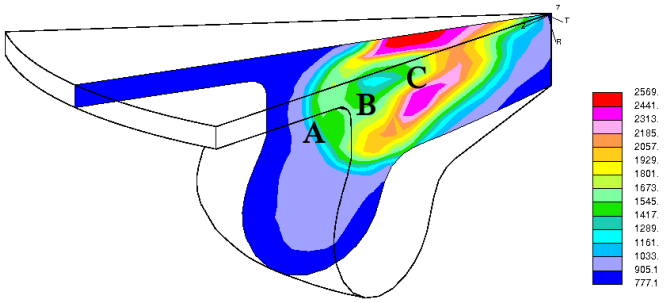

(b)

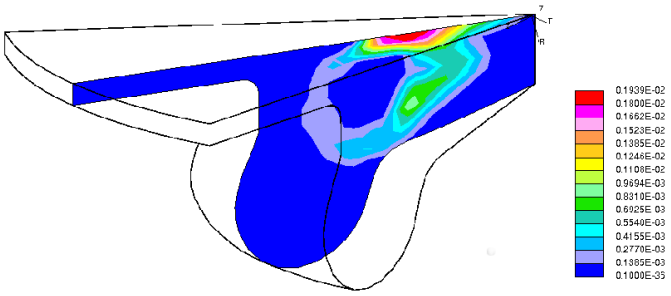

(c)

Figure 6.5: Isocontour of $\tilde{\xi}$ [-] (a), $\tilde{T}$ [K] (b), $\tilde{Y}_{OH}$ [-] (c) along the spray axis for the 100% load case 3 deg aTDC.

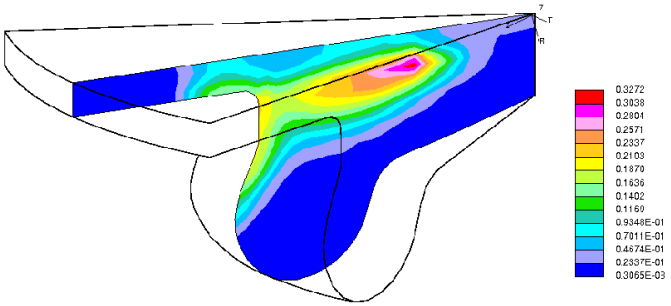

(a)

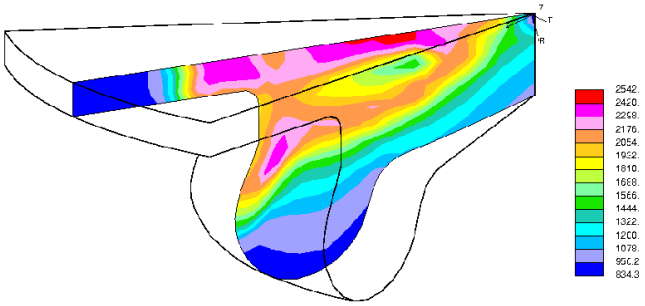

(b)

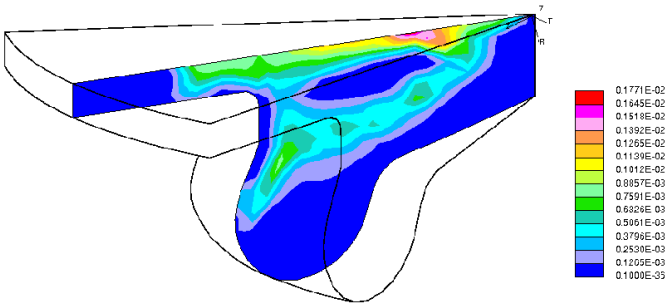

(c)

Figure 6.6: Isocontour of $\tilde{\xi}$ [-] (a), $\tilde{T}$ [K] (b), $\tilde{Y}_{OH}$ [-] (c) along the spray axis for the 100% load case 9 deg aTDC.

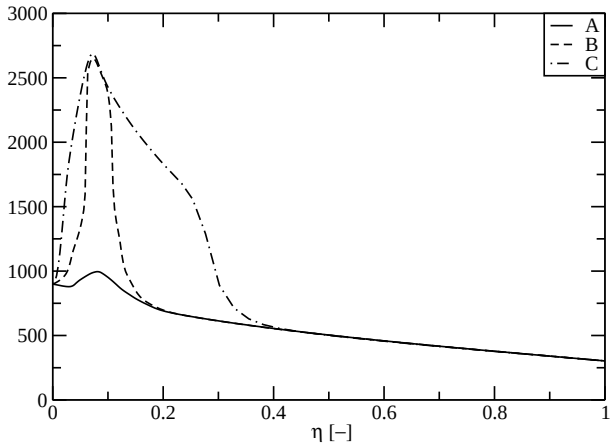

Figure 6.7: Conditional temperature [K] at 3 deg aTDC 100% load for three point.

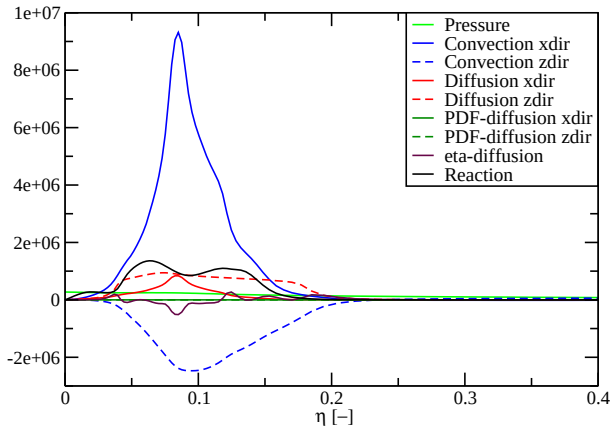

Figure 6.8: Balance of term [K/s] in the conditional temperature equation at point A in figure 6.7.

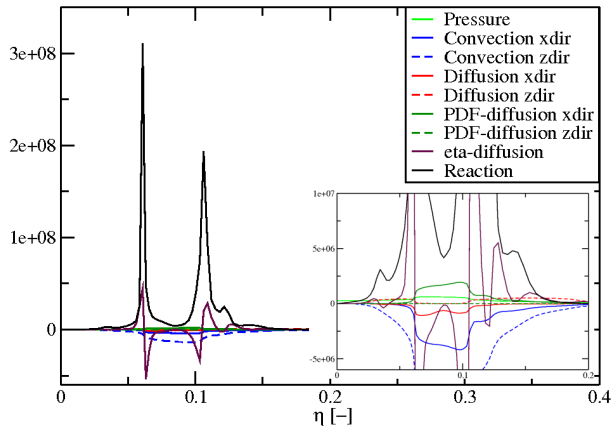

Figure 6.9: Balance of term [K/s] in the conditional temperature equation at point B in figure 6.7.

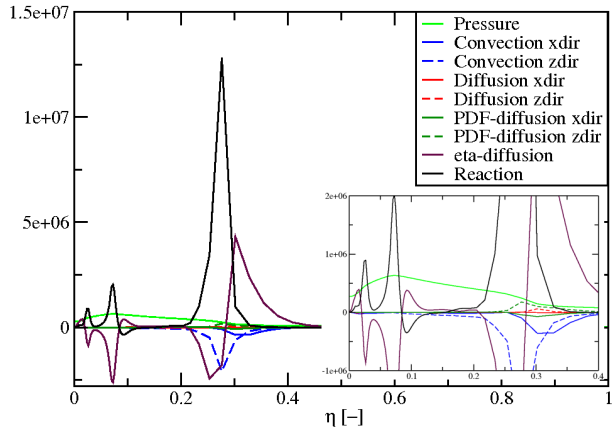

Figure 6.10: Balance of term [K/s] in the conditional temperature equation at point C in figure 6.7.

Chapter 7

Conclusions

The aims of this thesis are twofold: to investigate turbulent non-premixed autoignition in the Conditional Moment Closure (CMC) framework and to develop a computer code able to predict turbulent non-premixed combustion as for DI diesel engines. Simulations have been performed for two dedicated autoignition experiments respectively a steady turbulent n-heptane plume (chapter 4) and an unsteady n-heptane spray bomb (chapter 5) with the intent to assess the model behaviour and its implementation for simple cases. The developed code has been subsequently used to model a DI diesel engine cycle (chapter 6). Numerical and theoretical developments have been proposed to close the conditional chemical source term at first and higher-order and to implement the CMC for transient calculations. The results obtained are presented in the following. The chapter closes with suggestions for further research.

7.1 Turbulent non-premixed autoignition

Autoignition of a pre-vaporized n-heptane plume in an uncloased coflow of turbulent heated air has been investigated using a parabolic CMC formulation. The use of this relatively simple configuration allowed to investigate the effects of turbulent mixing on chemistry during the autoignition event.

It was found that both the scalar dissipation rate and the mixture fraction statistics are important factors to predict autoignition. As expected, autoignition occurs at the 'most reactive' mixture fraction (ξ_{MR}), which is function of the

fuel (i.e. the chemical mechanism), the composition (i.e. dilution), the initial temperature of the reactants and the conditional scalar dissipation rate.

The autoignition delay time of a reactive non-premixed mixture is bounded between two reference times: the ignition time of a homogeneous mixture at a composition defined by the 'most reactive' mixture fraction (τ_{REF}) and by the perfect mixing of the reactants (τ_{PREMIX}) as, respectively, its lower and upper limits. Hence, the mixture fraction statistics ($P(\eta)$) becomes an important parameter to distinguish between the non-premixed and the homogeneous autoignition. In the present configuration, for long autoignition delays $P(\eta)$ approaches a δ-function at its premixed composition, however, the autoignition delay is determined by the history of the reactive fluid particles and an evaluation of the autoignition delay time based on τ_{PREMIX} yields erroneous results. On the other hand, if ξ_{MR} does not belong to the realizable $P(\eta)$, autoignition can not be estimated by τ_{REF} and it can be delayed or even fails to happen within the domain length.

Autoignition occurs at low value of the conditional scalar dissipation rate. In particular, all conditions kept the same, the longer the time the fluid particle passes at high scalar dissipation rate, especially close to its critical value (χ_{CR}) at which autoignition fails to happen, the higher is the autoignition delay time.

In conditions of high conditional scalar dissipation rate the fluctuations above its conditional mean value become an important term for the evolution of autoignition. It has been shown, prior autoignition, that the contribution of the conditional covariance of scalar dissipation rate and the reactive scalars is the most important contribution to the balance of terms of the conditional covariance equation.

The first-order CMC was able to satisfactory predict autoignition time and location in both the coflow plume and the spray-driven flow. The success of the first-order formulation to predict autoignition is attributed to the rapid decay that the conditional scalar dissipation rate exhibits in both configurations studied. This does not imply that the conditional fluctuations are negligible at autoignition. It has been been shown, in fact, that using higher-order closure the PDF of conditional temperature exhibits a bimodal behaviour at the thermal 'run-away' and during the flame propagation phase consistently with DNS

results. It is expected that solving for second-order closure will improve predictions of autoignition at higher values of the conditional scalar dissipation rate or when prediction of minor species is required.

Higher order closure may have an influence also in the propagation velocity of the edge flames following autoignition. It was shown that the conditional fluctuations have a positive contribution in the evaluation of the conditional reaction rate during the initial development of the flame kernel in mixture fraction space. In physical space the conditional scalar flux represents an important generation term in the conditional covariance equations. At the edge of a flame this contribution may be significant and the turbulent flame speed may be affected.

Autoignition of a n-heptane spray in a diesel engine-like configuration has been studied in the effort of analyze the effect of turbulence. Results show that ignition occurs at the edge of the spray in particular at its tip where the conditions of existence of 'most reactive' mixture fraction and low conditional scalar dissipation rate coexist. High turbulence shortens the autoignition delay, which is explained by a faster decay of the conditional scalar dissipation rate. After autoignition the hot kernel propagates lighting the whole spray. The mechanism of flame propagation has been presented showing how after autoignition a double flame is formed ('premixed' phase of diesel engine combustion) to stabilize as a triple flame typical of a lifted jet flame. In this first attempt to represent spray combustion the contribution of the dispersed evaporating phase has not been considered in the CMC implementation. The results compare well with the experiments, however, the contribution of droplet evaporation may be significant and requires future research.

The combustion code developed has been employed to model a diesel engine cycle. Results compare well with the experimental pressure traces, which gives credibility to the model and the numerical method used. This constitutes a first validation of the flame propagation phase that was not feasible in the previous spray-driven autoignition experiment at constant pressure. The level of detail and insight that the CMC model provides on diesel engine combustion highlights its potential to be used as a practical tool for engine diagnostic.

7.2 Numerical implementation

One of the outputs of the present work is the two numerical codes whose results have been presented throughout this thesis. The first consists in a three-dimensional, transient code which has been coupled with a fluid mechanics solver for unsteady turbulent combustion calculations. The second has a parabolic one-dimensional radial formulation solving the first two conditional moments, therefore closing the conditional reaction rate at first or higher-order. In the following a short description of both is presented.

7.2.1 Elliptic, transient, first-order closure

A first-order elliptic CMC code has been coupled with a fluid mechanics solver for transient turbulent combustion simulations. The CMC model solves transport equations for conditional scalars, therefore, in the aim of resolving the spatial gradient of these last, its mesh requirement may differs form a typical unconditional fluid mechanics solver. Gradients of conditional scalars are present within the edge of a flame, at autoignition, at the interaction with a solid wall, etc... Whereas, in the coupling, the fluid mechanics solver needs to properly resolve the velocity and mixing field, with particular care to the conserved scalar statistics $\mathrm{P}(\eta)$ in temporal and spatial coordinates. An interface is, therefore, required to map the two computational meshes with the data transfer achieved by an appropriate averaging or by convolution with the local $\mathrm{P}(\eta)$ respectively proceeding from the CFD to the CMC mesh and vice versa.

A finite difference formulation has been used to discretize the CMC equations. This has been chosen in order to avoid estimation of the convective and diffusive fluxes from the CFD mesh which would have encountered high inaccuracies (a finite volume formulation would have been selected if there was coincidence of the cell faces between the two meshes).

Two different methods of integration have been implemented: the Method of Lines (MOL) and the Operator Splitting (OS) method. The former integrates simultaneously the full set of Ordinary Differential Equations (ODEs) obtained from the discretization of the CMC Partial Differential Equations (PDEs); the latter allows the sequential integration of the ODEs in various sub-steps of smaller

subsystems. The method has to be selected on the base of a compromise between accuracy and numerical efficiency. The MOL is the most accurate, nonetheless, it results to a very large and stiff ODE system to integrate due to the high dimensionality (i.e. five independent variables: three physical coordinates, η-space and time) and depending to the chemical mechanism used; MOL may be improbable for realistic geometries. The OS method has the advantage that splitting the equation in two substeps (OS1) (i.e. transport in physical space and reaction-diffusion in η space) or in three substeps (OS2) (i.e. physical space, diffusion and reaction in η space), allows the use of smaller array with resulting gain in memory storage and solver efficiency.

The use of an OS method introduces an error due to the sequential resolution of phenomena that are physically coupled. The error is function of the splitting timestep and of the phenomenon that needs to be resolved. It was found that a large timestep might predict earlier autoignition in particular in conditions of large conditional scalar dissipation rate and an under prediction in the flame propagation phase. It is important to underline that the solution obtained with the MOL may be recovered reducing the splitting timestep. In the present thesis the OS2 has been selected as the method of choice for practical calculations.

Additional advantages, using an OS formulation, can be achieved employing a solver tailored according to the nature of the substep. For stiff systems it may be convenient to use a solver with small restart costs (i.e. CHEMEQII). Based on an OS formulation the code developed has been parallelized solving the physical transport (non-stiff substep) part the equations on a single processor and the η-substep (stiff substep) in parallel on different processors of a CPU cluster. Good parallel efficiency has been demostrated.

Additional work has been done to allow the coupling of the present code with the unstructured mesh typical of the diesel engine combustion chambers. An algorithm of cell recognition was developed to identify the CMC nodes that had a correspondence with the CFD boundary in order to build a domain which represented a piece wise approximation of the CFD domain. Identified using the CFD boundary cells, the solid wall has been considered with the inclusion of additional terms into the CMC equation by modelling the heat flux to through the wall. In case of a moving grid formulation, as during the compression/expansion

stroke in a diesel engine cycle, an algorithm of cell removal/addition has been implemented for the CMC grid which allows the user to specify the cell density and their aspect ratio. The presence of a sliding grid, furthermore, has been modelled into the CMC equation as an additional convection term depending on the grid relative velocity.

The interface and the numerical developments here implemented in a RANS context can be easily extended to an LES framework with careful validation of the sub-models of the CMC equations.

7.2.2 Parabolic, steady, second-order closure

A parabolic formulation of the CMC has been used to implement a conditional reaction rate closure at higher order than first. Conditional second moments are conditional variances and covariances, given a chemical mechanism of n species additional $n \times (n-1)/2$ transport equations need to be added to a first order formulation.

Two higher-order implementations were investigated: a Taylor expansion and the conditional joint PDF method. In the first, the conditional reaction rate has been expanded up to second order assuming small, but not negligible conditional fluctuations. Evaluation of the reaction rate is done adding to the first-order contribution a second order term function on the Hessian of the reaction rate evaluated numerically. In the second, closure of the conditional reaction rate is obtained by the convolution of the reaction rate with the presumed conditional joint PDF of the reactive scalar over the reactive scalar sample space. In the latter, no conditions are imposed on the magnitude of the conditional fluctuations resulting in a more general formulation.

First and second moments are coupled only through the conditional reaction rate: in the Taylor expansion formulation variances and covariances are used to estimate the second-order contribution to the first order conditional reaction rate, in the PDF method to presume the conditional joint PDF of the reactive scalars.

The Taylor expansion method proved to be an efficient way to include the second order effects. However, the hypothesis of small conditional fluctuations does

not hold at ignition and the calculation could not proceed further due to instability in the evaluation of the Hessian of the reaction rate. Despite the difficulties to model the propagation following ignition, the method presented is general and the possibility of including mechanism of any complexity without selecting reduced set of chemical reactions for second order closure is an advantage. The Taylor expansion method may be used to predict the structure of autoignition before the thermal 'run-away' or applied to flame calculations with limited conditional fluctuations to improve pollutant prediction.

A second order correction based on temperature variance has been explored to assess the effects the closure using the full mechanism for an autoignition case. It was found that for complex chemistries as the n-heptane mechanism used here, only the temperature could not accurately predict the effects of the pre-ignition reactions resulting to an overall underestimation of the reaction rate.

A different conclusion was drawn using the conditional joint PDF method. Due to limitations in the mathematical formulation for multidimensional PDF, in the present work only the conditional temperature PDF was considered to close the conditional reaction rate, presuming the $P(T|\eta)$ to be a β-distribution. Results have shown that this method has similar prediction to what predicted by the Taylor expansion method with the advantage of not having assumption on the conditional fluctuations.

This last method is in general computationally more expensive since the reaction rate has to be calculated in each point of the selected manifold (in the present case in the two-dimensional space (η,T)), however tabulated chemistry may be used in the future to improve the numerical efficiency.

7.3 Future work

The application of the CMC for practical calculation introduces interesting challenges which can be used as guidelines for future work in terms of model developments and numerical implementation.

In the aim of applying the CMC as universal model for diesel engine combustion an accurate treatment of spray combustion is necessary. Combustion may occur in the inter droplet space as well as around dense clusters of droplets. The

mixture fraction distribution, its variance and dissipation rate need to reflect the effects of the dispersed phase (Reveillon and Vervisch (2000)). The CMC equations need to be revisited including additional terms due to the dispersed phase (Rogerson et al. (2007)) and the standard submodels further validated. Additional work has to be done on the boundary conditions in mixture fraction space since the interval of realizable mixture fraction bounds may be modified accounting for the saturation mixture fraction (Smith et al. (2000)) and the condition at eta boundaries (equations 2.73 and 2.74) may not hold.

The evaluation of modern diesel engine performance is generally based on power output and pollutant emissions in particular nitric oxides and soot. While the first can be included directly in the chemical mechanism used, the addition of soot requires the implementation of transport equation for the first conditional moments and special treatment if the differential diffusion effect of the solid particle need to be accounted. The implementation of soot particles in CMC was initially treated by Kronenburg et al. (2000) who suggested a differential diffusion formulation and accounting for soot only as a post processing substep decoupled from the main chemical mechanism. Future development aim to implement higher moments for the soot particles, include the soot chemistry into the main chemical mechanism and evaluating new formulations for differential diffusion as the one proposed by Hewson et al. (2006). Furthermore the radiation model used in gaseous flame calculation, may not be valid in case of sooty spray combustion and needs to be revisited.

In the presence of an HCCI type of combustion the charge in the cylinder has a high degree of homogeneity. Combustion occurs in multiple locations with little propagation of flame. The limit of realizability of the $P(\eta)$ and the treatment of the probability region may have an effect and needs further investigation.

Modelling of the flame-wall interaction is also becoming an important field of research. Heat transfer, radical recombination, absorption and desorption of fuel by the lubricant film at the wall are phenomena which may en effect on the engine combustion and the pollutant prediction. A careful resolution of the wall boundary layer is needed as well as to model for the fluxes of species at the solid boundary (Bilger (2001)).

The application of second-order closure to diesel engine combustion is also an interesting field of research. As presented in this thesis a simplified closure based on the conditional joint PDF method solving only the temperature variance may give important insight into diesel engine combustion at a relatively cheap computational cost.

Additional area of research intends to validate the model used for second-order closure. Of particular interest are the conditional scalar dissipation rate fluctuations which appear in the conditional covariance equation and which has been proven to be the driving term in autoignition simulations. The shape of the conditional joint PDF of the various scalars during autoignition and the flame propagation is also interesting and may validate the present mathematical formulations.

Further research has been carried out by Richardson and Mastorakos (2007) to validate the conditional turbulent flux model. One important output of that work consists in a modelling approach to account for counter gradient diffusion in the conditional turbulent flux term, find to be important for example in the propagation of an edge flame. Further work may be needed to implement that submodel.

It is important to mention that some of the development proposed here requires a high CMC resolution. An automatic grid refinement able to resolve the gradient in mixture fraction and physical space would allow a better resolution of the flame brush for an accurate study of the flame propagation phase, a better definition of the solid boundaries as well as generally higher accuracy of the discretization.

All the development proposed here may also be seen in the perspective of a full coupling of CMC with LES for diesel engine applications.

References

C. Bai and A.D. Gosman. Mathematical modelling of wall films formed by impinging sprays. *SAE Technical Paper 960626*, 1996. 155

G. Bikas. *Kinetic mechanisms for hydrocarbon ignition.* PhD thesis, University of Aachen, 2001. xii, 67, 70, 90, 115, 118, 156

R. W. Bilger. Marker fields for turbulent premixed combustion. *Combustion and Flame*, 138:188–194, 2004. 9

R.W. Bilger. Turbulent flows with non-premixed reactants. In P.A. Libby and F.A. Williams, editors, *Turbulent Reacting Flows*, chapter 3. Springer-Verlag, 1980. 7

R.W. Bilger. Conditional moment closure for turbulent reacting flows. *Physics of Fluids A Fluid Dynamics*, 5:436–444, 1993. 8, 12, 18, 47

R.W. Bilger. Boundary conditions at walls for conditional moment closure modeling (unpublished). 2001. 35, 47, 156, 178

G. Blanquart and H. Pitsch. Modeling autoignition in non-premixed turbulent combustion using a stochastic flamelet approach. *Proceedings of the Combustion Institute*, 30:2745–2753, 2005. 8, 10

J. D. Blouch, J-Y Chen, and C. K. Law. A joint scalar PDF study of nonpremixed hydrogen ignition. *Combustion and Flame*, 135:209–225, 2003. 10

R. Borghi. Turbulent combustion modelling. *Progress in Energy and Combustion Science*, 14:245–292, 1988. 7

G. Boudier, L.Y.M. Gicquel, T. Poinsot, D. Bissieres, and C. Berat. Comparison of LES, RANS and experiments in an aereonautical gas turbine combustion chamber. *Proceedings of the Combustion Institute*, 31:3075–3082, 2007. 6

K. Boulouchos, O.N. Margari, A. Escher, G. Barroso, B. Schneider, and S. Kunte. Optical siagnostic on diesel spray for the validation of computer aided simulation. *6. Internationales Symposium fur Verbrennungsdiagnostik, Baden-Baden*, 2003. 154

P. N. Brown, G. D. Byrne, and A. C. Hindmarsh. VODE, a variable-coefficient ODE solver. *SIAM Journal on Scientific and Statistical Computing*, 10:1038–1051, 1989. 50, 69, 116

P. N. Brown and A. C. Hindmarsh. Reduced storage matrix methods in stiff ode systems. *Journal of Computational and Applied Mathematics*, 31:40–91, 1989. 50, 116

W.K. Bushe and R.W. Bilger. Conditional moment closure modeling of turbulent non-premixed combustion with reduced chemistry. *Annual Research Briefs*, pages 139–154, 1999. 23

G.D. Byrne. Pragmatic experiments with Krylov methods in the stiff ODE setting. In J. Cash and I. Gladwell, editors, *Computational Ordinary Differential Equations*, pages 323–356. Oxford University Press, Oxford, 1992. 50, 116

C.M. Cha and H. Pitsch. Higher-order conditional moment closure modelling of local extinction and reignition in turbulent combustion. *Combustion Theory and Modelling*, 6:425–437, 2002. 29, 30, 69

H.H. Chiu, H.Y. Kim, and E.J. Croke. Internal group combustion of liquid droplets. *Proceedings of the Combustion Institute*, 19:971–980, 1982. 113, 130

H.K. Ciezky and G. Adomeit. Shock-tube investigationof self-ignition of n-heptane-air mixtures under engine relevant condition. *Combustion and Flame*, 93:4212–433, 1993. xii, 70, 90

M.J. Cleary, J.H. Kent, and R.W. Bilger. Prediction of carbon monoxide in fires by conditional moment closure. *Proceedings of the Combustion Institute*, 29: 273–279, 2002. 112, 116

O. Colin and A. Benkenida. The 3-zones extended coherent flame model (ECFM3Z) for computing premixed/diffusion combustion. *Oil & Gas Science and Technology*, 59:593–609, 2004. 152

O. Colin, A. Benkenida, and C. Angelberger. 3D modeling of mixing, ignition and combustion phenomena in highly stratified gasoline engine. *Oil & Gas Science and Technology*, 58:47–62, 2003. 152

T.J. Craft and B.E. Launder. Closure modelling near the two-component limit. In B.E. Launder and N.D. Sandham, editors, *Closure strategies for turbulent and transitional flows*, chapter 3, pages 102–126. Cambridge University Press, 2002. 65

P. A. Davidson. *Turbulence*. Oxford University Press, 2004. 13

J.E. Dec. A conceptual model of DI diesel combustion based on laser-sheet imaging. *SAE Technical Paper 970873*, 106(3)(1319-1348), 1997. 111, 113, 160, 161

F.X. Demoulin and R. Borghi. Assumed PDF modelling of turbulent spray combustion. *Combustion Science and Technology*, 158:249–271, 2000. 129, 130

C.B. Devaud, R.W. Bilger, and T. Liu. A new method of modeling the conditional scalar dissipation rate. *Physics of Fluids*, 16(6):2004–2011, 2004. 32, 74

C.B. Devaud and K.N.C. Bray. Assessment of the applicability of conditional moment closure to a lifted turbulent flame: First order model. *Combustion and Flame*, 132:102–114, 2003. 53

T. Echekki and J.H. Chen. Direct numerical simulation of autoignition in non-homogeneous hydrogen-air mixtures. *Combustion and Flame*, 134:169–191, 2003. 10, 62

FLUENT. FLUENT V*6*. FLUENT Inc., http://www.fluent.com, 2003. 65

S.S. Girimaji. On the modeling of scalar diffusion in isotropic turbulence. *Physics of Fluids A*, 4(11):2529–2537, 1992. 32

K. Gkagkas and R.P. Lindstedt. Transported PDF modelling with detailed chemistry of pre- and auto-ignition in CH4/air mixtures. *Proceedings of the Combustion Institute*, 31:1559–1566, 2007. 10

M.P. Halstead, L.J. Kirsch, and C.P. Quinn. The autoignition of hydrocarbon fuels at high temperatures and pressures - fitting of a mathematical model. *Combustion and Flame*, 30:45–60, 1977. 3, 151

C. Hasse and N. Peters. A two mixture fraction flamelet model applied to split injections in a DI diesel engine. *Proceedings of the Combustion Institute*, 30(2): 2755–2762, 2005. 8, 152

C. Hergart and N. Peters. Applying the representative interactive flamelet model to evaluate the potential effect of wall heat transfer on soot emissions in a small-bore DI diesel engine. *ASME Journal of Engineering for Gas Turbines and Power*, 124(1042-1052), 2001. 8, 35, 47, 152

J. C. Hewson, A. J. Ricks, S. R. Tieszen, A. R. Kerstein, and R. O. Fox. Conditional-moment closure with differential diffusion for soot evolution in fire. *Proceedings of Summer Program CTR*, pages 311–323, 2006. 178

J.C. Hewson. *Pollutant emission from nonpremixed hydrocarbon flames*. PhD thesis, University of California, San Diego, 1997. 67, 118

J.B. Heywood. *Internal combustion engine fundamentals*. McGraw-Hill, 1988. 2, 35

J.O. Hinze. *Turbulence*. McGraw-hill, 2nd edition, 1987. 13

C. Hollmann and E. Gutheil. Modelling of turbulent spray diffusion flames including detailed chemistry. *Proceedings of the Combustion Institute*, 26:1731–1738, 1996. 129, 131

H.G. Im, J.H. Chen, and C.K. Law. Ignition of hydrogen-air mixing layer in turbulent flows. *Proceedings of the Combustion Institute*, 27:1047–1056, 1998. 4, 10, 62

W.P. Jones and P. Musonge. Closure of the Reynolds stress and scalar flux equations. *Physics of Fluids*, 31(12):3589–3604, 1988. 65

W.P. Jones, S. Navarro-Martinez, and O. Rhl. Large eddy simulation of hydrogen auto-ignition with a probability density function method. *Proceedings of the Combustion Institute*, 31:1765–1771, 2007. 6, 10, 63

I.S. Kim. *Conditional Moment Closure for non-premixed turbulent combustion.* PhD thesis, University of Cambridge, England, 2005. 32

I.S. Kim and E. Mastorakos. Simulation of turbulent lifted jet flames with two-dimensional conditional moment closure. *Proceedings of the Combustion Institute*, 30:905–912, 2005. 9, 26, 33, 128

I.S. Kim and E. Mastorakos. Simulations of turbulent non-premixed counter-flow flames with first-order conditional moment closure. *Flow, Turbulence and Combustion*, 76:133–162, 2006. 5, 65, 73

I.S. Kim, G. De Paola, and E. Mastorakos. Simulations of n-heptane combustion in a constant-volume vessel with first-order conditional moment closure. Technical report, Hopkinson Laboratory, Cambridge University, 2007. 160

S.H. Kim. On the conditional variance and covariance equations for second-order conditional moment closure. *Physics of Fluids*, 14(6):2011–2014, 2002. 22, 23, 38, 39, 46

S.H. Kim, K.Y. Huh, and R.W. Bilger. Second-order conditional moment closure modeling of local extinction and reignition in turbulent non-premixed hydrocarbon flames. *Proceedings of the Combustion Institute*, 29:2131–2137, 2002. 28, 44, 47

S.H. Kim, K.Y. Huh, and R.A. Fraser. Modeling autoignition of a turbulent methane jet by the conditional moment closure model. *Proceedings of the Combustion Institute*, 28:185–191, 2000a. 112

S.H. Kim, K.Y. Huh, and L. Tao. Application of the elliptic conditional moment closure model to a two-dimensional nonpremixed methanol bluff-body flame. *Combustion and Flame*, 120:75–90, 2000b. 53

W.T. Kim and K.Y. Huh. Numerical simulation of spray autoignition by the first-order conditional moment closure model. *Proceedings of the Combustion Institute*, 29:569–575, 2002. 53, 63, 112, 131

A.Y. Klimenko. Multicomponent diffusion of various mixtures in turbulent flow. *Fluid Dynamics (ISSR)*, 25:327–334, 1990. 8, 18

A.Y. Klimenko. Note on the conditional moment closure in turbulent shear flows. *Physics of Fluids*, 7(2):446–448, 1995. 49, 66, 157

A.Y. Klimenko. On the relation between the conditional moment closure and unsteady flamelets. *Combustion Theory and Modelling*, 20:275–294, 2001. 8

A.Y. Klimenko and M.M. Abdel-Jawad. Conditional methods for continuum reacting flows in porous media. *Proceedings of the Combustion Institute*, 31: 21072115, 2007. 132

A.Y. Klimenko and R.W. Bilger. Conditional moment closure for turbulent combustion. *Progress in Energy and Combustion Science*, 25:595–687, 1999. 8, 10, 17, 20, 21, 22, 23, 26, 28, 29, 32, 33, 34, 36, 54, 129

S.C. Kong, Z. Han, and D. Reitz. Application of a diesel ignition and combustion model for multidimensional engine simulation. *SAE Technival paper no. 950278*, 1995. 151

H.J. Koss, D. Bruggemann, A. Wiartalla, H. Baker, and A. Breuer. Investigations of the influence of turbulence and type of fuel on the evaporations and mixture formation in fuel sprays. Technical report, Final Report JOULE Project on Integrated Diesel European Action (IDEA), 1992. xv, xvi, 113, 114, 135, 142, 143

A. Kronenburg. Double conditioning of reactive scalar transport equations in turbulent nonpremixed flames. *Physics of Fluids*, 16(7):2640–2648, 2004. 9, 128

A. Kronenburg and R.W. Bilger. Modelling differential diffusion in nonpremixed reacting turbulent flow: Model development. *Combustion Science and Technology*, 166:195,227, 2001. 24

A. Kronenburg, R.W. Bilger, and J.H. Kent. Second-order conditional moment closure for turbulent jet diffusion flames. *Proceedings of the Combustion Institute*, 27:1097–1104, 1998. 44

A. Kronenburg, R.W. Bilger, and J.H. Kent. Modeling soot formation in turbulent methane-air jet diffusion flames. *Combustion and Flame*, 121:24–40, 2000. 178

A. Kronenburg and M. Kostka. Modeling extinction and reignition in turbulent flames. *Combustion and Flame*, 143:342–356, 2005. 30, 46, 69

K.N. Lakshmisha, Y. Zhang, B. Rogg, and K.N.C. Bray. Modelling auto-ignition in a turbulent medium. *Proceedings of the Combustion Institute*, 24:421–428, 1992. 10

H. Lehtiniemi, F. Mauss, M. Balthasar, and I. Magnusson. Modeling diesel spray ignition using detailed chemistry with a progress variable approach. *Combustion Science and Technology*, 178:1977–1997, 2006. 8, 152

M. Lesieur and O. Metais. New trends in large-eddy simulation of turbulence. *Annual Review of Fluid Mechanics*, 28:45–82, 1996. 6

J.D. Li and R.W. Bilger. Measurement and prediction of the conditional variance in a turbulent reactive-scalar mixing layer. *Physics of Fluids*, 5(12):3255–3264, 1993a. 44, 45

J.D. Li and R.W. Bilger. A simple theory of conditional mean velocity in turbulent scalar-mixing layer. *Physics of Fluids*, 6(2):605–610, 1993b. 33

A. Liñan and A. Crespo. The asymptotic structure of counterflow diffusion flames for large activation energies. *Combustion Science and Technology*, 14:95, 1976. 10, 61, 69, 86

S. Liu, J.C. Hewson, J.H. Chen, and H.Pitsch. Effects of strain rate on high-pressure nonpremixed n-heptane autoignition in counterflow. *Combustion and Flame*, 137:320–339, 2004. 118

B.F. Magnussen. On the sturcture of turbulence and a generalixed eddy dissiaption concept for chemical reaction n turbulent flow. *AIAA*, 19, 1981. 3, 151

C.N. Markides. *Autoignition in turbulent flows*. PhD thesis, Cambridge University, 2005. 63, 64, 71, 72, 76, 78, 79

C.N. Markides and E. Mastorakos. An experimental study of hydrogen autoigniton in a turbulent co-flow of heated air. *Proceedings of the Combustion Institute*, 30:883–891, 2005. 63, 78, 79

C.N. Markides and E. Mastorakos. Measurements of scalar dissipation in a turbulent plume with planar laser-induced fluorescence of acetone. *Chemical Engineering Science*, 61(9):2835–2842, 2006a. 63, 65

C.N. Markides and E. Mastorakos. Measurements of the statistical distribution of the scalar dissipation rate in a turbulent axisymmetric plume. *The 5th International Symposium on Turbulence, Heat and Mass Transfer in Dubrovnik, organized by ICHMT*, 2006b. 45

C.N. Markides, G. De Paola, and E. Mastorakos. Measurements and simulations of mixing and autoignition of an n-heptane plume in a turbulent flow of heated air. *Experimental Thermal and Fluid Science*, 31(5):393–401, 2007. xii, 63, 89

A. R. Masri, R. W. Dibble, and R. S. Barlow. The structure of turbulent nonpremixed flames of methanol over a range of mixing rates. *Combustion and Flame*, 89:167–185, 1992. 17, 27

A. Massias, D. Diamandis, E. Mastorakos, and D.A. Goussis. An alhorithm for the construction of global reduced mechanism with CSP data. *Combustion and Flame*, 117:685–708, 1999. 67

E. Mastorakos, T.A. Baritaud, and T.J. Poinsot. Numerical simulations of autoignition in turbulent mixing flows. *Combustion and Flame*, 109:198–223, 1997a. 4, 10, 45, 61, 62, 68, 71, 78, 86, 115, 127

E. Mastorakos and R.W. Bilger. Second-order conditional moment closure for the autoignition of turbulent flows. *Physics of Fluids*, 10(6):1246–1248, 1998. 10, 62, 63, 72, 81, 82

E. Mastorakos, A. Pirez Da Cruz, and T.A. Baritaud. A model for the effects of mixing on the autoignition of turbulent flows. *Combustion Science and Technology*, 125:243–282, 1997b. 61, 72

W.E. Mell. A validity investigation of the conditional moment closure model for turbulent combustion. 1995. 23

M. Mortensen. Consistent modeling of scalar mixing for presumed, multiple parameter probability density functions. *Physics of Fluids*, 17(1)(18106), 2005. 31, 32, 33, 74

M. Mortensen and A. Bengt. Presumed mapping functions for eulerian modelling of turbulent mixing. *Flow, Turbulence and Combustion*, 72(2)(199-219), 2006. 31

D.R. Mott, E.S. Oran, and B. van Leer. A quasi-steady-state solver for the stiff ordinary differential equations of reaction kinetics. *Journal of Computational Physics*, 164:407–428, 2000. 50, 117, 119

R. Mustata, L. Valiño, C. Jimenez, W.P. Jones, and S. Bondi. A probability density function eulerian montecarlo field method for large eddy simulation: Applications to a turbulent piloted methane/air diffusion flame (sandia d). *Combustion and Flame*, 145:88–104, 2006. 9

S. Navarro-Martinez, A. Kronenburg, and F. Di Mare. Conditional moment closure for large eddy simulations. *Flow, Turbulence and Combustion*, 75:245–274, 2005. 11

E.E. O'Brien and T. Jiang. The conditional dissipation rate of an initially binary scalar in homogeneous turbulence. *Physics of Fluids A*, 3(12):3121–3123, 1991. 32

N. Peters. Laminar diffusion flamelet models in non-premixed turbulent combustion. *Progress in Energy and Combustion Science*, 10:319–339, 1984. 7, 151

N. Peters. Laminar flamelet concepts in turbulent combustion. *Proceedings of the Combustion Institute*, 21:1231–1250, 1986. 7, 151

N. Peters. *Turbulent combustion*. Cambridge University Press, 2000. 7

L.M. Pickett and D.L. Siebers. Soot in diesel fuel jets: effects of ambient temperature ambient density, and injection pressure. *Combustion and Flame*, 138: 114–135, 2004. 111

H. Pitsch, H. Barthsand, and N. Peters. Three-dimensional modelling of NO_x and soot formation in di-diesel engines using detailed chemistry based in the representative interactive flamelets. *SAE Technical Paper 962057*, 1996. 8, 152

H. Pitsch, C.M. Cha, and S. Fedotov. Flamelet modelling of non-premixed turbulent combustion with local extinction and re-ignition. *Combustion Theory and Modelling*, 7:317–332, 2003. 8, 47

S.B. Pope. PDF methods for turbulent reactive flows. *Progress in Energy and Combustion Science*, 11:119–192, 1985. 9, 13, 33

S.B. Pope. *Turbulent flows*. Cambridge University Press, 2000. 4, 5, 6, 9, 13

J. Reveillon and L. Vervisch. Spray vaporization in nonpremixed turbulent combustion modeling: a single droplet model. *Combustion and Flame*, 121:75–90, 2000. 129, 130, 131, 178

S. Richard, O. Colin, O. Vermorel, A. Benkenida, C. Angelberger, and D. Veynante. Towards large eddy simulation of combustion in spark ignition engines. *Proceedings of the Combustion Institute*, 31(2):3059–3066, 2007. 6

E.S. Richardson, N. Chakraborty, and E. Mastorakos. Analysis of direct numerical simulations of ignition fronts in turbulent non-premixed flames in the context of conditional moment closure. *Proceedings of the Combustion Institute*, 31(1): 1683–1690, 2007. 33, 128

E.S. Richardson and E. Mastorakos. Simulations of non-premixed edge-flame propagation in turbulent non-premixed jets (to appear). *Proceedings of the European Combustion Meeting*, 2007. 9, 33, 128, 179

J.W. Rogerson, J.H. Kent, and R.W. Bilger. Conditional moment closure in a bagasse-fired boiler. *Proceedings of the Combustion Institute*, 31(2):2805–2811, 2007. 112, 116, 129, 131, 178

T.W. Ryan and T.J. Callahan. Homogeneous charge compression ignition (HCCI) of diesel fuel. *Society of Automotive Engineers 961160*, 1996. 3

D.A. Schwer, P. Lu, W.H. Green, and V. Semiao. A consistent-splitting approach to computing stiff steady-state reacting flows with adaptive chemistry. *Combustion Theory and Modelling*, 7:383–399, 2003. 116

N.S.A. Smith, C.M. Cha, H. Pitsch, and J.C. Oefelein. Simulation and modeling of the behavior of conditional scalar moments in turbulent spray combustion. *Proceedings of Summer Program CTR*, pages 207–218, 2000. 129, 130, 131, 178

B. Sportisse. An analysis of operator splitting techniques in the stiff case. *Journal of Computational Physics*, 161:140–168, 2000. 53

S. Sreedhara. *Studies on autoignition in a turbulent nonpremixed medium using direct numerical simulation*. PhD thesis, Indian Institute of Science - Bangalore, 2002. 45

S. Sreedhara and K.Y. Huh. Assessment of closure schemes in second-order conditional moment closure against DNS with extinction and ignition. *Combustion and Flame*, 143:386–401, 2005a. 43, 46

S. Sreedhara and K.Y. Huh. Modeling of turbulent, two-dimensional nonpremixed CH4/H2 flame over a bluffbody using first- and second-order elliptic conditional moment closures. *Combustion and Flame*, 143:119–134, 2005b. 40, 46

S. Sreedhara and K.Y. Huh. Conditional statistics of nonreacting and reacting sprays in turbulent flows by direct numerical simulation. *Proceedings of the Combustion Institute*, 31:2335–2342, 2007. 130

S. Sreedhara and K.N. Lakshmisha. Assessment of conditional moment closure models of turbulent autoignition using DNS data. *Proceedings of the Combustion Institute*, 29:2069–2077, 2002a. 62, 63

S. Sreedhara and K.N. Lakshmisha. Autoignition in a non-premixed medium: DNS studies on the effects of three-dimensional turbulence. *Proceedings of the Combustion Institute*, 29:2051–2059, 2002b. 4, 10, 62

P. Sripakagorn, G. Kosaly, and H. Pitsch. Local extinctionreignition in turbulent nonpremixed combustion. *Annual Research Briefs*, page 117128, 2000. 29

STAR-CD. STAR – CD V*3.20, Methodology*. CD adapco Group, http://www.adapco.com, 2004. 54, 114, 115, 154, 155

G. Strang. On the construction and comparison of difference schemes. *SIAM J. Numer. Anal*, 5(3):506–517, 1968. 53

K. Suga. *Development and application of a non-linear eddy viscosity model sensitized to stress and strain invariants*. PhD thesis, Faculty of Technology, University of Manchester, 1995. 65, 73

N. Swaminathan and R.W. Bilger. Study of the conditional covariance and variance equations for second order conditional moment closure. *Physics of Fluids*, 11(9):2679–2695, 1999. 30, 43, 44, 45, 69

N. Swaminathan, R.W. Bilger, and G.R. Ruetsch. Interdependence of the instantaneous flame front structure and the overall scalar flux in turbulent premixed flames. *Combustion Science and Techology*, 128:73–97, 1997. 9

D. Thevenin and S. Candel. Ignition dinamics of a diffusion flame rolled up in a vortex. *Physics of Fluids*, 4:434, 1995. 61

L. Thielen, K. Hanjalic, H. Jonker, and R. Manceau. Predictions of flow and heat transfer in multiple impinging jets with an elliptic-blending second-moment closure. *International Journal of Heat and Mass Transfer*, 48:1583–1598, 2005. 65, 73

L. Valiño. A field Monte Carlo formulation for calculating the provability density function of a single scalar in a turbulent flow. *Flow Turbulence and Combustion*, 60(2)(157-172), 1998. 9

D. Verhoeven, J.L. Vanhemelryck, and T. Baritaud. Macroscopic and ignition characteristics of high-pressure sprays of single-component fuels. *SAE Technical Paper 981069*, 107(3)(1654-1668), 1998. 111, 113

L. Vervisch. personal communication. 2006. 129, 130

D. Veynante and L. Vervisch. Turbulent combustion modelling. *Pregess in Energy and Combustion Science*, 28(193-266), 2002. 5, 33

Y.P. Wan, H. Pitsch, and N. Peters. Simulation of autoignition delay and location of fuel sprays under diesel engine relevant conditons. *SAE Technical Paper 971590*, 1997. 152

F.A. Williams. *Combustion theory*. Benjamin/Cummings, 2nd edition, 1985. 16

Y.M. Wright. *Numerical investigation of turbulent spray combustion with conditional moment closure*. PhD thesis, Swiss Federal Institute of Technology Zurich, 2005. 35, 153

Y.M. Wright, G. De Paola, K. Boulouchos, and E. Mastorakos. Simulations of spray autoignition and flame establishment with two-dimensional CMC. *Combustion and Flame*, 143:402–419, 2005. 9, 53, 63

Y. Yu, S.K. Kim, and Y.M. Kim. Numerical modelling for auto-ignition and combustion processes of fuel sprays in high-pressure environment. *Combustion Science and Technology*, 168:85–112, 2001. 8, 127

Y. Zhang, B. Rogg, and K.N.C. Bray. 2-D simulation of turbulent autoignition with transient laminar flamelet source term closure. *Combustion Science and Technology*, 105:211–227, 1994. 152

Y.Z. Zhang, E.H. Kung, and D.C. Haworth. A PDF method for multidimensional modeling of HCCI engine combustion: effects of turbulence/chemistry interactions on ignition timing and emissions. *Proceedings of the Combustion Institute*, 30(2):2763–2771, 2005. 152